UNIVERSITY OF CANTERBURY
Te Whare Wānanga o Waitaha
CHRISTCHURCH NEW ZEALAND

Active Control of Noise through Windows

A thesis submitted in practical fulfilment of the

requirements for the Degree of

Masters in Engineering

at the

University of Canterbury

by

Jeremy Lane

University of Canterbury

Christchurch, New Zealand

2013

Table of Contents

Abstract

Windows are a weakness in building facade sound transmission loss (STL). This coupled with the detrimental effects of excessive noise exposure on human health including: annoyance, sleep deprivation, hearing impairment and heart disease, is the motivation for this investigation of the STL improvements active noise control (ANC) of windows can provide.

Window speaker development, ANC window experiments and analytical modelling of ANC windows were investigated. Five different window speaker constructions were characterised then compared with a previously developed window speaker. ANC window testing used three different ANC configurations and was performed in two different environments, one with a reverberant receiving room, and the other with an anechoic receiving room. Optimisation of ANC systems with particular control source locations was the aim of the modelling. This enabled comparison with the ANC window tests and would aid in further development of ANC windows.

Window speaker constructions were characterised by sound pressure level (SPL) measurements performed in an anechoic room. These measurements were made in a way that enabled comparison with the previously developed window speaker.

Total sound energy reduction calculations were used to determine the relative performance of the tested ANC windows.

An STL model, based on a modal panel vibration model, was initially created and verified against published STL data before it was expanded to include ANC control sources. The model was used to simulate the performed anechoic environment tests and an ideal ANC case.

Acknowledgements

The author would like to thank Fletcher Aluminium, and the Ministry of Science and Innovation for funding this project. A special thank you is also extended to Aiotec Ltd who was the driving force behind this project aiding with technical support and sourcing of materials and components.

The author also would like to thank all the individuals associated with the University of Canterbury Acoustics Research Group (ARG) for the feedback on ideas, testing advice, reviews of work and most importantly for the enjoyable working environment.

Thank you to the following individuals who have helped during the duration of this project including:

John Pearse for his supervision.

Bart Wenmeckers and Peter Squires for their advice and assistance with the experimental work and their technical input.

John Davy for his expert advice on acoustics in general.

Stefanie Gutschmidt for her expert advice on piezoelectric materials and modal analysis.

Shayne Crimp for making the whole project happen.

Symbols

Symbol	Physical Quantity	Unit
a	Horizontal panel dimension	m
b	Vertical panel dimension	m
c	Speed of sound in air; 340m/s	m/s
d	Inter pane spacing of double wall system	m
D	Bending stiffness	Nm^2
E	Young's modulus; for glass ($70GN/m^2$)	N/m^2
f	Frequency	Hz
f_c	Critical frequency for wave co-incidence	Hz
f_R	Resonant frequency	Hz
f_{mn}	Modal frequency for mode (m,n)	Hz
F	Point force magnitude	N
h	Material thickness	m
$\bar{I}_m$	Coupling co-efficient m	-
$\bar{I}_n$	Coupling coefficient n	-
I_m	Radiation coefficient m	-
I_n	Radiation coefficient n	-
I^t	Transmitted sound intensity	Pa/m^2
k	Wave number; defined as ω/c	rad/m
k_m	Wave number for horizontal direction	rad/m
k_n	Wave number for vertical direction	rad/m
m	Horizontal mode number	-
M	Surface density	kg/m^2
n	Vertical mode number	-
p	Sound pressure	Pa
p^t	Transmitted sound pressure	Pa
P_{mn}^c	Modal control forces	Pa
P_{mn}^d	Modal disturbance forces	Pa
P_i	Incident pressure	Pa
r	Radius of sound power calculation surface	m
t	Time	s

TL	Sound transmission loss	dB
TL_0	Normal incident sound transmission loss	dB
TL_θ	Sound transmission loss for angle of incidence θ	dB
TL_{random}	Sound transmission loss for a diffuse field incidence	dB
w	Panel displacement	m
W_{mn}	Modal contribution factor of mode (m,n)	-
x	Displacement in the horizontal direction from origin	m
x_f	Horizontal position of control force	m
y	Displacement in the vertical direction from origin	m
y_f	vertical position of control force	m
θ	Angle of incidence	rad
θ_t	Angle of sound transmission	rad
λ	Wavelength of airborne sound	m
λ_B	Bending wave is glass wavelength	m
ν	Poisson's ration; 0.23 for glass	-
$\prod_r$	Radiated sound power	W
$\prod_i$	Incident sound power	W
ρ	Density of air	kg/m^3
ρ_p	Density of panel material	kg/m^3
φ_i	Incident planar direction	rad
Ψ	Total sound energy	J/m^3
Ψ_R	Sound energy reduction	dB
$\Psi_{ANC\ off}$	Total sound energy when ANC is off	J/m^3
$\Psi_{ANC\ on}$	Total sound energy when ANC is on	J/m^3
ω	Angular frequency	rads^{-1}
ω_{mn}	Angular modal frequency	rads^{-1}

1 Introduction

1.1 Introduction

Environmental noise pollution and its effects on human health are a topic of much research [1-3]. Effects include hearing impairment, hypertension, ischemic heart disease, annoyance and disturbed sleep [4]. Low frequency noise in particular has been linked to disturbed sleep and annoyance [5].

Studies of building facades in relation to increasing noise levels in cities [6-9] have identified that windows and doors are the weak link in terms of the sound transmission loss (STL) of facades [10, 11]. Passive solutions for windows involve adding mass or air cavities by way of double and triple glazed windows. Yu [12] describes an innovative solution using active noise control (ANC) applied to windows.

1.2 Project Objective and Scope

The main objective of this project was to explore the viability of applying an ANC platform to a single glazed window application. Improvements in STL at low frequencies (50-500Hz), were targeted.

The initial goal was to create a window speaker that could output high sound pressure levels (SPL) in that if the control source were able to output high SPL it would be an effective control source.

Another approach used was implementing an ANC window application. This approach utilised multiple point control sources in order to minimise the vibration of the glass. The assumption was that if the vibration were minimised then so would be the STL.

In conjunction implementing the ANC window application, prediction work was undertaken to provide enhanced understanding. An experimentally verified model was developed for STL and then further developed to incorporate ANC control sources so was able to simulate ANC window applications.

1.3 Project Approach

Chapter 2 contains a review of the STL of glass windows and how different configurations of single, double, triple and laminated glazed windows affect the STL. Consideration of boundary conditions such as framing and sealing are explored. This chapter also contains a review of ANC window applications and their parameters such as the control method and reference signal generation.

Chapter 3 describes the parallels between an ANC window and an ANC duct application which highlights the need for a high output control source. An experimental study is performed on five different window speaker control source constructions developed utilising PVDF film. These investigated film attachment methods and window materials. Each window speaker construction is described along with the corresponding results which were compared to previously developed window speakers.

Chapter 4 focuses on the implementation of an ANC window application. The experimental study covers both reverberant and anechoic receiving rooms. These tests highlight what is possible with an ANC window application.

Chapter 5 describes an STL model for a single glazed window. This model is used to predict STL and is further extended to model ANC point force control sources. Simulations of the anechoic room experiments (described in chapter 4) and an ideal ANC case is presented and results compared with measurements. The benefits and limitations of the model are then discussed.

Chapter 6 summarises the project findings including a discussion of the viability of ANC window applications and where any future work could be focussed.

2 Sound Transmission Loss of Windows

A review of the literature relating to the sound transmission loss (STL) of windows was conducted. The literature establishes the mechanisms relating to STL of glass and these are related to potential active noise control (ANC) applications for sound reduction. Single, double, triple and laminated glazing type windows were considered along with boundary conditions, and cavity size. Previously studied ANC applications are also included in this review. Cavity and panel control type ANC applications are identified and control source and reference signal considerations discussed.

2.1 Single Glazed Windows

Beranek [13] explains theory relating to the STL of finite panels. He considers a typical transmission loss curve, shown in Figure 2.1, which is broken up into 3 regions. Each region of the STL curve is governed by a different property of the glass. The low frequency STL region is governed by the stiffness and resonances of the panel, the mid frequency region is governed by mass and the high frequency region is governed by wave coincidence. The low frequency region governed by stiffness and resonances is of most interest and potentially the lower part of the mid frequency region. For completeness all regions are covered in this review.

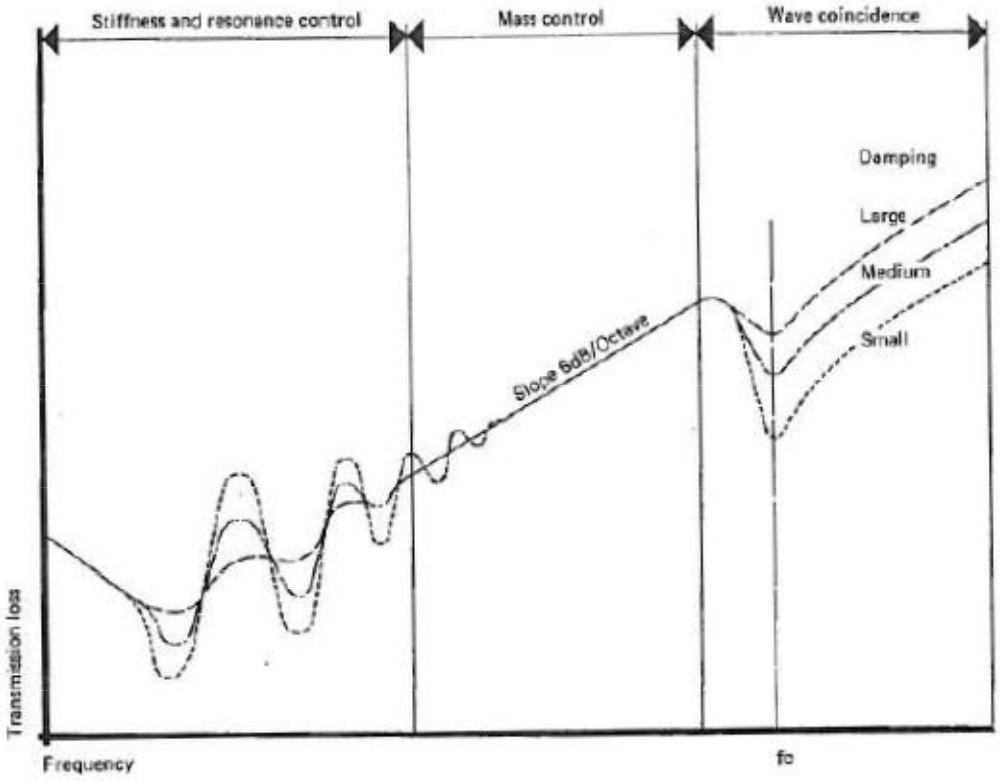

Figure 2.1 A typical transmission loss curve for a panel [13].

2.1.1 Mass law

Beranek's [13] definition of mass law for a plane wave with arbitrary angle of incidence is shown in Equation 2.1. The normal incidence case is shown in Equation 2.2. In both cases it is obvious that for each doubling of mass, the STL increases by approximately 6 dB. Beranek then derives an expression which accounts for all angles of incidence by

integrating Equation 2.1 between 0° and 90°. The resulting approximation is stated in Equation 2.3.

$$TL_\theta = 10\log_{10}\left[1 + \left(\frac{\omega M cos\theta}{2\rho c}\right)^2\right] \quad \text{Equation 2.1}$$

$$TL_0 = 10\log_{10}\left[1 + \left(\frac{\omega M}{2\rho c}\right)^2\right] \quad \text{Equation 2.2}$$

$$TL_{random} \approx TL_0 + 10\log_{10}[0.23TL_0] \quad \text{Equation 2.3}$$

Incident sound of all angles up to 90° is usually not reflected in practice. Therefore smaller limiting angles have been found to give agreement with experimental work [13]. A limiting angle of 80° is typically chosen which reduces to the approximation in Equation 2.4.

$$TL_{random} \approx TL_0 - 5\,dB \quad \text{Equation 2.4}$$

Utley [14] found that experimental results of sound insulation vary widely between studies; therefore many variations of the mass law have been developed. An investigation by Jones [15] explored these different mass law expressions and concluded that Equation 2.5 below had the best fit with several laboratory tests. Utley [14] suggested that laboratory transmission loss facilities be calibrated using a lead panel to combat laboratory variations. Quirt [16] also noticed this variation in STL results specifically in windows. This led Quirt to undertake an extensive series of STL tests on windows to eliminate the variation of results between laboratories.

$$TL = 10log_{10}\left[1 + \left(\frac{\omega M}{4\rho c}\right)^2\right] \quad \text{Equation 2.5}$$

2.1.2 Wave coincidence

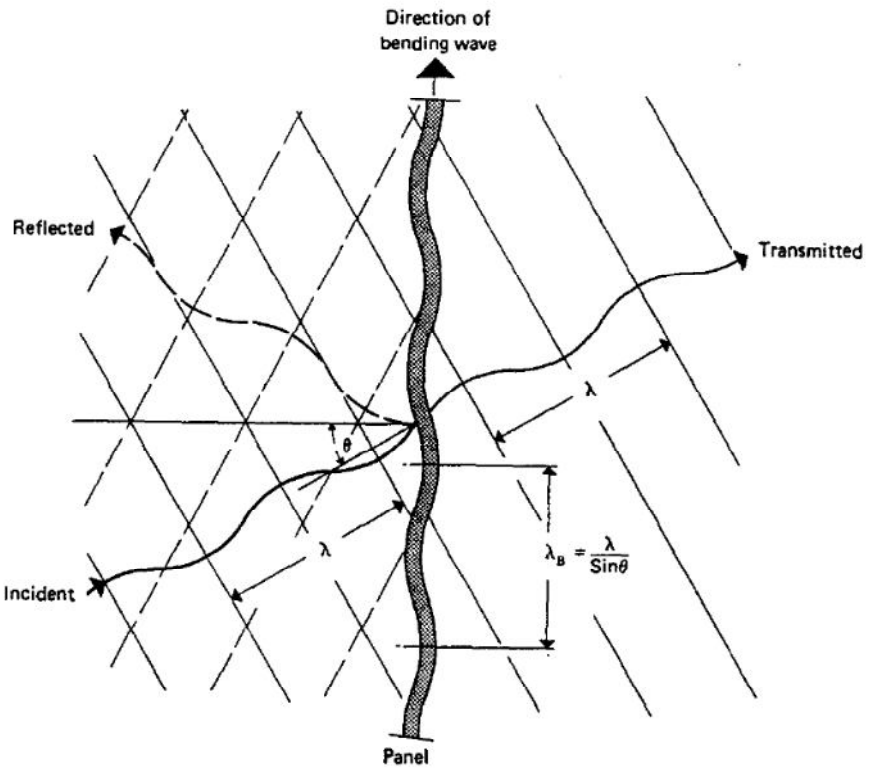

Figure 2.2 Illustration of wave coincidence [17].

Wave coincidence is described by Marsh [17], as a matching of the projected wavelength of the incident airborne sound onto the panel and the free bending waves in the panel. This is illustrated in Figure 2.2. This relationship is described in Equation 2.6. Sound transmission is improved in this frequency range due to the efficient coupling of the panel and air [17, 18].

$$\frac{\lambda}{\sin\theta} = \lambda_B \qquad \text{Equation 2.6}$$

$$f_C = \frac{c^2}{2\pi sin^2\theta}\left[\frac{12\rho_p(1-\nu^2)}{Eh^2}\right]^{1/2} \qquad \text{Equation 2.7}$$

Wave coincidence typically occurs at higher frequencies and usually presents as a dip in the STL curve. The centre frequency of this coincidence dip is calculated in Equation 2.7

for an arbitrary panel. This frequency sets the upper bound of the frequency range over which mass law has a significant effect on the STL curve.

For glass the coincidence dip is significant due to the lower internal damping of glass in compared with other materials [19]. This is illustrated by Marsh [18] in Figure 2.3 along with the significant improvement that is possible with added damping by way of laminated glazing.

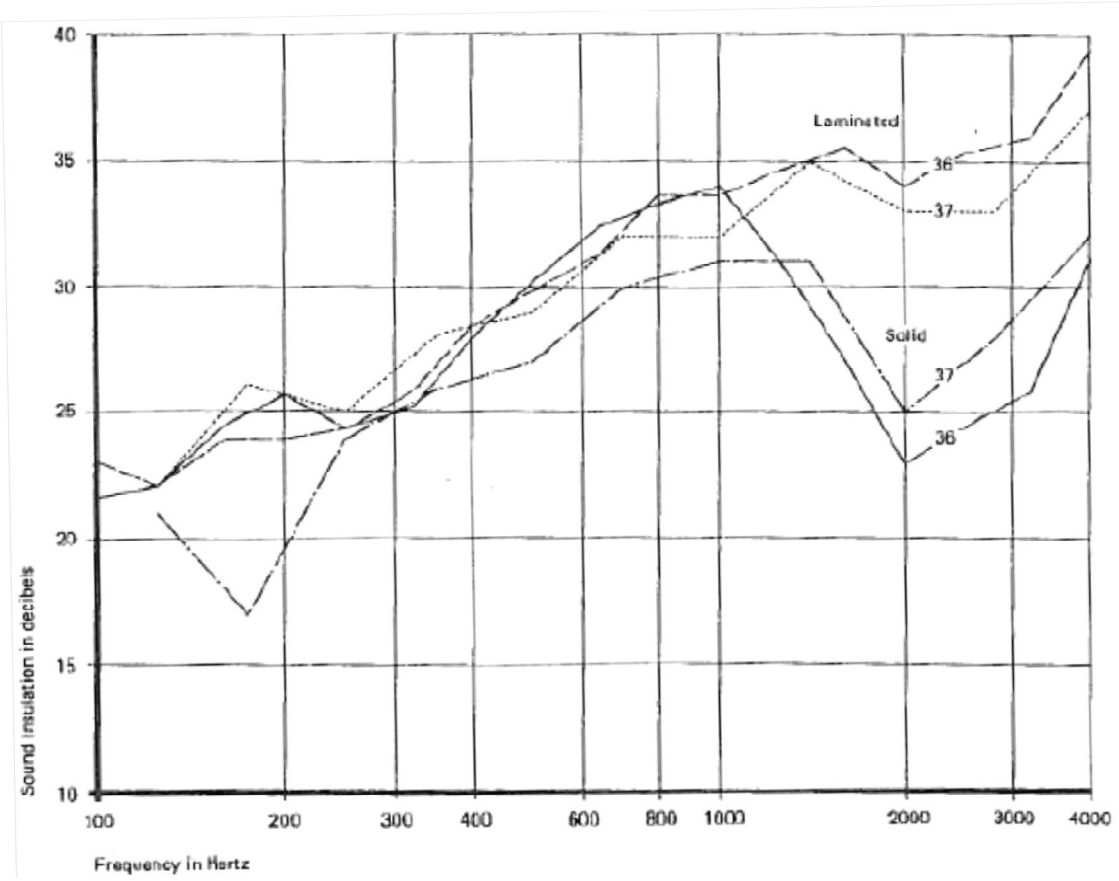

Figure 2.3 Pilkington (36) and Libbey-Ford-Owens (37) manufacturer's data comparison of laminated glazing and solid glazing of same thickness.

Double glazed windows offer a way of minimising the significance of the coincidence dip. Double glazing with unequal thickness panes shows improved STL of the coincidence dip over equally glazed double glazed windows as illustrated in Figure 2.4. Despite the improvements possible with unequal double glazing, laminated glazing provides higher improvements in STL over the coincidence region.

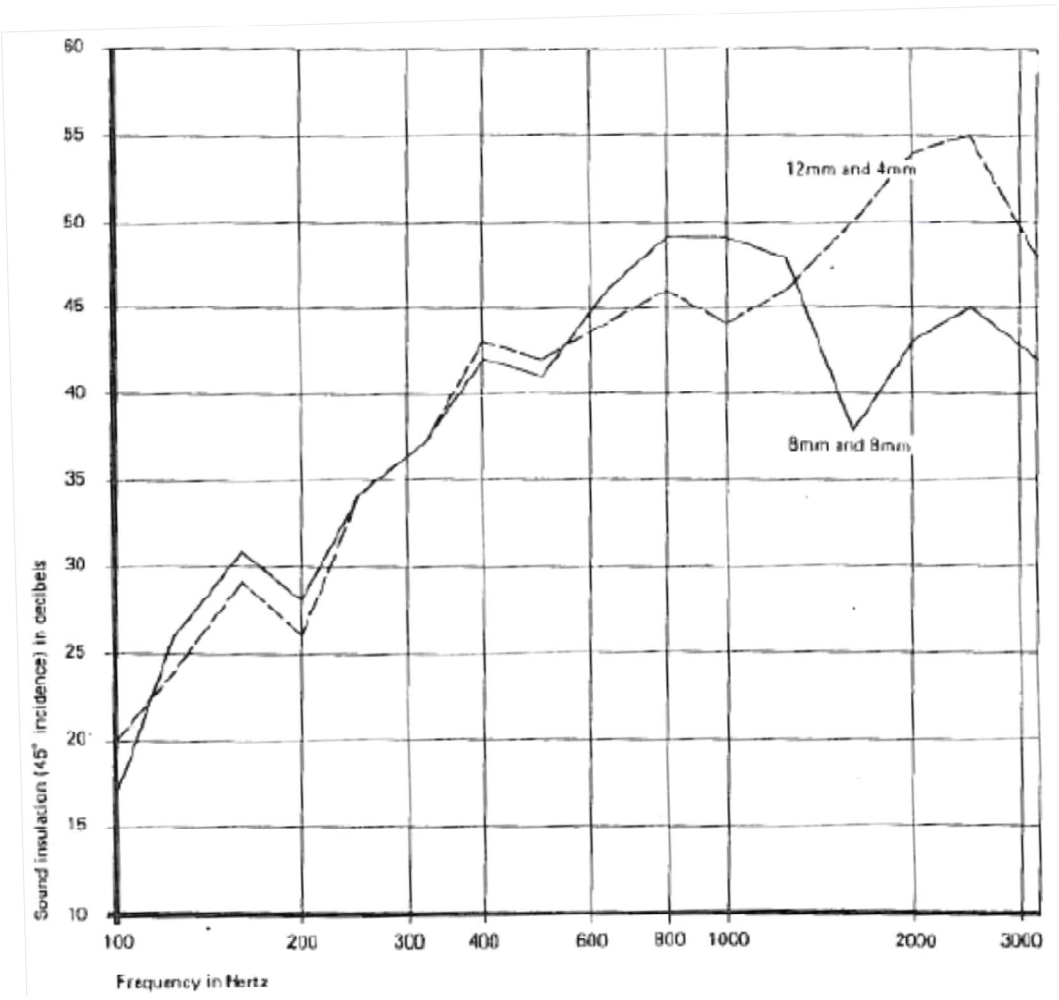

Figure 2.4 Comparison of equal (8mm and 8mm) and unequal (12mm and 4mm) thickness double glazed windows (Oosting [20]).

2.1.3 Resonance

Resonant frequencies occur at specific frequencies where the magnitude of the amplitude of panel vibration is at a relative maximum. These resonant frequencies cause low STL due to the efficient vibration of the panel at these frequencies; hence more efficient sound transmission occurs. Resonant frequencies come about due to finite panels. Equation 2.8 shows the calculation of the resonant frequencies $f_{R,}$ using mechanical properties and dimensions of the panel [17]. An approximation for glass panels is shown in Equation 2.9.

$$f_R = \frac{\pi}{2}\left[\frac{Eh^2}{\rho_p 12(1-\nu^2)}\right]^{\frac{1}{2}}\left[\frac{m^2}{a^2}+\frac{n^2}{b^2}\right] \quad \text{Equation 2.8}$$

$$f_R \approx 2.5\, x\, 10^3 h\left[\frac{m^2}{a^2}+\frac{n^2}{b^2}\right] \quad \text{Equation 2.9}$$

Below the first resonance the stiffness of the panel alone controls the panel movement [13]. This region is usually neglected in research due to the likelihood of it falling below the audible range of the average person.

In a similar fashion to coincidence, resonance is affected by damping. Figure 2.1 shows that poor STL due to resonance can also be improved by higher damping. Unfortunately glass has low internal damping as previously mentioned therefore the damping provided by sealing or edge conditions becomes particularly important.

2.1.4 Pane size

Effects of the pane size on STL performance have not been shown to be significant. Resonant frequencies are impacted by pane size which can be seen in Equations 2.8 and 2.9 but experimental results show little deviation due to pane size. Experimental work by Michelsen [21] concluded that variations in STL performance due to varied panel size are only a few decibels. The Saint-Gobain [22] results also show a maximum variation of 3 dB in STL in any one-third octave band between different pane sizes. Eisenberg [23] suggested that pane size is unimportant in comparison to other considerations such as window sealing and damping.

2.1.5 Sealing

Sealing of the glass in a frame is a key issue as sound easily leaks around the edges of a panel. Hood [24] concluded that sealing on average provides a 6 dB improvement at low frequencies.

2.1.6 Framing

Framing or boundary conditions of glass panels are more important than that for most other building materials due to the low internal damping of glass [19]. Utley [25]

demonstrated that added damping through the use of flexible framing, such as neoprene gaskets, provide superior performance over rigid frames like wood or concrete. The advantages are usually seen at higher frequencies and noticeably in the coincidence region.

Lewis [26] investigated the design of framing for unsealed windows for comparison with models of windows with apertures around the perimeter. Lewis concluded that avoiding small overlaps is critical for unsealed frame design and that sealed window exhibit superior sound insulation performance. These findings are consistent with those of Hood [24] and Michelsen [21] where leakage around the perimeter of a window adversely affect the STL.

2.1.7 Laminated glazing

Laminated glazing provides increased STL across the coincidence region as mentioned above. Probably because of the damping effects of the polyvinyl butyral (PVB) interlayer which is discussed by Marsh [18]. The improvement is of the order of 10dB compared to solid glass. It was found that there is little if any advantage to using a thicker PVB interlayer once above 0.4mm [27] with although thicknesses of PVB up to 1.5mm were compared. Extending the laminated idea to a three pane, two interlayer laminated glazing gives no definitive advantage over a single interlayer [18].

2.2 Double and Triple Glazing

2.2.1 Double glazing

Double glazed windows generally have higher STL than single glazed windows due to the added mass of the additional pane as well as the enclosed air gap or cavity. For unequal thickness double glazing the effects of coincidence are staggered resulting in improved performance over single glazing as aforementioned. The downside of double glazing is the increased number of resonant frequencies. Unequal thicknesses introduce more resonant frequencies whilst unequal thicknesses exacerbate the effect of each resonant frequency. In both cases cavity resonances are added. Double glazing generally gives a higher STL than single glazing mainly due to significant improvements in the mass law region.

2.2.1.1 Mass-air-mass resonance

Mass-air-mass resonance is a resonance frequency inherent in double glazed windows. Single glazed window do not have this resonance as there is no encapsulated air as in double glazed windows. The frequency at which the mass-air-mass resonance occurs is given by London [28] in Equation 2.10.

$$f = \frac{1}{2\pi \cos\theta}\left[\frac{2\rho c^2}{Md}\right]^{\frac{1}{2}} \qquad \text{Equation 2.10}$$

2.2.1.2 Cavity

In general as the cavity width of double glazing is increased an increase in STL performance is observed. Brüel [29] investigated sound insulation as a function of distance between panels, including glass, and concluded that the general rule is increased cavity width leads to improved STL.

Figure 2.5 below shows sound insulation curves for three different separations. This work was carried out by Bazley [30] and clearly shows that increased spacing improves low frequency STL with a little expense at higher frequencies.

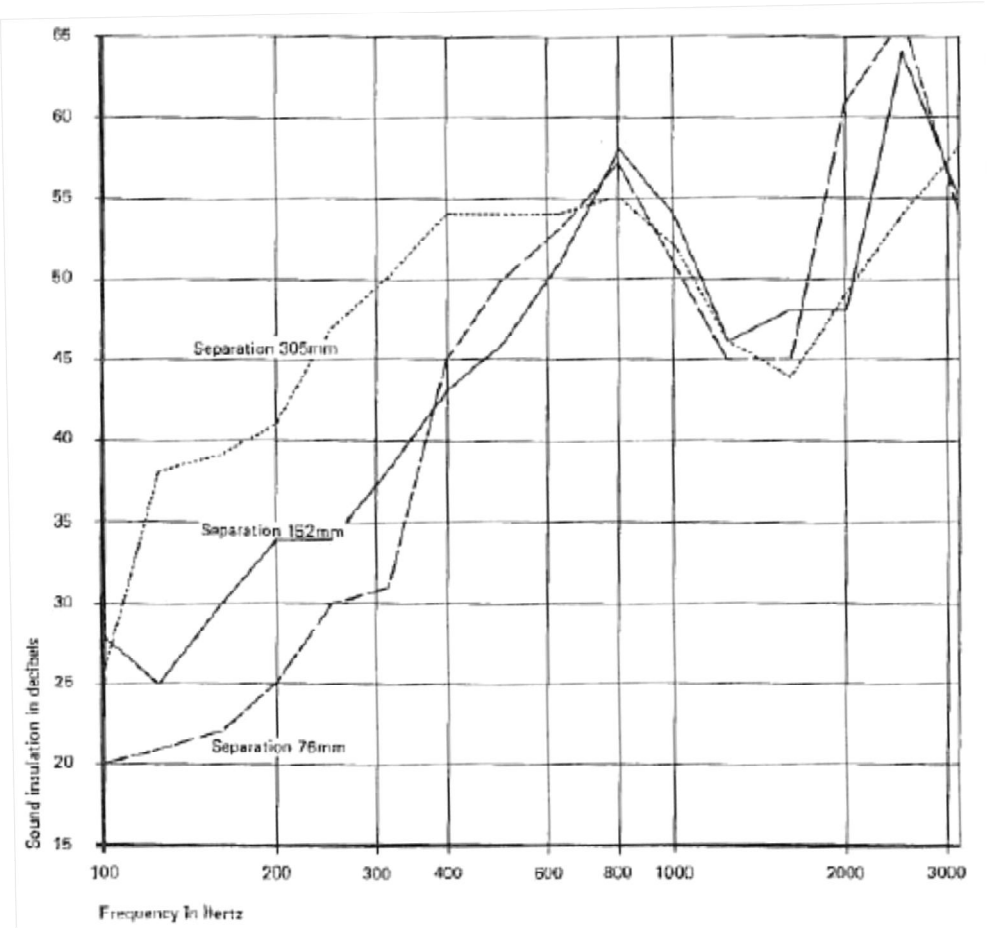

Figure 2.5 Sound insulation curves for differing separations of double glazed windows [30].

The STL of double glazed window can be increased through lining the cavity with absorptive material. Bazley [30] found that lining the cavity with acoustic tiles increased the mean sound insulation by 6dB. Woolley [31] showed improvements of up to 3dB.

2.2.1.3 Non-parallel double glazing

Non-parallel double glazing does not appear to exhibit any benefit over parallel glazing with same mean pane spacing [17]. Mackle [32] drew the same conclusion but with comparison to parallel glazing with the same maximum spacing. The experimental findings of Mackle generally agree with that of Quirt [16]. Therefore non-parallel glazing is not usually employed as a means of increasing the STL.

2.2.1.4 Mechanical linkage

For a double window there are two paths for the sound to travel between the panes, the first is across the cavity, and the other is structurally through the frame. This

mechanical linkage through the frame is believed to provide the primary path when inter-pane spacing reaches 200mm yet quantitative assessment of this appears to be lacking [18]. Fort inter-pane spacing <200mm isolated framing for each pane may be appropriate.

2.2.2 Triple glazing

Tadeu [33] showed that triple glazing exhibits no major advantage over double glazed windows in terms of STL .Marsh [18] states that the larger spacing is more important in terms of STL than the additional glazing. Quirt's work [34] agrees with that of Marsh; but also found advantages for triple glazing below the mass-air-mass resonance and in the coincidence region when compared to double glazing. Triple glazing appeared to have little advantage over double glazing when STL is the sole consideration.

2.2.3 Sound transmission loss data

A comprehensive collation of sound insulation data across all single, laminated, double and triple glazing configurations with third octave band STL decibel values and an overall STC rating was collated by Marsh [35]. Quirt [36] has a similar set of data from all his testing.

2.3 Active Noise Control Applied to Windows

In the building industry it has been realised that windows are the weak link in the sound insulation of building walls [37]. This becomes the motivation for active noise control (ANC) window research. There are two basic ways to attack this problem, panel control and cavity control. Cavity control will be considered first.

2.3.1 Cavity control of double glazed windows

ANC can be applied to windows by controlling the sound pressure within the cavity of a double glazed window system. This is known as cavity control and tends to show a higher increase in STL than panel control [38-40]. Although cavity control has given the higher increases in STL, these windows tend to compromise thermal insulation [41] due to the larger inter-pane spacing required for loud speaker control sources.

2.3.1.1 Cavity size

The size of the cavity required for cavity control is usually relatively large due to the need for speakers to be fitted within it with consequences for the thermal insulation as discussed above. Jakob addresses this problem in [42] with the use of long thin speakers. These speakers allow for the glazing spacing to be reduced to 40mm, from previous spacing sizes were 84mm, 100mm, and 200mm. STL was increased by around 5 dB.

Fabio [43] looked at an active window as part of applying ANC technology to building components. Their ANC window was different in only the window sill was lined with speakers. The idea was to treat the system like a short duct which is described further in Chapter 3. This achieved increases in STL of 12 dB for general band noise.

2.3.1.2 Window material

Windows used in ANC application are not all made of glass. Jakob used acrylic [38, 44, 45] and glass [42]. There is no mention of the effect this has on the performance of the ANC windows.

2.3.2 Panel control windows

Panel controlled ANC window applications are scarce. One reason for this might be the difficulty of producing a control source out of a window without compromising window aesthetics. The more likely reason is that cavity control yields higher STL improvements [38-40].

Panel control takes a similar approach to that of an ANC duct. The primary unwanted noise is transmitted through the window; while the window is simultaneously used as a speaker control source, producing the anti-phase noise required for cancelation as discussed in Chapter 3.

2.3.2.1 Control sources

Endeavouring to preserve the aesthetics of the window leads to some innovative control source solutions. Polyvinylidene Fluoride (PVDF) film was used by Yu et al [12, 46] in conjunction with transparent carbon nano-tube based electrodes to provide a transparent control source window speaker. The technology presented by Yu has been patented [47]. While the conductivity of these electrodes is significantly less than typical electrodes, the results showed ANC insertion losses of 12-15 dB across a 200x200mm window. The window size of 200mm x200mm is a limitation as most windows are significantly larger than this. Comparison of the film speaker with a point source exposed the inability of a point source to achieve attenuation across the whole window. Therefore the distributed nature of the film speaker is probably important.

Zhu [48] used a rare earth actuator with specially designed distributed characteristics. The window size in this study was 175mm x 175mm, which is too small to be useful in practice. Insertion losses of 20 dB were observed for tonal noise and 10-15 dB for broadband noise. This study used plane wave excitation implemented through directing the noise source through a wave guide directed at the window.

2.3.3 Feedforward control versus feedback control

Feedforward control generally exhibits the best results, which is not surprising given its utilisation of prior knowledge of the incident sound. This is demonstrated in a study by Kaiser [37]. This study used two feedforward and two feedback ANC control strategies; feedback control produced an insertion loss at the mass-air-mass resonance of 13dB, this

was eclipsed by feedforward control which provided 18dB insertion loss in the same region.

Jakob [38] has also investigated both feedforward and feedback control. Jakob completed a comprehensive study of feedforward control, which found insertion losses of more than 12dB around the mass-air-mass resonance and 8dB total across 50Hz to 3150Hz third octave bands. This can be compared to Jakob's investigation of feedback control [44] where insertion losses of more than 8dB in the mass-air-mass region with a total reduction of 5dB were achieved. Both feedforward and feedback control obtained 10 dB overall insertion losses for harmonically dominant noise but other noise sources gave 7dB and 3.4dB to 6dB for feedforward and feedback, respectively. Therefore it can be seen that feedforward control appears superior based on the work of Jakob [45] and Kaiser [37].

The quality of the reference signal has a significant impact on the performance of feedforward control. In Kaiser's work [37] the reference signal was taken directly from the noise source. This would not be possible in most applications; hence feedback control may provide a more practical control method.

2.3.4 Feedforward reference signal

The reference signal required in a feedforward control system poses a challenging question ignored by most studies [37, 49] but acknowledged by Jakob [38]. All these studies use a reference signal directly from the noise source, as in Kaiser's work, which is not possible in reality. Yu [46] gives this problem more thought with a system that uses four reference microphones. These are placed 1m above, left , right and below the window. The data from these microphones is then used in an algorithm which identifies the source direction. This was used with a panel control type window. It is difficult to determine how effective this was as it was not compared to an ideal reference signal. This issue applies to all versions of feedforward control applied to windows.

2.4 Summary

The STL of glass windows has been reviewed. The key points from this review for this work are that low frequency STL performance is determined by resonant frequencies and mass. These resonant frequencies can be calculated from the properties of the glass. Damping and sealing are also critical for low frequency STL performance. Applying ANC to glass windows is attempting to improve the STL at these resonant frequencies and effectively improve the STL without adding mass to the window.

There is an absence of work on ANC windows using panel control which is the subject of this work. In contrast cavity control has been explored more comprehensively hence the performance of cavity controlled ANC window is better understood.

3 Piezoelectric PVDF Film Speakers

PVDF (polyvinylidene fluoride) film is a material that exhibits a very high piezoelectric effect. It is a transparent plastic material making it suitable for use with windows. Experimental work presented in this chapter is based on a window speaker developed by Yu [46] out of PVDF film. The aim was to improve on Yu's window speaker performance through the use of different configurations or boundary conditions, window materials and application methods. Sound pressure level (SPL) measurements were made at 50mm from the window surface which is consistent with Yu's measurement position. This enabled direct comparison between the results obtained in this work and Yu's speaker response.

3.1 Introduction

3.1.1 Piezoelectricity

'Piezoelectricity' is an effect that was discovered in 1880 by Jacques and Pierre Curie [50], where an electric field induces mechanical deformation of a material. The Curie brothers found this property present in quartz. They also found the converse effect, mechanical deformation inducing an electrical charge, a year later in 1881 [51].

Piezoelectric materials have been used in hydrophones [52], crystal oscillators, and transducers [53]. The majority of piezoelectric materials used today are ceramics although some are polymers. These polymers exhibit much larger deformations then the ceramic materials but with much lower force output.

3.1.2 PVDF film

PVDF is an example of a piezoelectric polymer which exhibits one of the largest piezoelectric effects. It was discovered in Japan by Kawai [54] in 1969. This piezoelectric material is now widely used as a transducer material, especially in smart structures employing active vibration or noise control [55-58].

PVDF is also desirable in work concerned with windows for its transparent properties. Constructing a transparent window speaker with this material is possible with the use of transparent electrodes.

3.1.3 Window speakers and panel control

Window speakers are required as control sources for panel controlled active noise control (ANC) windows. Panel control can be approached in a similar fashion to that of an ANC duct application. The duct analogy assumes that all noise is transmitted through the window. This assumption is valid since windows tend to be the weakest element in a wall in terms of sound transmission loss (STL) (see chapter 1). The analogy is illustrated in Figure 3.1 where a reference signal is picked up outside the window, and then filtered in order to produce the anti-phase noise signal which is then played through the window speaker control source. The filtering is optimised using feedback from the error microphone.

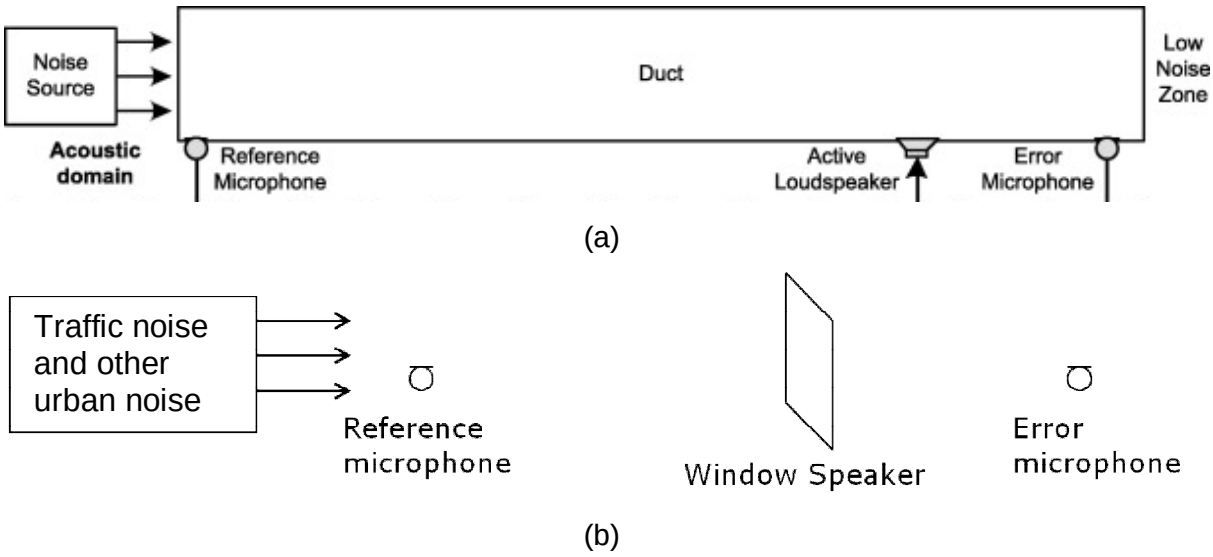

Figure 3.1 Demonstrating the parallels between (a) a duct ANC example and (b) the ANC window.

Previous panel control studies have produced mixed results. Davy [59] used PVDF film in his construction of a window speaker which attempted to move the glass window in order to produce a control source. Davy concluded that the SPL achieved was inadequate for producing the required STL.

Zhu [48] used a rare earth electromagnetic actuator in the centre of a glass panel. While 10-15 dB reductions were achieved, the aesthetics of the window were compromised.

Yu [46] measured reductions of up to 15dB on a small window (200mm x 200mm). Yu also demonstrated that PVDF film could be used with transparent electrodes so window aesthetics could be preserved.

The work presented in this chapter employs variations of Yu's window speaker [12] seeking to obtain higher sound levels in the 50-500 Hz frequency range. Yu's window speaker response is shown in Figure 3.2 with a red box indicating the frequency range of interest. The interest in this frequency range is due to the reported effects of fatigue and tiredness it induces in people [2, 3].

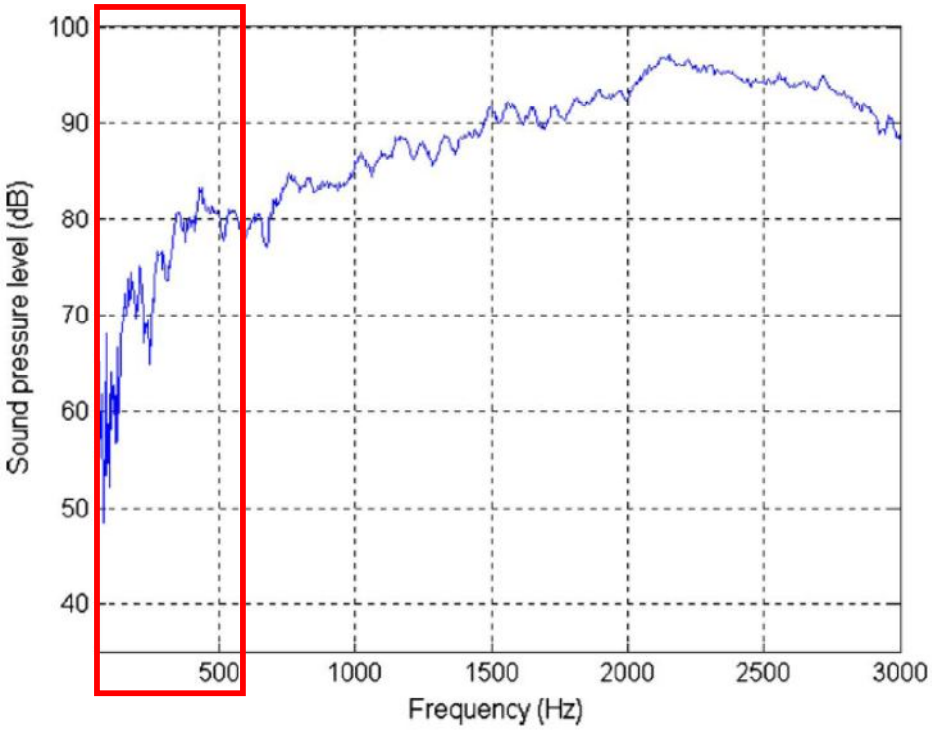

Figure 3.2 Yu's film speaker response [12] with the 50-500Hz frequency range of interest highlighted.

The testing presented in this chapter aimed to construct a viable PVDF film speaker for use in an ANC window application. The practicality of the window came into consideration when evaluating each speaker's likelihood of success in the proposed application. Transparency was initially ignored in this experimental study.

The PVDF film was available with opaque electrodes pre-attached in sizes up to 203mm by 280mm. For larger sizes, a custom order would be required.

3.2 Equipment

3.2.1 Wooden frames

Wooden frames were constructed specifically for housing the window materials. Drawings of these frames are in Appendix A.

3.2.2 Window materials

Three different window materials were used in construction of the window speakers, polycarbonate, acrylic and glass. Two different sizes were used: 300mm x 300mm sheets

were used in the initial speaker constructions and 280mm x 340mm sheets for the vacuum method speakers.

3.2.3 PVDF film

The PVDF film used in this experiment was sourced from Measurement Specialties Inc and was a 280mm x 203mm film with thickness of 28μm and silver ink electrodes.

3.2.4 Vacuum pump

A small vacuum pump was used to create and maintain an attachment of the film to the window material in the vacuum method of window speaker construction. The pump fed into a transparent container of fluid which helped evaluate the vacuum seal with bubbles representing a poor seal and the absence of bubbles indicating a good seal. This technique ensured the film was flat against the window material.

3.2.5 Copper tape

3M electro-magnetic interference (EMI) embossed copper shielding tape 1245 was used to attach leads to the electrodes. This tape was conductive through the adhesive.

3.2.6 Anechoic room

An anechoic room was used as a testing environment for the speakers. This room had a raised metal grate floor, a room volume of 64m^3.

3.2.7 B&K Pulse analyser 3560C

The B&K pulse analyser 3560C was the measurement platform with which all the measurements are conducted. Measurements were setup and controlled by a Dell laptop with Pulse software installed.

3.2.8 B&K measurement microphone

The measurement microphone was a B&K type 4189 microphone fitted with a type 2669-C preamplifier.

3.2.9 B&K type 2713 amplifier

The B&K type 2713 amplifier is a special amplifier that can drive reactive loads such as the PVDF film and was used here. It is capable of high gain but clips the output once 100Vrms is reached.

3.3 Experimental Procedure

Each window speaker was constructed and placed in the anechoic room in turn. The speaker was isolated from the metal grated floor by placing carpet between the speaker and the floor.

The B&K measurement microphone was then placed 50mm from the speaker for measurement of the SPL response. The Pulse analyser was then used for recording of the microphone signal and for subsequent processing. Fast Fourier transform (FFT) analysis was performed in real time on measurements. The FFT analysis used a Hanning window with 67% overlap of each window of data. Pressure squared measurements were repeated 3 times and averaged before conversion to SPL.

The B&K analyser also produced the excitation signal for the PVDF film speakers. The excitation signal was an infinitely repeating swept sine from 50-600Hz, sweeping at a rate of 50Hz/s. This excitation signal was amplified to 100 Vrms (141 Vpeak) with the type 2713 amplifier before being fed to the PVDF film.

3.4 Window Constructions and Results

PVDF film was used in a progression of window speakers constructions, some involving window materials and others not. These window speaker constructions are described before presenting the corresponding set of results. Explanations for each construction are provided and developed. The initial window speaker construction was the tape attached window speaker construction.

3.4.1 Tape attached window speaker construction

This construction used 300mm square sheets of window material inserted into the wooden frames and pressure sensitive tape to attach of the PVDF film to the window material. Separate wooden frames were constructed to house 2mm, 4mm and 6mm thick window material. Wire leads were required to be attached to the film before the window

material was tested. These wire leads were attached by copper tape which allowed conduction through the adhesive. The wire leads were soldered to lengths of copper tape before attachment to the film. The lengths were then attached to the film and run off the top left corner, as shown in Figure 3.3. This avoided bulky solder connections which could affect the seal of the film to the window material. Insulation tape was used to insulate the copper tape to safeguard against short circuiting the film. The PVDF film was applied to the window material and fixed only around the perimeter with strong pressure sensitive tape. A fully constructed PVDF film speaker is shown in Figure 3.3.

Figure 3.3 Fully constructed PVDF film speaker

A small pocket of air between the film and the window material was intended to provide a baffle effect similar to that of a speaker box, as in Yu's film speaker patent [47].

The SPL achieved from this window speaker construction was lower than that presented by Yu. Figure 3.4 shows the SPL results; (a) for a 6mm glass window material, (b) for a 2mm acrylic window material and (c) shows Yu's window speaker response. These were the best performing thicknesses for the respective window materials. For a complete set of results see appendix B. The average SPL outputs over the frequency range of interest were 25dB and 35dB for the 6mm glass and the 2mm acrylic respectively. These SPL outputs are significantly lower than the 60db to 80 dB achieved by Yu's window speaker response in the frequency range of interest.

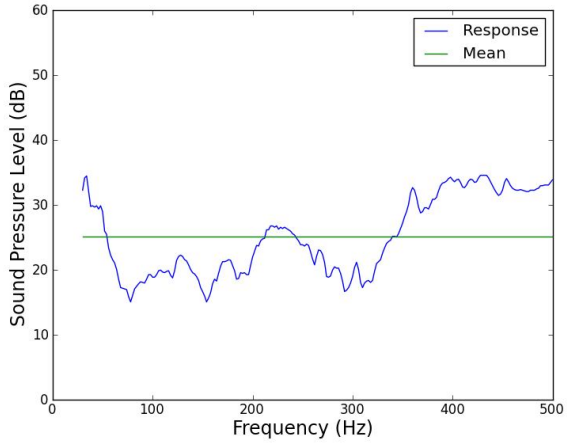

(a)

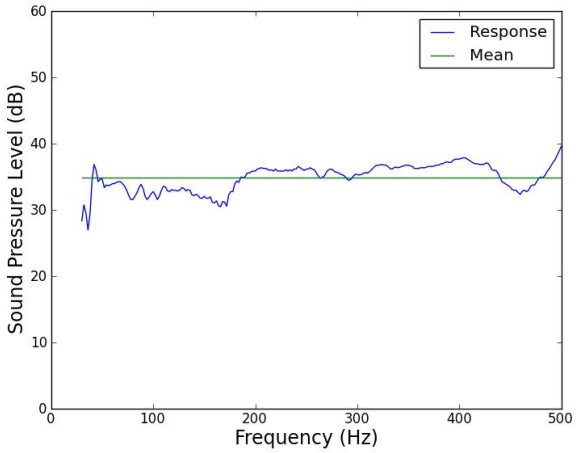

(b)

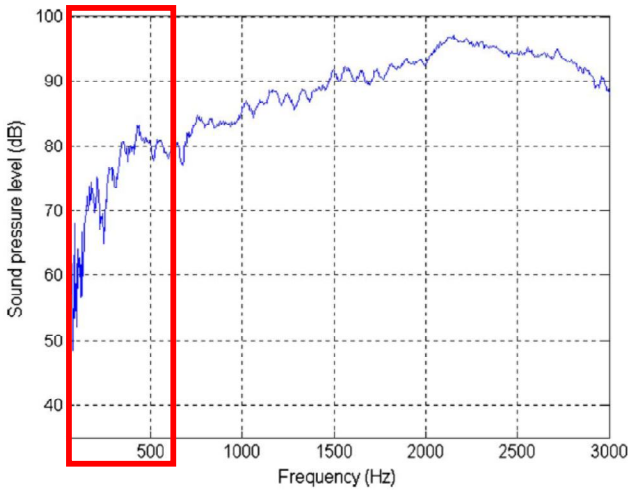

(c)

Figure 3.4 (a) 2mm acrylic SPL frequency response and mean (b) 6mm glass SPL frequency response and mean (c) Yu's window speaker response

The air pocket between the film and the window material was a design detail taken from [47] which has shown little effect in increasing the SPL output. The acrylic window material produced larger SPL outputs than the glass window material of the same thickness in all cases (see appendix B). It was observed that materials with less stiffness allowed production of higher SPL . This is probably due to the greater ability of the film to induce movement in the window material. Subsequent tests therefore attempted to achieve completely flat and taut film application in order to amplify this bending effect.

The next three window constructions were all aimed at inducing movement in the window material to increase the SPL output of the window speaker. These window constructions in order of discussion were:

- Vacuum window speaker construction
- Film window speaker construction
- Glue-attachment window construction

3.4.2 Vacuum window speaker construction

The vacuum window speaker construction was used to ensure the film was applied in completely flat manner to the window material. This was achieved by using a 0.2mm thick sheet of polyvinylchloride (PVC) and sealing this with silicon over the entire film. A pump was then used to remove air forcing the PVC and PVDF film flat against the window material.

The constructions method is illustrated in Figure 3.5 and described as follows:

1 A 280mm x 340mm sheet of window material was cut.

2 A 10mm hole was drilled in the top right corner of the material.

3 The PVDF film was placed with leads running off the material close to the 10mm hole.

4 A silicon perimeter was applied around the film and the PVC sheet was then placed over the top.

5 A vacuum pump was attached to the 10mm hole and the pump switched on. This ensured the PVC and film were flat against the window material.

G-clamps were used to fix two wooden frames in place, one either side of the film. These frames were 200mm x 280mm with frame thickness 15mm. This completes the speaker construction. A completed window speaker is shown in Figure 3.6.

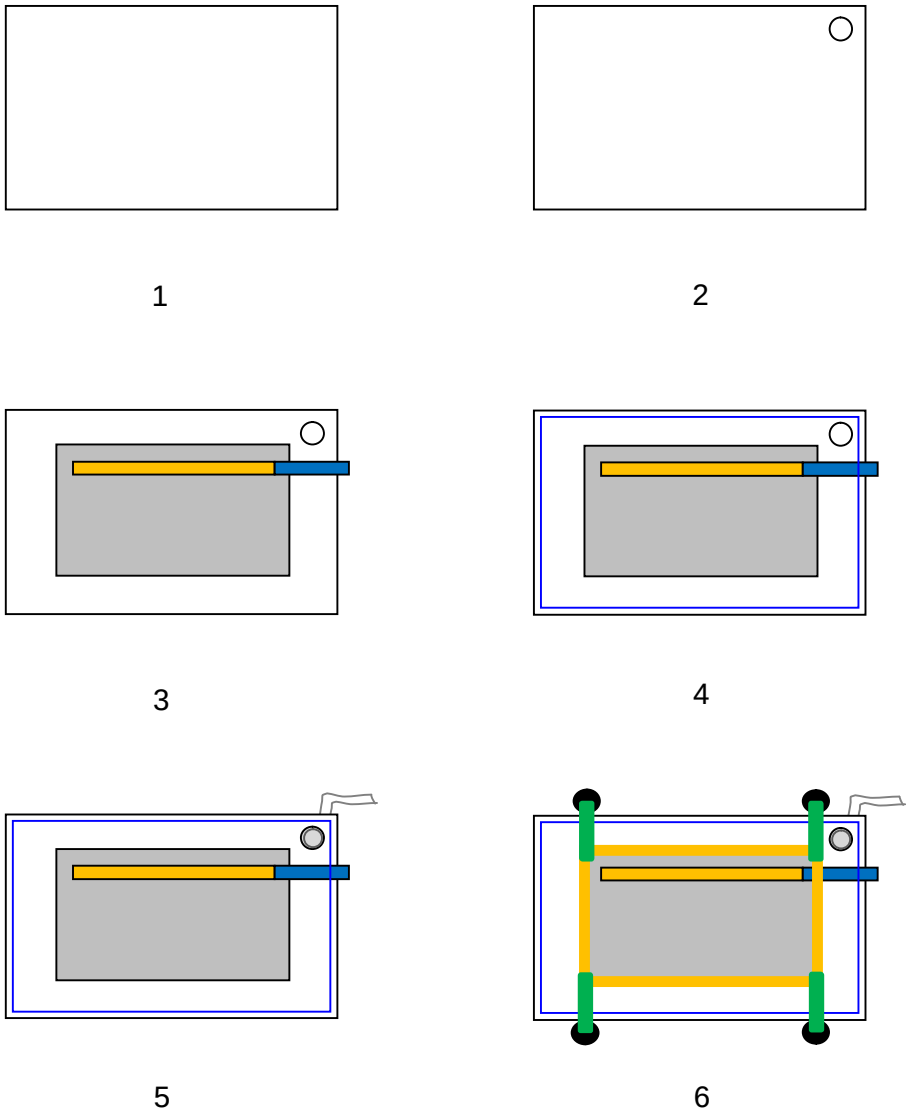

Figure 3.5 Steps In constructing a window speaker using the vacuum method

Figure 3.6 A completed window speaker using the vacuum construction method.

Results for two thicknesses of glass sheet are displayed in Figure 3.7. The glass window materials yielded a relatively high SPL above 300Hz than that below 300Hz. The frequency range of interest is 50Hz to 500Hz and more than half of this range exhibited relatively low SPL. For this reason this speaker construction using a glass window material is unlikely to make a successful ANC application.

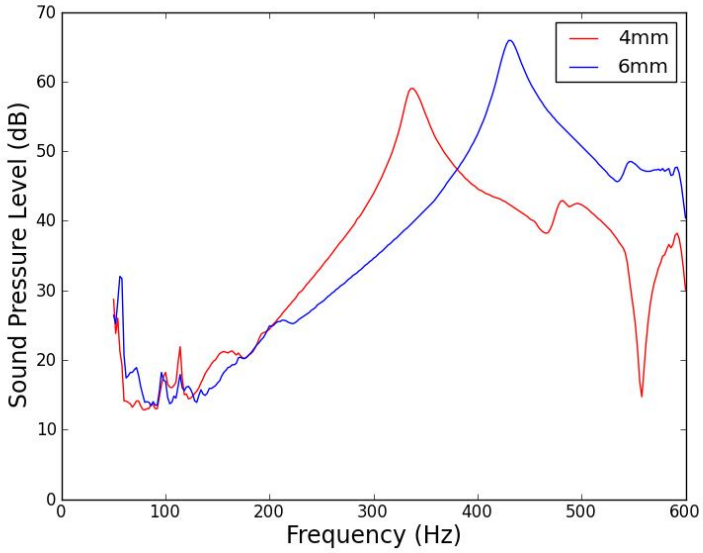

Figure 3.7 SPL frequency response from the vacuum window speakers using 4mm and 6mm glass.

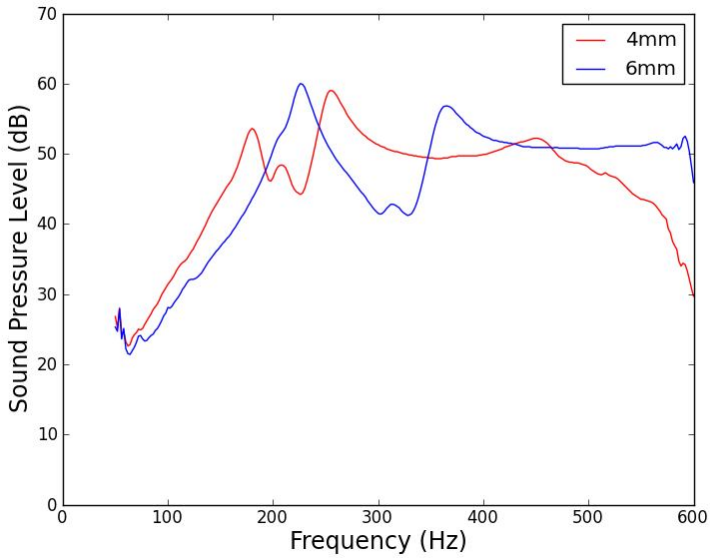

Figure 3.8 SPL frequency response for the vacuum window speakers using 4mm and 6mm acrylic.

Figure 3.8 shows the results for 4mm and 6mm acrylic window materials. The results are similar to the glass results in Figure 3.7 except the SPL output is higher above 150Hz. While acrylic exhibits improved performance over glass it would not be suitable for an ANC window application for the same reason as the glass, it performs relatively poorly for a portion of the frequency range of interest.

In both Figure 3.7 and Figure 3.8 it can be seen that the thinner window materials produce increased SPL over the thicker window materials. 2mm window materials were then used as the window materials on subsequent window speaker constructions. The use of only acrylic and polycarbonate was due to the earlier conclusion which stated that the stiffer a material the poorer its performance. This ruled out the testing of glass.

Figure 3.9 presents the responses obtained with 2mm acrylic and polycarbonate. These SPL responses are much flatter with an average output of about 40 dB. It is noted that the polycarbonate window has a substantial dip in response at 300Hz. Ignoring this dip both of these speakers could be of use in an ANC system.

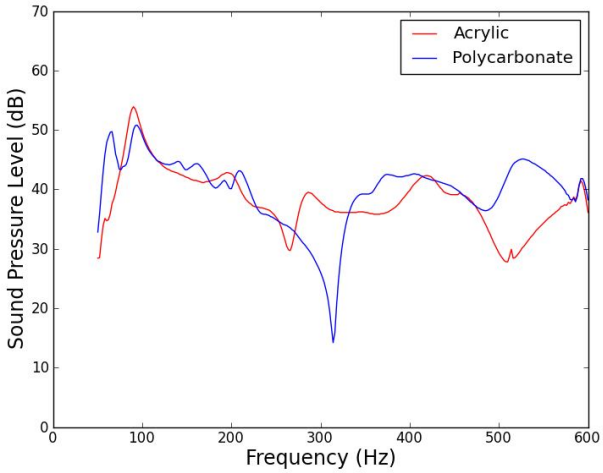

Figure 3.9 2mm acrylic and polycarbonate window material SPL responses for the vacuum window speaker construction.

Due to the relative success with the thinner materials, 1mm polycarbonate was used with the expectation of additional improvement. Figure 3.10 shows the result for 1mm polycarbonate compared with the 2mm polycarbonate. The responses are similar except for the enlarged dip in response now at around 180Hz. Therefore the 1mm polycarbonate would provide a good control source although it would struggle to be effective around 180Hz, due to its inadequate SPL output at this frequency.

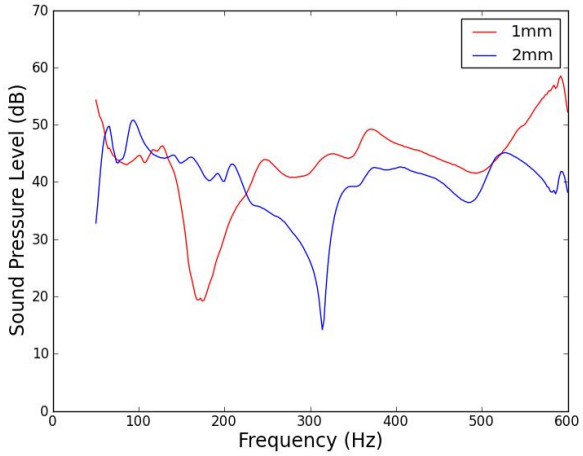

Figure 3.10 1mm and 2mm polycarbonate window material SPL responses for the vacuum window speaker construction.

3.4.3 Film window speaker construction

This window speaker variation consisted of just the film itself clamped between the wooden frames with G-clamps, no window material was used. Tautness was ensured by taping two edges of the film to the bottom frame and pulling the film tight before clamping. Figure 3.11 below shows a constructed film window speaker.

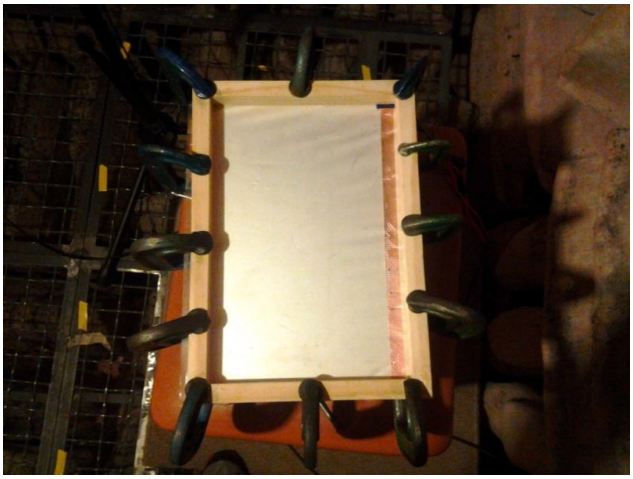

Figure 3.11 Film window speaker.

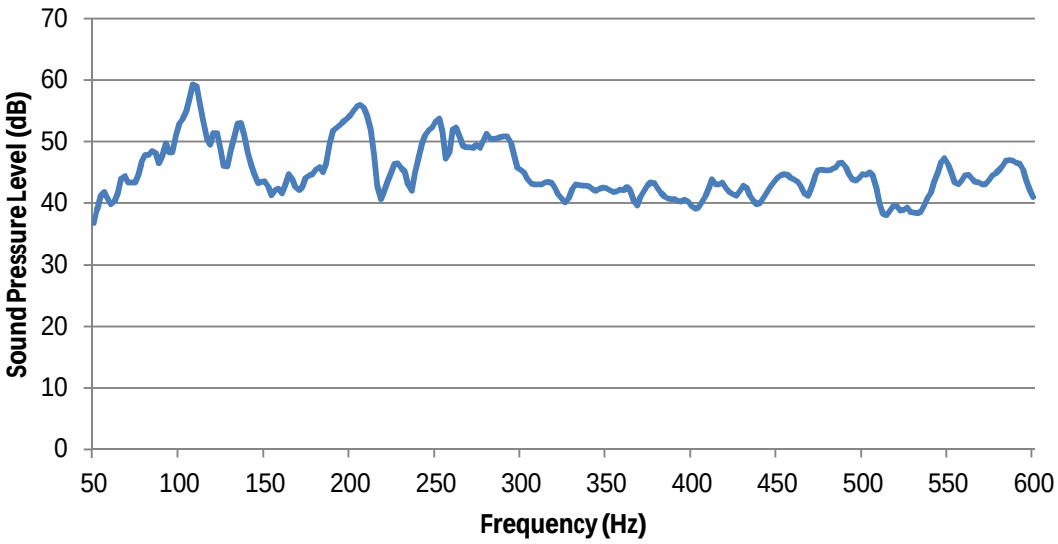

Figure 3.12 SPL output of the film speaker at 50mm.

The film by itself produced the most consistent results to date, see Figure 3.12. The SPL is above 40dB throughout the majority of the measured frequency range. Higher SPL is observed in the 50-300Hz frequency range. In this range nearly 60dB is reached just

above 100 Hz. This is an encouraging result and is thus far the most suitable speaker tested, for use in an ANC window application.

3.4.4 Glue attached window construction

The glued film speaker was identical to the tape attachment window speaker except that the film was attached with glue instead of pressure sensitive tape. The same 300mm square 2mm acrylic sheet was used for this speaker. The film was glued in place before the acrylic material was inserted into the frame. This made film application easier. The 2mm acrylic was the only window material tested as it performed best in the earlier tests and resources were limited. A constructed glue attached window speaker is below in Figure 3.13.

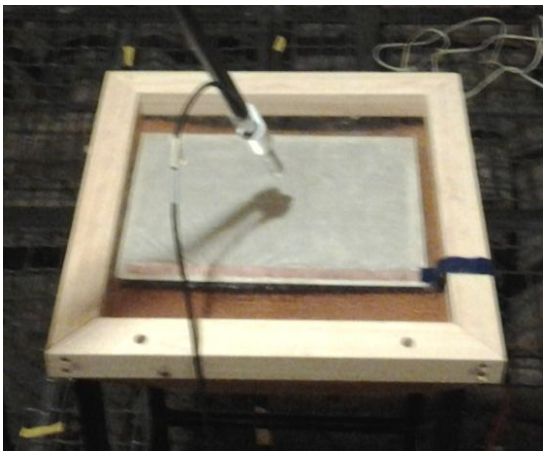

Figure 3.13 Glued film speaker in test situation, glued to 2mm acrylic.

The SPL response of the glued film speaker is shown in Figure 3.14. The response is consistently 40dB except for one dip around 220Hz. This dip would make ANC difficult around 220Hz. Apart from this limitation; this speaker would be suitable for ANC window applications.

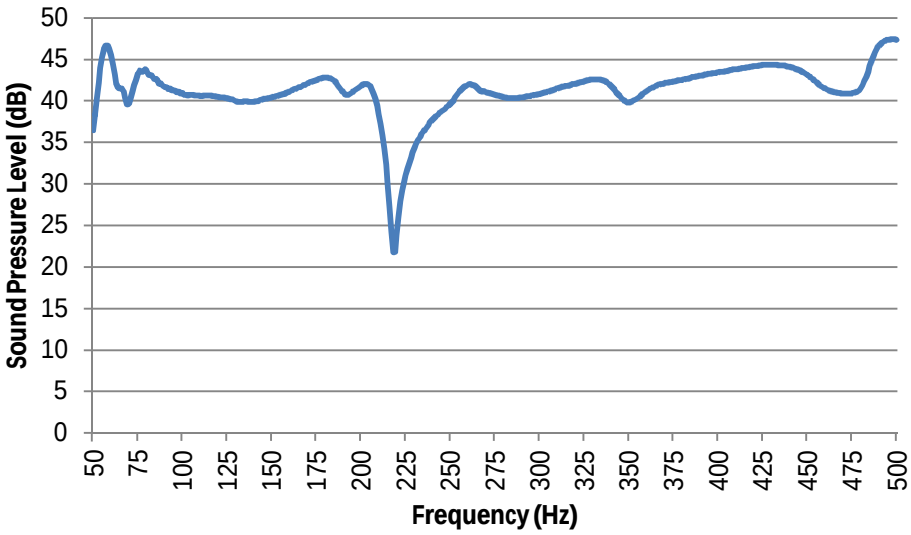

Figure 3.14 Response of the 2mm acrylic speaker with glued film application.

All window speaker constructions presented thus far failed to produce SPL equal to that presented by Yu.

The next speaker construction ignores ANC window practicality and is focused on achieving the highest SPL output from the PVDF film. Bowed film speakers were tested as it was anticipated that the bowing of the film would increase the displacement of the film and therefore increase the SPL output.

3.4.5 Bowed film speakers

The bowed film speaker construction was tested to determine what is possible with PVDF film and compare with the other constructions. Due to the bowed nature of this construction, it is not a practical solution. This is because even a bowed transparent film will distort the window aesthetics through significant diffraction. The construction method is illustrated in Figure 3.15 below.

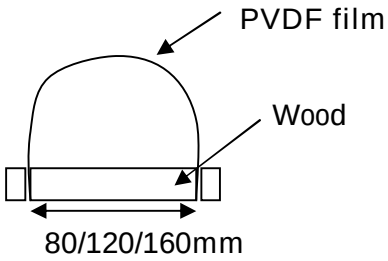

Figure 3.15 An end view of a bowed film speaker construction

The bowed film speaker construction used three pieces of wood all 280mm long. The outside pieces were 20mm wide and used to clamp the film up against the middle piece of wood with a G-clamp. The middle piece of wood was varied in width to vary the extent of bowing in the film (shown in Figure 3.16) and determine the most effective arrangement. The widths used were 160mm, 120mm and 80mm. The 160mm bowed film speaker is in Figure 3.17.

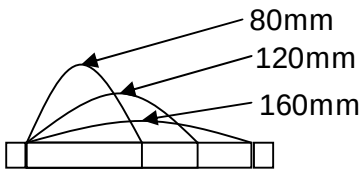

Figure 3.16 Demonstration of bowing variation.

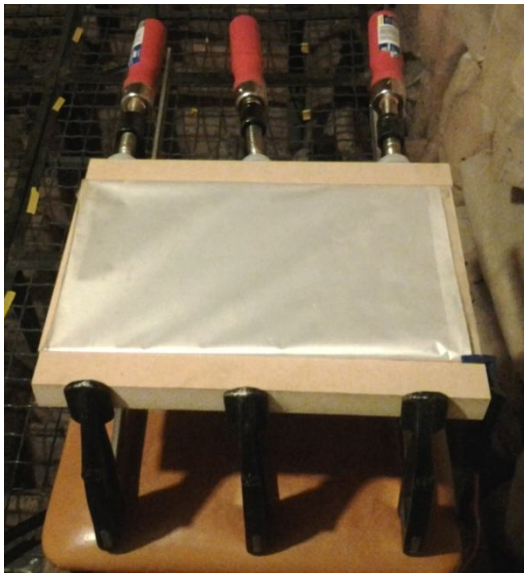

Figure 3.17 160mm bowed film speaker

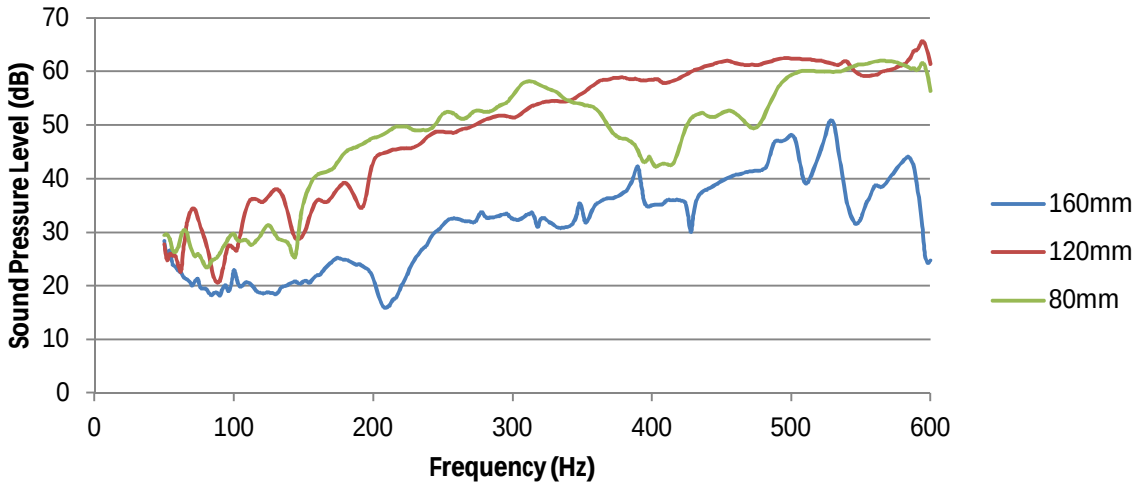

Figure 3.18 Bowed film speaker SPL responses for 160mm, 120mm and 80mm.

Results for the bowed film speakers are shown in Figure 3.18. The best performance was with the 120mm bowed film which exhibited a smoothly increasing SPL response with frequency, reaching around 60 dB in the 400Hz to 600Hz frequency range. The 80mm bowed film speaker was expected to perform best due to its potential for the largest film displacement. This was not the case due to a wide dip in its response in the 300Hz to 500Hz range. The 80mm speaker still exhibited comparable SPL to the 120mm speaker. The 160mm bowed film speaker was the speaker with the least amount of bowing and expectedly performed worst. While for frequencies below 200Hz other speakers tested have shown larger SPL, the results of the 80mm and 120mm are the largest SPL responses observed.

It was observed that the 80mm bowed film speaker struggled to support its own weight; therefore a nicely curved shape was not achieved. This may account for the dip in response observed in Figure 3.18. A wire cage was then used to support and shape the 80mm bowed film speaker. It was anticipated that this would improve the 80mm bowed speaker response. The supported and unsupported 80mm bowed film speakers are shown in Figure 3.19.

(a) (b)

Figure 3.19 Photos of the 80mm with (a) and without (b) a wire support cage inserted under film.

In Figure 3.20 the responses for the 80mm bowed film speaker with and without wire support is displayed. It can be seen that the wire support did not improve the response of the unsupported bowed film speaker. The same test was conducted on the 120mm bowed film speaker but not the 160mm bowed film speaker as the wire support was unable to fit underneath it Figure 3.21 exhibits the comparison of the 120mm bowed film speaker with and without the wire support. The responses are similar although there is an apparent improvement in performance for the supported response over the unsupported at frequencies up to 200Hz. This is offset a little by degradation in the response at higher frequencies. Overall the 120mm supported bowed film speaker provided improved SPL output.

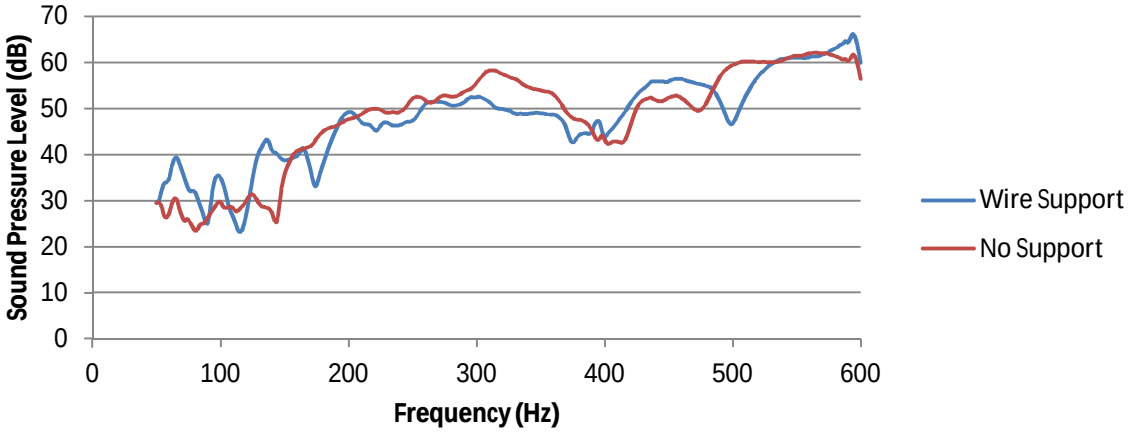

Figure 3.20 Responses for 80mm bowed film speaker with and without wire cage support.

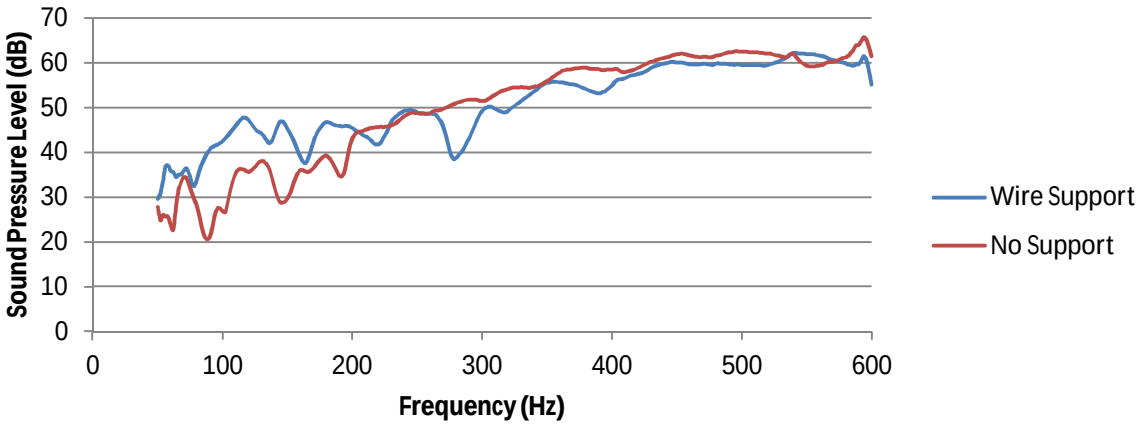

Figure 3.21 Responses for 120mm bowed film speaker with and without wire cage support.

The comparison of the 80mm and the 120mm supported bowed film speakers are shown in Figure 3.22. These responses are more similar then the 80mm and 120mm unsupported cases. These responses are less smooth then the initial unsupported responses. The 120mm performs best over the majority of the frequency range tested.

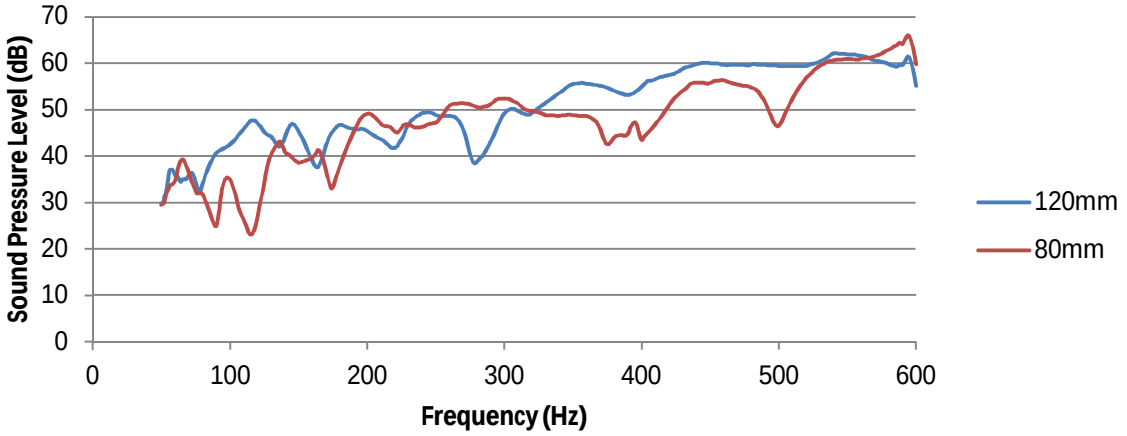

Figure 3.22 Responses for 80mm and 120mm bowed film speakers which use a wire cage for support.

Overall the bowed film tests yielded higher SPL output than the flat film speakers excluding the 160mm bowed film speaker. An exception to this would be that the flat film speakers tested generally performed better for frequencies up to 200Hz. The bowed film speakers did not reach an SPL over 40 dB until 200Hz. Although below 200Hz the bowed film speakers did not perform as poorly as the tape attached window speaker

construction. The best response was provided by the 120mm bowed film speaker. This response was not as smooth as the unsupported speaker but exhibited much improved performance in frequencies up to 200Hz. While the 120mm wire supported bowed film speaker performed best of all the speakers tested in this work it falls about 20 dB short of the 60dB to 80dB presented by Yu (see Figure 3.2).

3.5 Summary

A total of five different methods of constructing speakers out of PVDF film were evaluated. The methods that provided the highest SPL results were:

- Bowed film speaker
- Film window speaker
- Vacuum window speaker

Of the high performing window speakers, the film window speaker is considered the most suitable for an ANC window application. The film window speaker exhibited the highest SPL response of 40 dB over the 50 Hz to 500 Hz range with higher SPL achieved at frequencies up to 300Hz. This speaker was chosen over the bowed film speaker due to its practical advantages.

The bowed film speakers produced the highest SPL response with the 120mm wire supported bowed film speaker. The impracticality of the bowed film construction ruled it out of use in an ANC application despite the relatively high SPL obtained.

From the construction methods tested that involved the use of a window material it was observed that window materials with lower stiffness achieved higher SPL output. This principle also extended to these materials when thickness was reduced (a reduction in thickness corresponds to a reduction in stiffness). The extreme case of this is no material; this explains the relative success of the film only speaker over the other constructions that used window materials.

All speaker configurations tried in this work did not perform as well as the window speaker presented by Yu. The test environment details for Yu's film speaker results are unclear from his paper. This work used an anechoic testing environment to determine the absolute SPL produced so that the results are not coloured by any room acoustics. This colouring would typically increase the measured SPL due to acoustic reflections

which are not present in anechoic environments. Therefore Yu's film speaker could have been advantaged by its testing environment.

All window speakers constructed in this chapter were relatively small in size. The largest window constructed in this work was the 300mm by 300mm square window. This is significantly smaller than most typical windows. This work was limited by the maximum size of the PVDF film size (203mm by 280mm). Future work might investigate larger window speaker creations using a small film, multiple small films, or larger sized films.

An ANC application with the film window speaker construction could also be developed. As the film window speaker has no window material associated with its construction, it would need to be added to a single or double glazed window in some way. Therefore using this speaker in a double glazed window situation could be useful as the sound insulation of the double glazed window would be relatively high therefore the speaker would not need to provide a high SPL control signal in order to control noise

4 Testing of Active Noise Control Windows

This chapter describes an experimental investigation of the attenuations possible through windows using active noise control (ANC). Tests were performed using three different ANC configurations of control sources and error microphones and two different test situations, one in using a reverberant receiving room, and the other using an anechoic receiving room. Three different types of disturbance noise were used: tonal, third octave band and broadband noise. The attenuations were measured using total sound energy reductions of the receiving room. These energy reductions allowed evaluation of each ANC system.

4.1 Introduction

ANC employing panel control has rarely been tested. This is likely due to the greater success of cavity control [38-40]. The work here uses panel control rather than cavity control so that the thermal insulation window properties are not affected. Windows using panel control in the literature have been smaller than typical size windows [12, 46, 48] with Davy's window being the largest at 304mm x 304mm [59]. This work investigates larger, more commonly used size windows.

All windows have natural or modal frequencies at which they vibrate more easily than at others. For smaller windows these frequencies are much higher than for larger windows. Smaller windows can therefore neglect these modes for low frequencies and effectively produce a piston type window speaker as the ANC control source. Modal frequencies must be considered when using a larger window due to the lower frequency at which they occur. Therefore in this study modal frequencies and their respective vibration patterns are considered when positioning the ANC control sources.

Trevathan [60] looked at sound transmission loss (STL) of gypsum panels and found that the fundamental mode makes the greatest contribution to the panel's overall transmission loss. This was discovered by the comparison of a complete STL model to a STL models which only considered an individual mode. It is clearly imperative that the fundamental mode of a panel be controlled in this work. It is known that the ideal location for controlling the fundamental mode is the centre of the panel which corresponds to the anti-node of the fundamental mode. For windows, using the centre of the panel is not desirable as this would impair the view through it. The testing in this chapter attempts to invoke control of the fundamental mode via multiple control sources around the perimeter of the window. These locations provide options for hiding these actuators in order to preserve the window aesthetics.

4.2 Aims

The primary objective of this testing was to prove whether active control of window noise transmission provides significant improvement of sound transmission loss (STL) for tonal and band noise sources. Other objectives were to:

- Determine whether piezoelectric stack actuators will provide sufficient force and displacement to achieve control
- Determine what frequencies can be controlled
- Characterise whether the noise reductions achieved are global or local reductions
- Ensure that a window can be used effectively as a control source with aesthetically non invasive actuation.

4.3 Theory

Consequently the theory of the control system is similar to that for an ANC employed in a duct (see section 3.1.3). Thus if a large sound pressure level (SPL) is generated from the window speaker, this will result in greater noise control.

There are difficulties with creating a piston type speaker out of a window with point sources around the edges. Since the window will vibrate in different mode shapes at different frequencies this made positioning the control sources a difficult but important task. Some consideration of modes and their respective mode shapes was made before choosing control source locations.

4.3.1 Plate vibration

The windows used in this work have a thickness to width ratio of 0.004 to 0.005 which is less than the typical 0.1 required for plate theory to hold [61]. The plate vibration theory of interest is the modal frequencies at which the plate vibrates with most ease. These frequencies are where sound transmission is optimised. Therefore control of these modal frequencies is critical.

Modal frequencies of a plate can be calculated as per Equation 4.1.

$$\omega_{mn} = \sqrt{\frac{D}{\rho_p h}}\left(\left(\frac{m\pi}{a}\right)^2 + \left(\frac{n\pi}{b}\right)^2\right) \qquad \text{Equation 4.1}$$

Where:

$$D = \frac{Eh^3}{12(1-\nu^2)}$$

Each natural frequency has a corresponding mode shape; two examples of mode shapes are shown below in Figure 4.1.

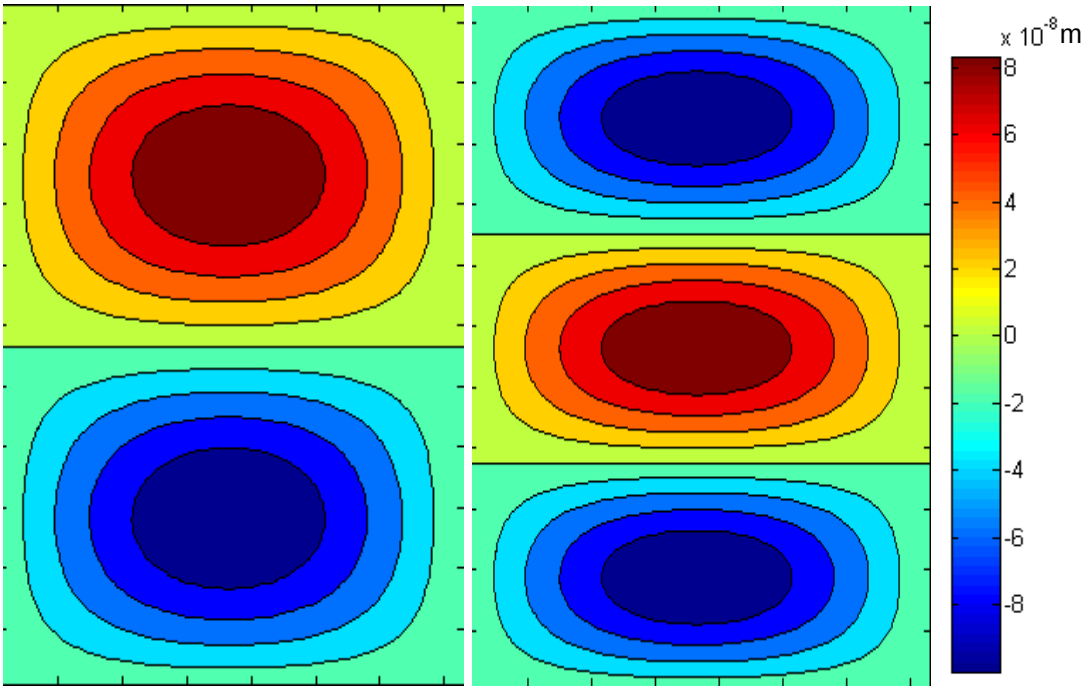

Figure 4.1 Example mode shapes for modes (1,2) (left) and (1,3) (right).

Control sources will ideally be placed at or near antinodes for the best control of a particular mode. To achieve broader cancellation, control sources must be placed such that they are located at anti-node locations for as many modes as possible.

4.3.2 Control source placement

Before the actuators were placed, consideration was given to actuator locations which need:

1. To preserve the aesthetics of a window.
2. To control as many modes as possible.

The actuators were placed as shown in Figure 4.2.

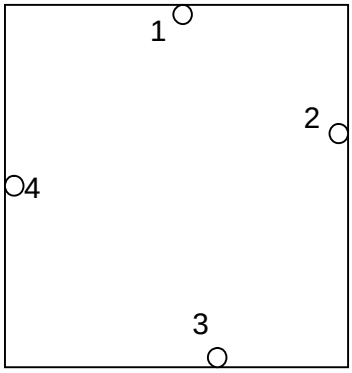

Figure 4.2 Control source locations for the ANC box test.

The control sources were placed 40mm from the edge of the glass. These varied locations along each edge of the window enabled control of multiple modes; whilst keeping the control sources relatively central, along each edge, attempted to control the fundamental mode.

4.4 Equipment

4.4.1 ANC box

Figure 4.3 ANC box test setup.

The ANC box is displayed in the Figure 4.3. It is a box constructed from 19mm MDF, reinforced with 90mm x 45mm supports, with internal dimensions are 2.4m x 1.9m x 1.5m and a 1.2m^2 opening where the window was installed [62].

4.4.2 Anechoic room

The anechoic room has a volume of 64m^3. A transmission loss rig was built into the doorway (Figure 4.4). The top section holds the window and the bottom section has a removable wall to enable access into the anechoic room.

Figure 4.4 Transmission loss rig built for anechoic room doorway

4.4.3 ANC control system

The ANC platform used was developed by Aiotec who hold the intellectual property. It can be configured to any multiple input multiple output (MIMO) system desired.

- Four input-two output,
- four input-four output,
- and eight input-four output

MIMO configurations were used. The adaptive filters can be adjusted in length. In this work the filter lengths used were either 1024 taps or 2048 taps depending on available ANC system resources.

4.4.4 Error microphones

The microphones used by the EZANC III are ECM-F8 SONY electret condenser microphones. These were modified to take phantom power from the ANC control system rather than using batteries.

4.4.5 Actuators and amplifiers

4.4.5.1 Electromagnetic shakers

Figure 4.5 Electromagnetic shaker

Figure 4.5 shows a moving magnet non-comm DC voice coil linear actuator (NCM08-17-050-2LB) of which 4 were used in the ANC box tests.

4.4.5.2 Shaker amplifiers

Two Digitech 2 x 100Wrms stereo amplifiers were to amplify the signal applied to the shakers.

4.4.5.3 Piezoelectric stack actuators

The P-010.20P Physik Instrumente (PI) PICA Power actuator was used. This is a piezoelectric stack actuator (PSA) and is used as it is small and would be easily concealed within a window frame.

4.4.5.4 Piezoelectric amplifier

The piezoelectric amplifier used to drive the above actuators was a Piezomaster VP7206-24Y805 (Figure 4.6). One was required for each PSA.

Figure 4.6 Piezoelectric actuator amplifier.

4.4.6 Measurement equipment

The following equipment was all Bruel & Kjaer (B&K) equipment.

4.4.6.1 Pulse analyser 3560C

The pulse analyser 3560C is a measurement platform in which all the measurements are conducted through. It is controlled and setup by a Dell laptop with Pulse software installed. The system performs real time fast fourier transform (FFT) analysis on the microphone inputs.

4.4.6.2 Measurement microphones

Microphones used for measurement are 4189 type microphones. They were all fitted with a 2669-C type preamplifier. At most 5 of these microphones were used at any one time during testing.

4.4.7 Sound source

This powered speaker was used as the noise source.

4.5 Experimental Procedures

This section describes the two experimental setups and the testing procedures used to perform these tests. Before these are described an outline of the tests conducted is presented below.

- ANC box tests
  - (1) A 4 error microphone, 4 control source (4x4) ANC control system was tested using tonal frequencies between 60Hz and 1000Hz in 20Hz increments. The overall sound energy reduction was calculated from the error microphone data.
  - (2) A 4x4 ANC control system was tested using tonal frequencies between 60Hz and 500Hz in 20Hz increments.
  - (3) An 8x4 ANC control system was tested as described in (2).
- Anechoic room tests
  - (1) A 4x2 ANC control system was tested as described in ANC box test (2).
  - (2) A 4x2 ANC control system was tested using one-third octave band white noise from centre frequencies 63Hz to 500Hz and 50-850Hz broadband white noise.
  - (3) An 8x4 ANC control system was tested as in anechoic room test (2) with an additional 50-250Hz broadband white noise test.

The overall sound energy reduction calculated from the measurement microphones is used for ANC box test 2 through to anechoic room test 6.

4.5.1 ANC box tests

4.5.1.1 Setup

Figure 4.3 in section 4.4.1 shows the experimental setup of the ANC box tests. The actuators are positions as described in section 4.3.2. The powered speaker was positioned outside the box, 1m from the window as shown in Figure 4.3.

(a) (b)

Figure 4.7 Error microphone locations within the ANC box for (a) 4 error microphones and (b) 8 error microphones.

Figure 4.7 shows the ANC system error microphone positions used for (a) the 4x4 ANC control system and (b) 8x4 ANC control system. Five measurement microphones were evenly distributed throughout the inside of the ANC box. Symmetry between locations was avoided in order to obtain an accurate indication of the total sound energy within the room.

4.5.1.2 ANC setup

Before measurements can be made the ANC control system needs to be configured and trained. The ANC control system is configured to the specific MIMO control system being tested. Then each cancellation path, one for each control source, is trained for 30 seconds so that the ANC control system can perform optimally.

4.5.1.3 Procedure

Each test used the following procedures:

- The desired excitation signal was initiated.
- Once a stable response was found, Pulse was used to record the squared pressure frequency response for each measurement microphones.
- The ANC control system was then enabled.
- Then wait for a stable response and record the squared pressure frequency response from Pulse.

These procedures produce two SPL frequency responses, ANC off and ANC on, for each measurement microphone within the room. These are used to calculate the reduction in sound energy due to ANC.

Sound energy was calculated from the sum of squared pressure measurements from each measurement microphone as shown in Equation 4.2.

$$\Psi = \frac{\sum_{n=1}^{n=N} p_n{}^2}{N\rho c} \qquad \text{Equation 4.2}$$

The sound energy reduction due to ANC is then calculated using Equation 4.3 given that the both the ANC on and off sound energy values have been calculated.

$$\Psi_R = 10log_{10}\left(\frac{\Psi_{ANC\ off}}{\Psi_{ANC\ on}}\right) \qquad \text{Equation 4.3}$$

Energy reductions were presented for each tonal frequency test in a bar graph with a total energy reduction calculation. This total energy reduction is calculated by summing all frequency and microphone pressure squared values of the ANC off and ANC on cases individually and then using Equation 4.3.

4.5.2 Anechoic room ANC tests

4.5.2.1 Setup

The window used in the anechoic room tests fits within a 0.8m x 1.2 m opening in the transmission loss rig shown in Figure 4.8. The error microphones locations for (a) the 4x2 and (b) the 8x4 ANC control systems are shown in Figure 4.9. All error microphones were attached to the doorway frame 400mm from the glass on the receiving room side.

(a) (b)

Figure 4.8 Anechoic room experimental setup for both (a) the 4x2 ANC system and (b) the 8x4 ANC system.

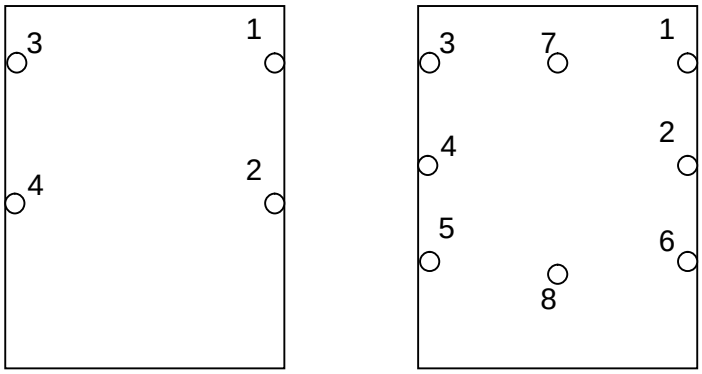

(a) (b)

Figure 4.9 Error microphone locations for the (a) 4x2 and (b) 8x4 ANC control systems.

Five measurement microphones were positioned as illustrated in Figure 4.10. Microphones 4 and 5 were at error microphone locations 1 and 4 respectively while the remaining measurement microphones were placed 800mm from the glass on the receiving room side.

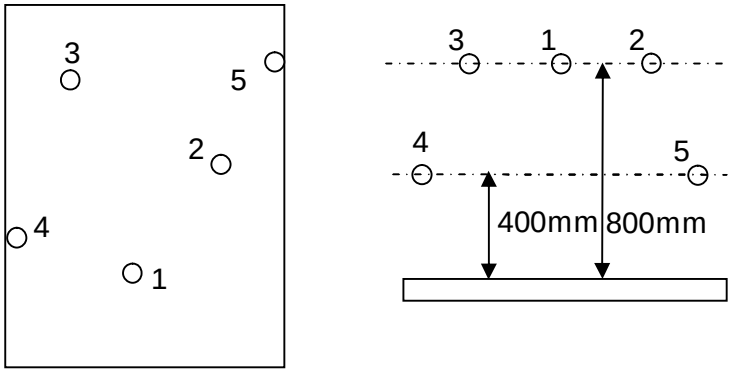

Figure 4.10 Measurement microphone locations (a) from an end view and (b) a plan view.

Actuators were positioned as per the actuator placement section 4.3.2. These positions were similar to that used in the ANC box tests and shown in Figure 4.8 for both test cases. PSA's were used for all anechoic room tests performed. These were mounted using 6mm thick L brackets with a bolt and nut arrangement as in Figure 4.11 pressing the actuator hard up against the window.

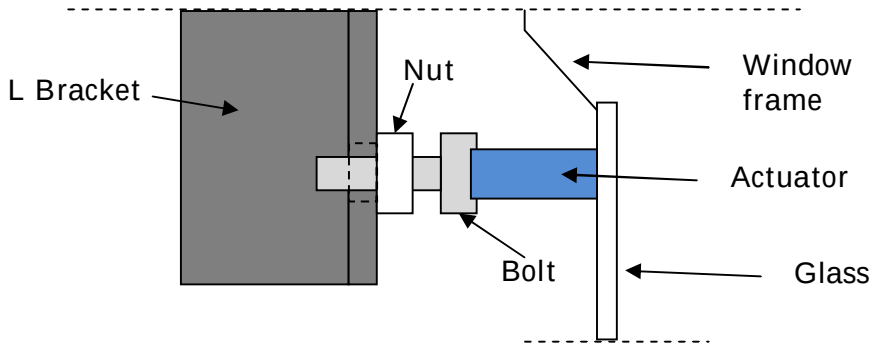

Figure 4.11 Diagram of PSA mounting.

4.5.2.2 ANC setup

The ANC system was configured as desired per section 5.1.2 for the ANC box tests.

4.5.2.3 Procedure

The experimental procedure was the same as described in section 4.5.1.3 for the ANC box tests for the tonal frequency tests.

The anechoic room tests included one-third octave band white noise and broadband white noise excitation. The data from tests using this excitation mainly was presented in one-third octave bands. Some narrowband SPL data is shown to illustrate points.

4.6 Results and Discussion

4.6.1 ANC box and 4x4 ANC control system results

The first test did not use separate measurement microphones. The data was therefore not recorded by Pulse but recorded manually off a spectrum analyser output of each error microphone. The results for the 4x4 ANC control system are shown in Figure 4.12.

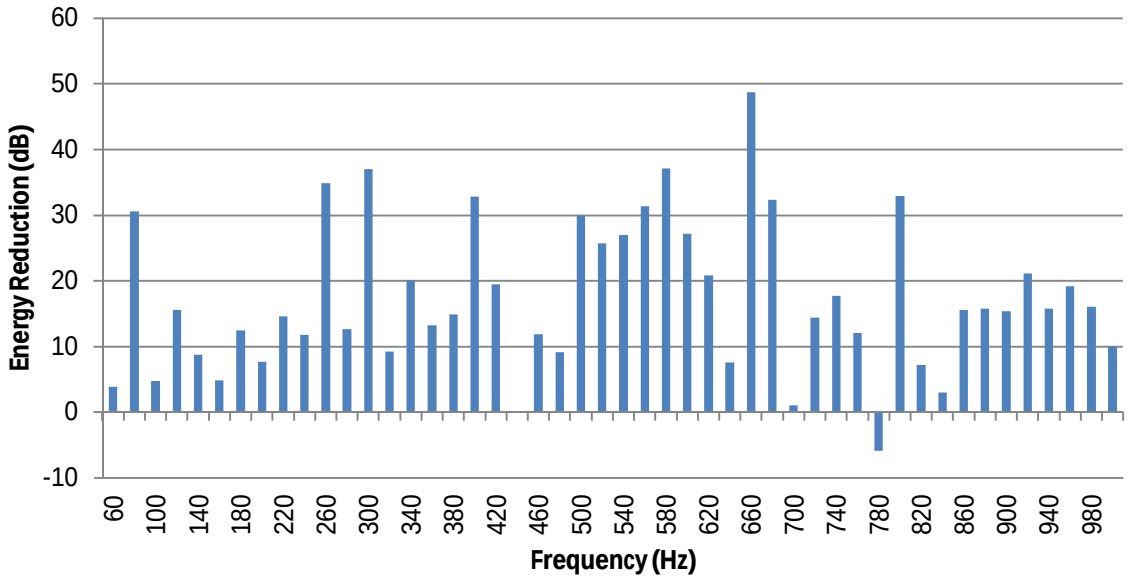

Figure 4.12 Sound energy reduction at the error microphones due to ANC

No measurement was taken at 440Hz as no steady state was achieved for the 'ANC on' case. It was observed that usually one microphone would limit the success of the overall system. The poor attenuation at a particular microphone quite often caused other microphones to exhibit less attenuation in steady state than initially observed.

These results exhibit reductions of 20 dB or more at ten different frequencies. The tonal frequency tests were expected to perform well due to the predictability of the tonal noise source. The error microphone measurements were the best case scenario because the ANC system is optimising for these locations and not the ANC box as a whole. Therefore the next test used measurement microphones placed throughout the ANC box as described in section 4.5.1.1.

ANC box test (2) as per the outline of tests in section 4.5 only considered data from the measurement microphones throughout the room. The results are shown in Figure 4.13.

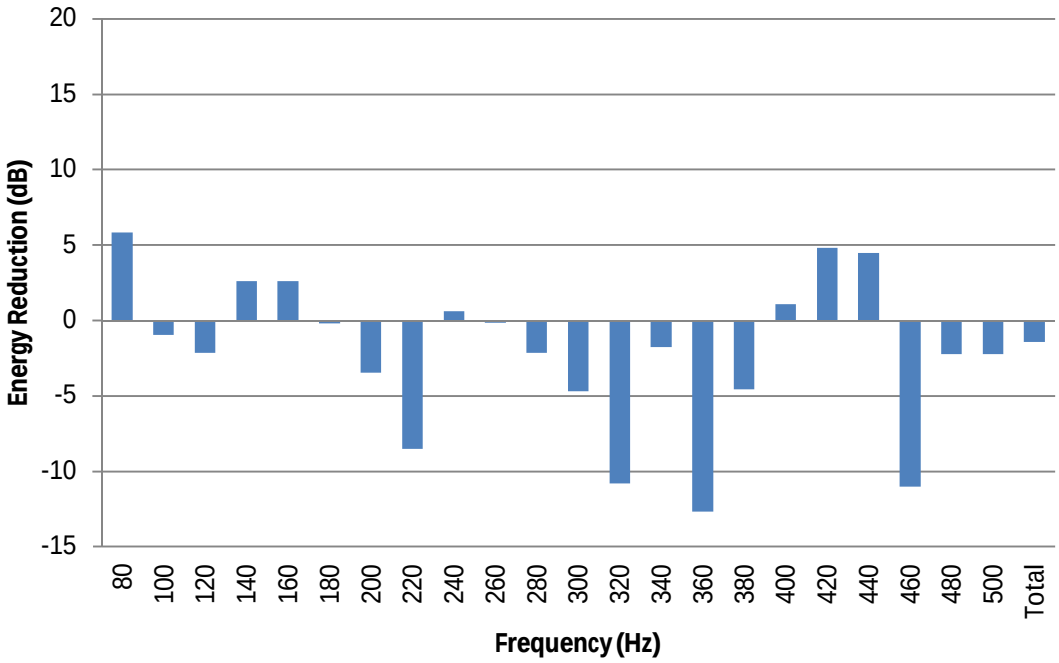

Figure 4.13 Energy reductions for the 4x4 ANC System

Figure 4.13 clearly shows that the overall control of sound energy in the ANC box is poor as the most frequencies exhibit an increase in sound energy. This suggests that the ANC control system is effectively introducing different constructive and destructive interference patterns. This would allow the error microphones to exhibit a reduction while the overall sound was not reduced and possibly increased.

Due to the poor performance it was decided that using 8 error microphones positioned in all corners of the ANC box would provide improved global sound energy reductions. It

was anticipated that due to the full coverage of the receiving room corners, improved sound energy reductions would result.

4.6.2 ANC box and 8x4 ANC control system results

The third ANC test performed used the 8x4 ANC configuration and the results are displayed in Figure 4.14. The sound energy reductions were 5dB or less for most frequencies except a few larger reductions below 200Hz and a few gains at higher frequencies. Overall these results were better than those of a 4x4 ANC system.

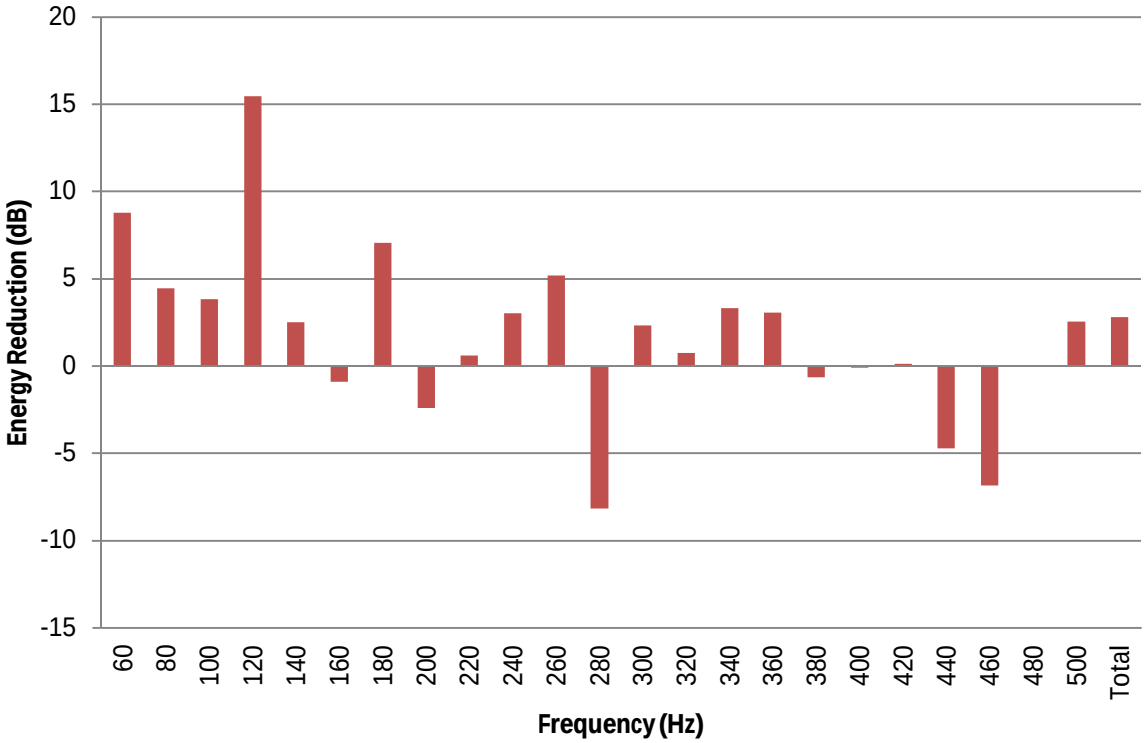

Figure 4.14 Energy reductions calculated from separate measurement microphones for an 8 error microphone system.

The total energy reductions were calculated as -1.4dB and 2.8dB for the 4x4 and 8x4 ANC control systems respectively. The 8x4 ANC control system exhibited the best performance of the two control systems by 4.2 dB in total energy reduction. From these tests is has been shown that 8 corner positioned error microphones provide increased global sound reduction compared to 4 corner positioned error microphones.

No one-third octave band or broadband white noise measurements were recorded. A few one-third octave band observations determined that minimal band noise control was possible in the ANC box.

Due to the relatively low total sound energy reductions observed in the last two ANC box tests and the difficulty with controlling band noise, insertions loss tests were performed on the window opening. This would determine whether the majority of noise was transmitted through the window versus the ANC box walls. If noise were to be transmitted through the MDF walls at a similar level to the window, this would be limiting the ANC systems performance.

4.6.3 Insertion loss tests

These tests were performed in order to determine the credibility of the results obtained from the ANC box. The test required the five measurement microphones within the ANC box and the power speaker noise source. A broadband white noise signal was used as excitation and data analysis was completed in one-third octave bands. The test involved measurements of the total sound energy (Equation 4.2) with no window, with a window and with 25mm MDF covering the opening. The insertion loss was calculated using Equation 4.3 to compare the no window case with the window and MDF cases.

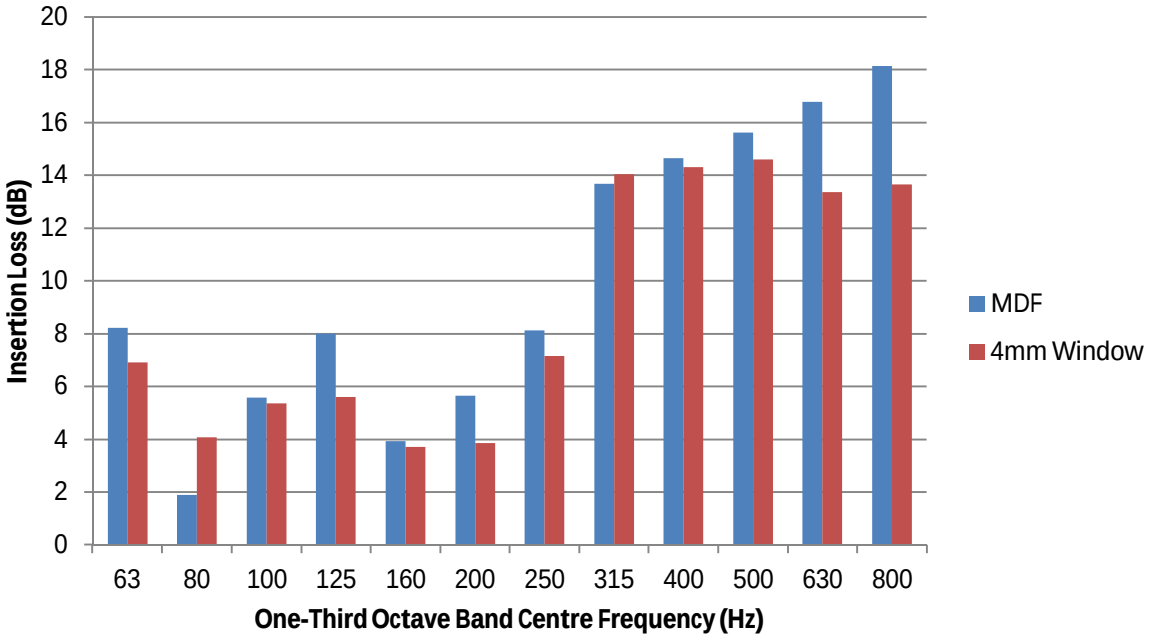

Figure 4.15 The sound energy insertion loss of 25mm MDF and the 4mm window.

The insertion loss results for MDF and the 4mm window are shown in Figure 4.15. The insertions loss of the 25mm MDF and the 4mm window were very similar suggesting that the MDF walls were likely to be transmitting similar levels of sound to that of the window. This will compromise the ANC control system's control ability as it can only reduce the sound transmission of noise transmitted through the window. Therefore if similar levels of noise are transmitted through the walls of the ANC box then the ANC is unable to effectively reduce the total sound energy in the ANC box.

In order to effectively test an ANC window, the test setup requires walls of high STL surrounding the window. The anechoic room was chosen as it is an isolated room hence the STL of the walls are high.

4.6.4 Anechoic room and 4x2 ANC control system results

Anechoic room test (1) (see section 4.5) was the tonal frequency test using a 4x2 ANC control system. Figure 4.16 shows the results of this test compared with test 3 in the ANC box (the best performing test of the ANC box tests).

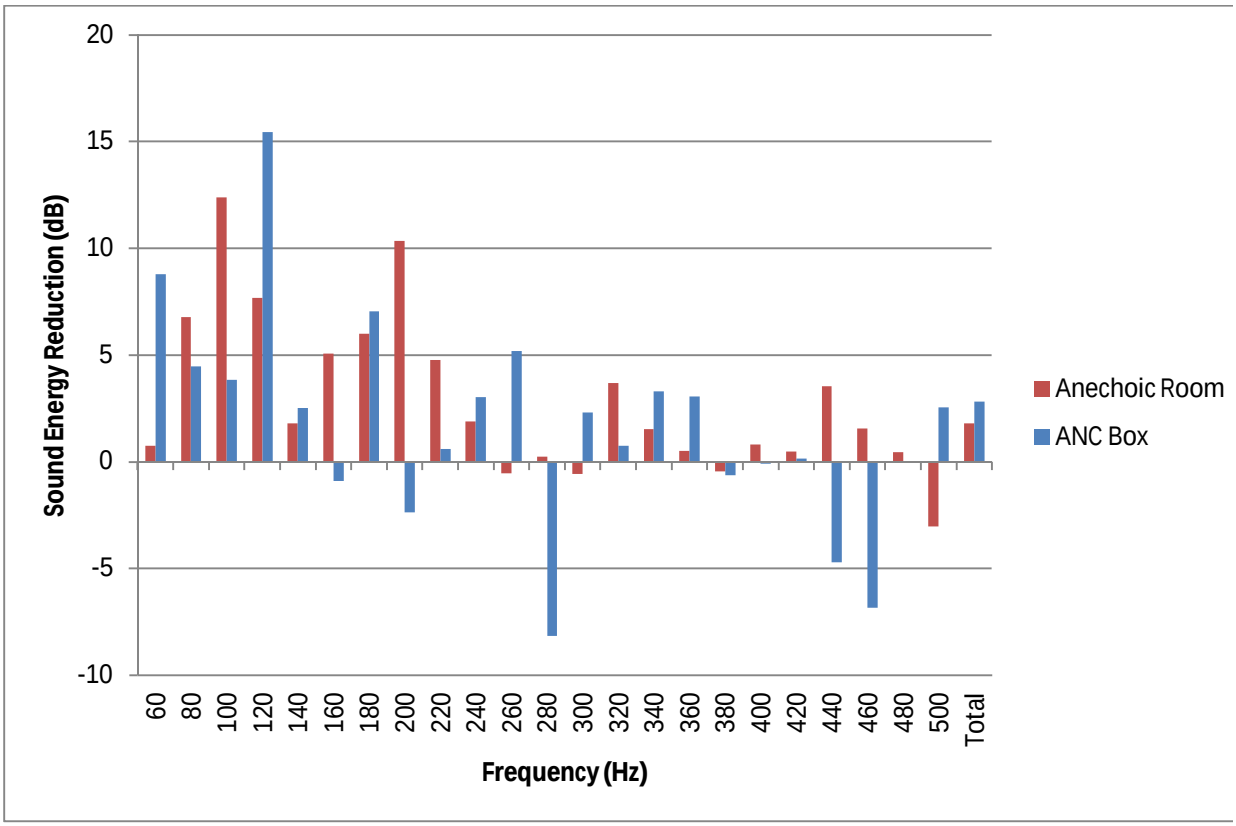

Figure 4.16 Tonal frequency ANC test comparison between the anechoic room (using a 4x2 ANC system) and the ANC box (using a 8x4 ANC comparison).

Figure 4.16 shows the ANC box test produced the largest sound energy reduction at 120Hz, whilst at a higher frequencies relatively large increases in sound energy were observed. The anechoic room tests did not exhibit the same increases in sound energy until 500Hz and below 240Hz showed consistent sound energy reductions. The total sound energy reduction values for the ANC box and anechoic room were 2.8dB and 1.8dB respectively. Although the total energy reductions indicate the ANC box test performed best, the consistent reductions and absence of large increases in sound energy for the anechoic room test suggests the converse. A relatively high particular frequency or microphone measurement could dominate the total sound energy calculation sum used in Equation 4.2 which could account for the ANC box result. The conclusion being that the anechoic room tests performed best due to the absence of relatively large sound energy increases which allowed band noise control unlike the ANC box tests.

The results for the one-third octave band tests (anechoic room test 2 in section 4.5), shown in Figure 4.17, show good reductions in one-third octave bands up to the 160Hz band. Energy reductions above 200 Hz were minimal. The total sound energy reduction calculated was 3dB. Whilst results are promising for frequencies up to 200 Hz the overall sound reductions is 3dB which is only just perceivable to the human ear [63].

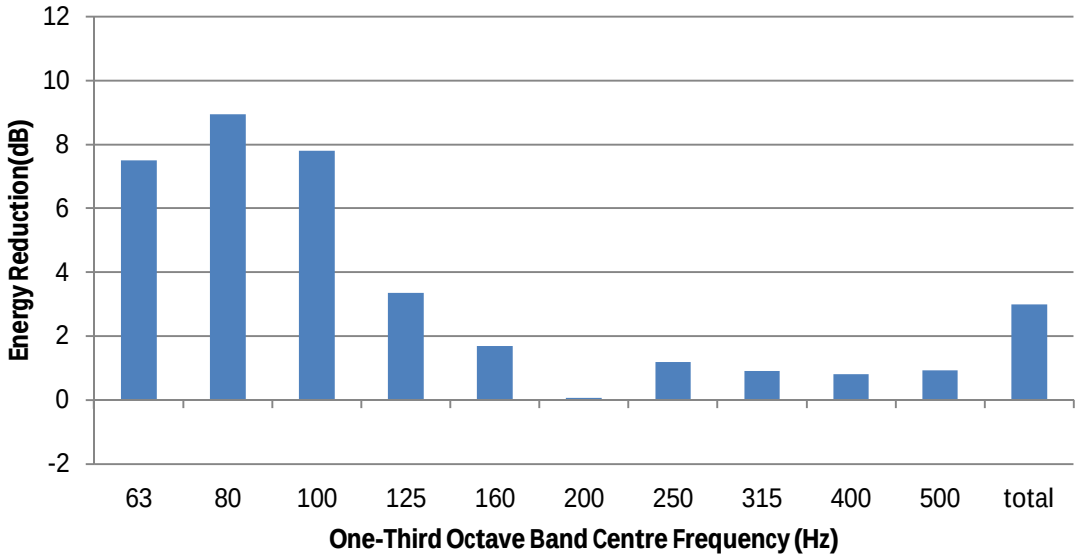

Figure 4.17 Individual one-third octave band test reductions collated.

The PSA's appear to be providing a sufficient level of actuation for acoustic control. Figure 4.18 shows no added harmonics at microphone 1 to due to the ANC system in the 100Hz band. Observation of microphones 2 and 3 confirmed that this response was

typical of microphones 1, 2 and 3. The measurement microphones at the error microphone locations closer to the window show some evidence of harmonics. The 3rd harmonic around 300Hz is apparent in Figure 4.19. Harmonic behaviour will provide issues for broadband control.

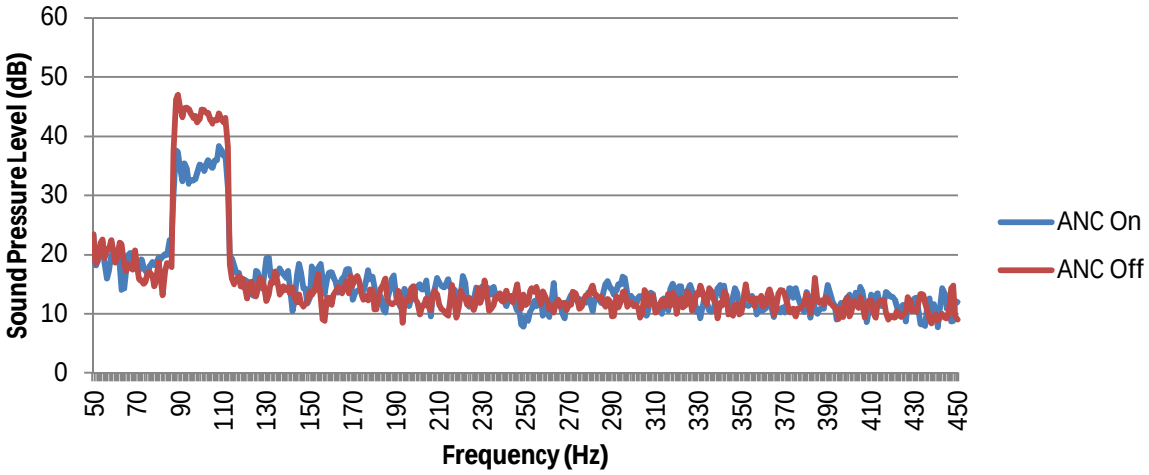

Figure 4.18 100Hz one-third octave band, narrowband SPL comparison at Microphone 1.

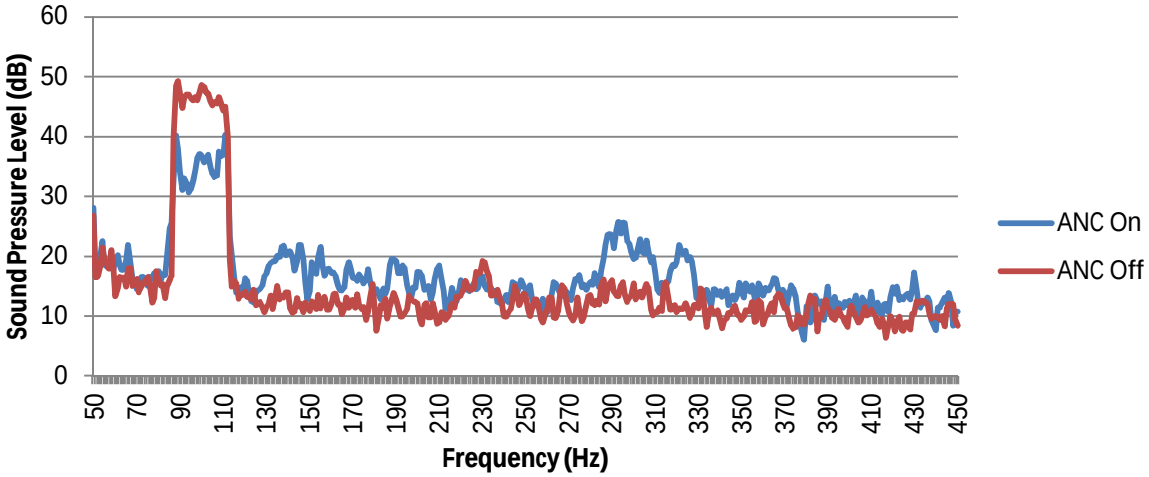

Figure 4.19 100Hz one-third octave band, narrowband SPL comparison at Microphone 5.

Figure 4.20 shows the one-third octave band results for the broadband noise ANC window test. These results were significantly lower than that presented in the one-third octave band test results with no one-third octave band reaching an energy reduction of 3dB. The total energy reduction of the broadband test was 1.3 dB which is unlikely to be picked up perceived by the human ear. The likely cause of the reduced performance is

the harmonics created by the actuators as shown in Figure 4.19. To improve on the broadband noise results these harmonics need to be minimised or eliminated from the system.

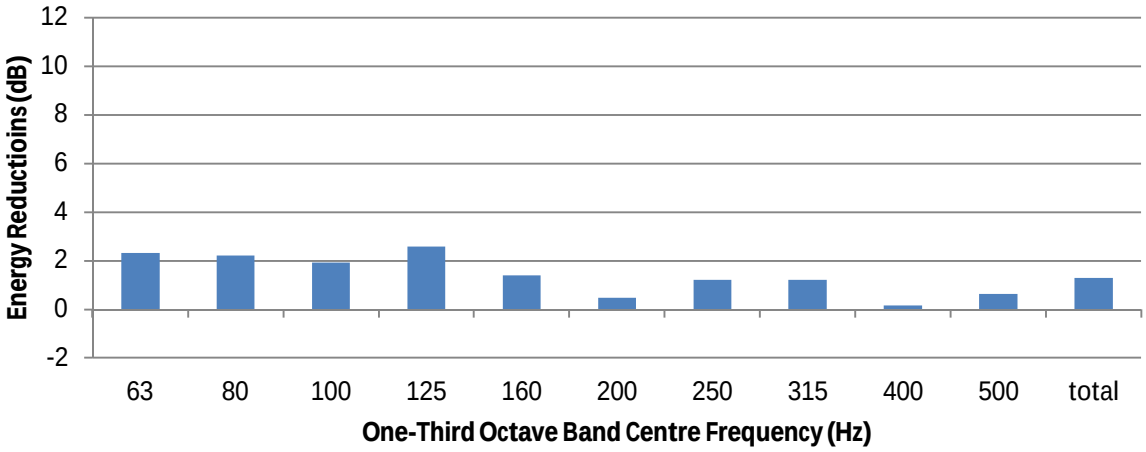

Figure 4.20 One-third octave band reductions for a broadband noise test.

4.6.5 Anechoic room and 8x4 ANC control system results

It was thought that more control sources would obtain increased or wider control of the sound energy transmitted or both. Figure 4.21 displays the energy reductions achieved by the 8x4 ANC window system. Relatively high control was seen in the lower frequency range up to the 200 Hz band. In comparison to the 2x4 ANC control system the 63Hz and 80Hz did not perform as well with reductions less than 3 dB. The overall energy reduction of all bands is 3.6 dB which was an improvement on the 3dB achieved by the 4x2 ANC control system. This improvement was not significant and again a reduction of this magnitude is only just perceivable to the human ear.

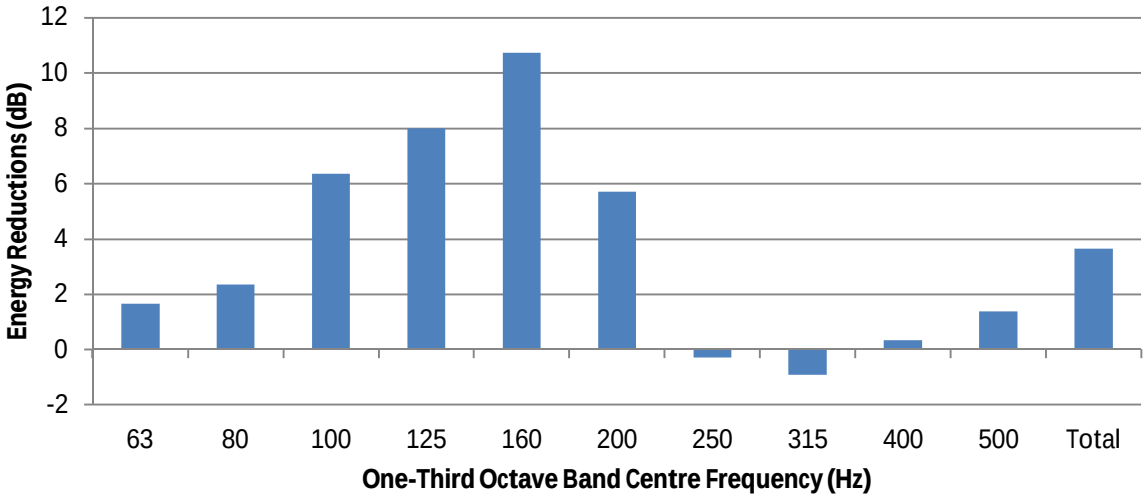

Figure 4.21 Individual one-third octave band test reductions collated for 8x4 ANC window system.

The one-third octave band results for the 8x4 ANC control system broadband test are shown in Figure 4.22. All reductions were 1dB or less with 0.6dB achieved as the overall total energy reduction due to ANC. Again the limited performance of the ANC to control broadband noise test was attributed to the harmonics seen at the error microphones.

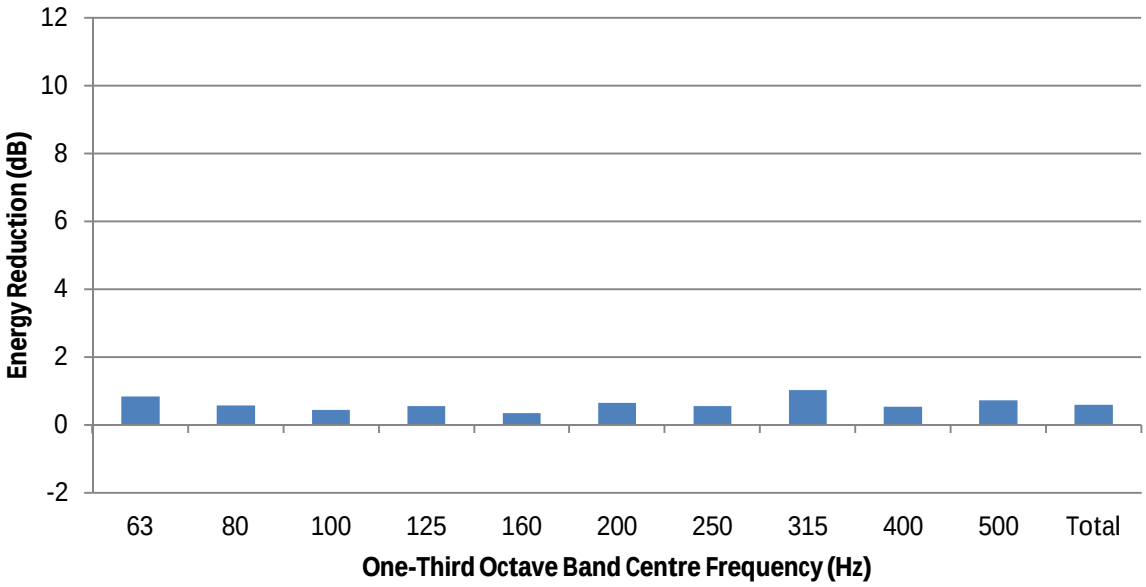

Figure 4.22 One-third octave band reductions for a broadband noise test.

Figure 4.23 shows evidence of harmonics present at microphone 5 around 300 Hz for the 100Hz one-third octave band. Microphones 1, 2 and 3, the microphones further from the window, do not exhibit these harmonics as in shown in Figure 4.24.

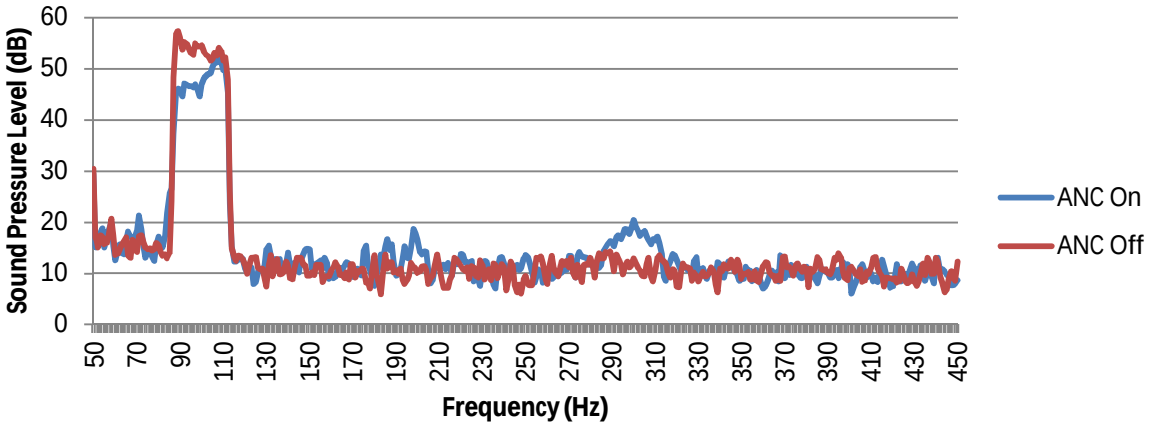

Figure 4.23 100Hz 1/3 octave band SPL comparison at Microphone 5

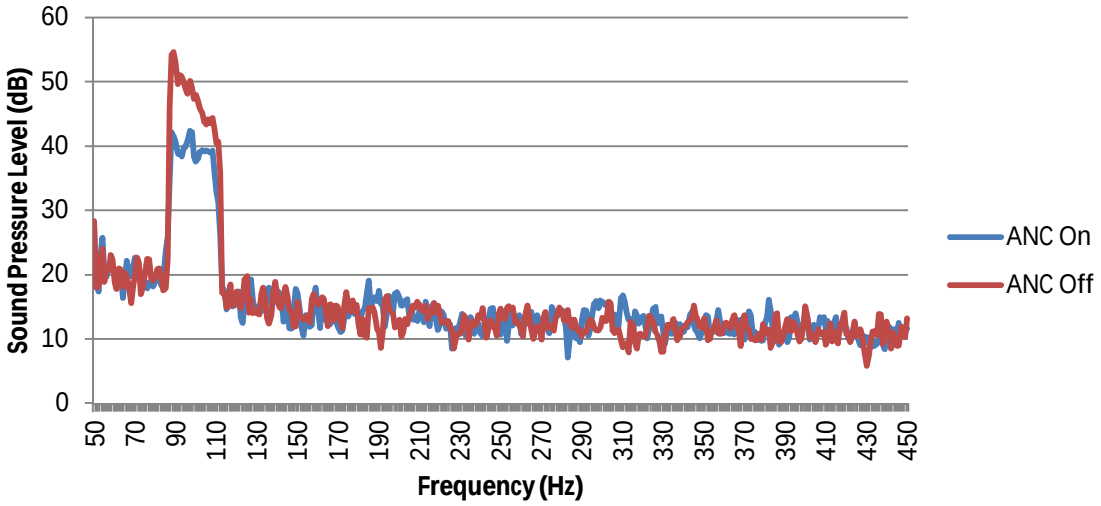

Figure 4.24 100Hz 1/3 octave band SPL comparison at Microphone 1

The poorer performance of the 8x4 system is likely due to the ANC control system attempting to optimise control of more error microphone locations which are in close proximity. Better global sound control was expected as seen in the ANC box tests. The total sound reductions were 0.6dB and 1.3dB for the 8x4 and the 4x2 ANC control systems respectively.

Audio recordings were made during the individual one-third octave band tests for subjective assessment. The results of this were ineffective as the recordings were hardly audible. Figures 4.18, 4.19, 4.23 and 4.24 all show maximum primary noise levels near 50dB for the 100Hz one-third octave band. The A-weighting of this produces a level of 30.2dB(A) which is exceptionally low. Hence, the difficulty in hearing the recordings let alone detect a reduction in SPL. For this reason the 8x4 ANC system test was conducted again with a higher primary noise level.

4.6.6 Higher power anechoic room and 8x4 ANC control system results

The higher noise level tests did not achieve a significant difference in results for the one-third octave band tests. The one-third octave bands performed well up to the 200 Hz band with an overall reduction of 3 dB (Figure 4.25). The lower frequency bands do not exhibit as higher peak reductions as in the previous tests. Therefore the system did not increase sound energy reductions when larger noise levels were tested. This is likely a limitation of the PSA's.

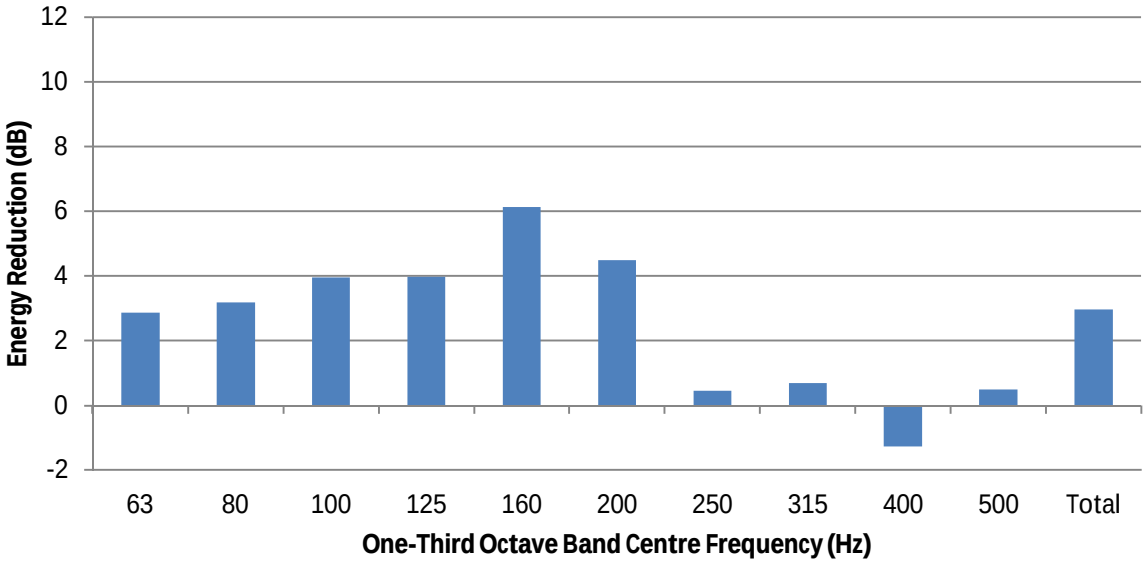

Figure 4.25 One-third octave band test sound energy reductions at higher primary noise power.

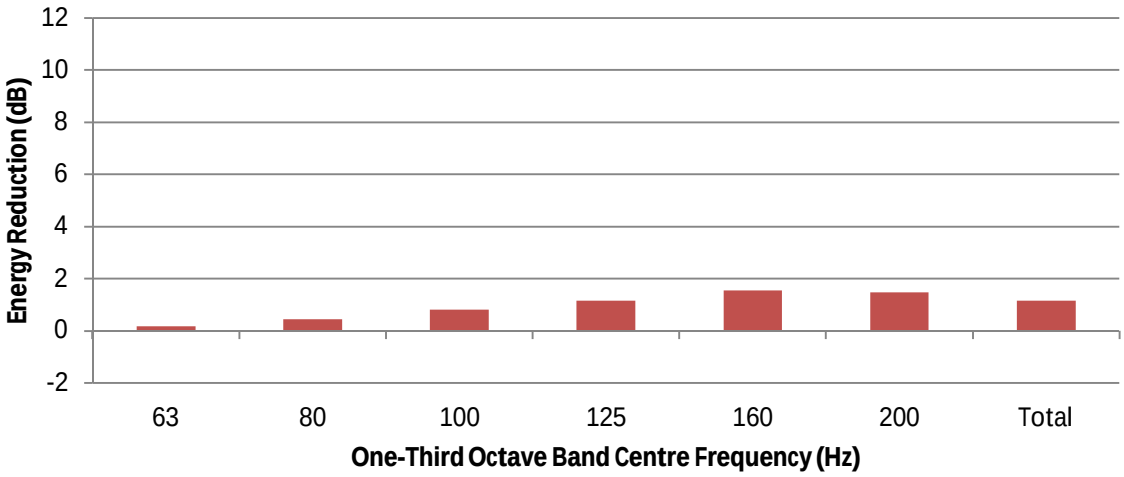

Figure 4.26 One-third octave band results for the broadband test with higher primary noise power.

The high power broadband noise test frequency range was reduced to 50-250Hz. This was used due to the good performance observed in previous individual one-third octave band tests. This was anticipated to enable the ANC system to focus its resources on improved performance in the frequency range where promising results had been observed. The results in Figure 4.26 are improved over the previous 8x4 ANC system broadband test yet the improvements are not overly significant. The total sound energy reduction was 1.2dB.

Harmonics were again likely the culprit for this decreased performance. Figure 4.27 clearly shows harmonic distortion of the actuators in the 200Hz and 300Hz regions corresponding to 2nd and 3rd harmonics respectively. In Figure 4.28, second, third and fourth harmonics are present although the ANC off response also exhibits harmonics. Despite the small presence of harmonics in the primary noise the actuators were to blame for the increase of these harmonics.

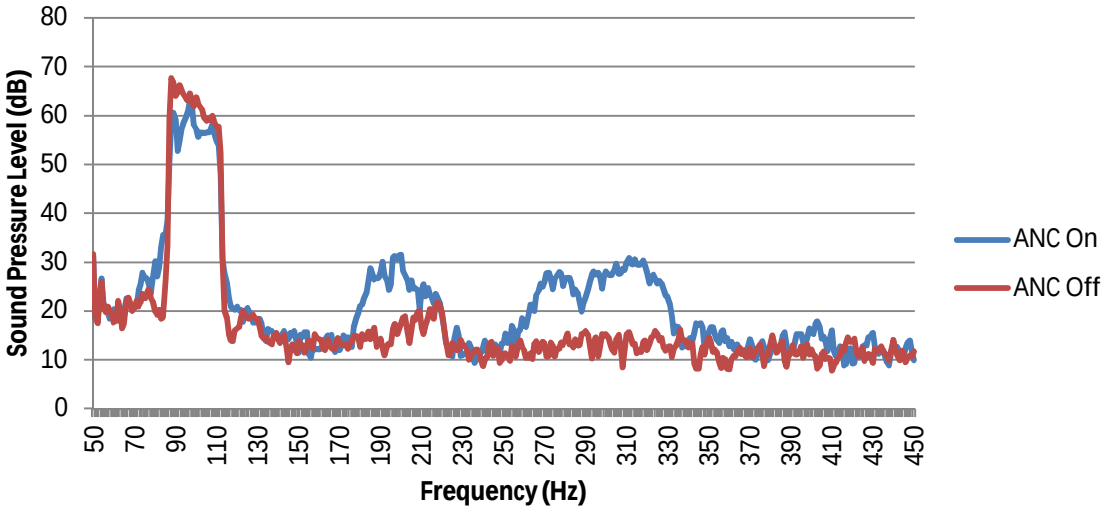

Figure 4.27 100Hz 1/3 octave band response at microphone 1

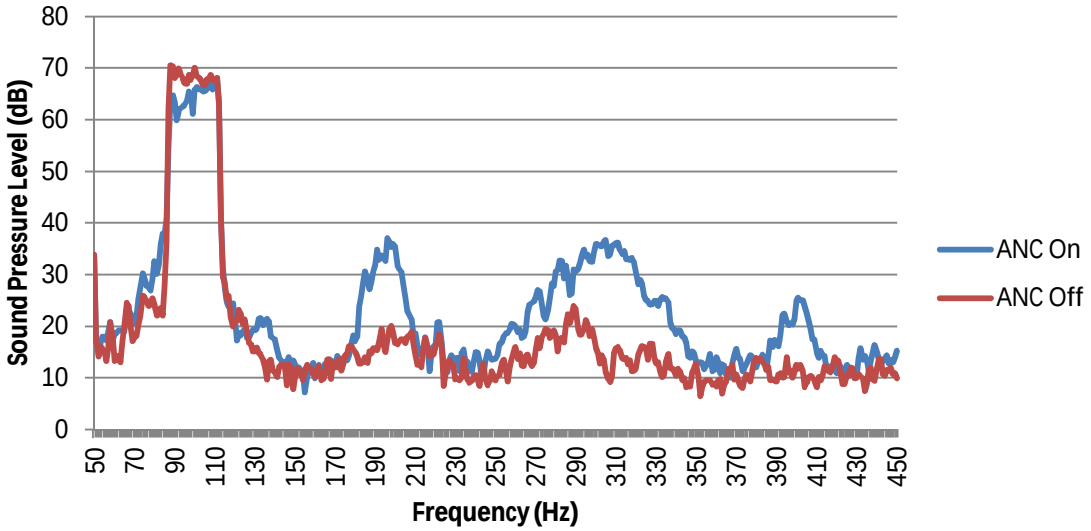

Figure 4.28 100Hz 1/3 octave band response at microphone 5

4.7 Summary

Three different ANC control systems were tested with two different experimental setups. The largest total sound energy reduction of 3.6dB was observed using the 8x4 ANC control system while testing the individual one-third octave bands in the anechoic room. This was relatively small and would only just be perceivable to the human ear.

Using the ANC box it was discovered that using 8 corner located error microphones achieves larger global cancellation within the ANC box then 4 corner located error microphones.

Throughout all tests using measurement microphone it was observed that the lower frequencies up to 200Hz achieved the largest sound energy reductions. This could be for two reasons: one being that the ANC control system can only produce control signals fast enough for frequencies up to 200Hz, and two was that the ANC control system can only effectively control a smaller band of frequency up to 50Hz in range. The former was thought, due to the approximate 50Hz range of the 200Hz third octave band and the relatively small energy reductions achieved above this one-third octave band.

Broadband noise was the most difficult to control with the best performance coming from the 4x2 ANC control system tested in the anechoic room. The total sound energy reduction was 1.3dB. The difficulty with broadband noise control was that any harmonics generated by the control sources limited the effectiveness of the system. Harmonics became more of an issue when attempting to control larger SPL.

This work was limited by number of microphones available for measurements as five microphones was not a sufficient number for accurate sound energy calculations. This work used comparative testing which may not be completely accurate but presents a good indication of the sound energy reductions are likely to be.

Future work would investigate targeted ANC control systems where the frequency range of interest is of a short range less than 50Hz. This allows focussing of ANC control system resources. This would also determine whether 200Hz is indeed a limiting frequency for effective ANC window as no 50Hz frequency bands were tested above 200Hz in this work. This future work would also investigate the use of large PSA's in order to minimise the harmonics generated. This would be achieved through highly over rating the PSA and then only requiring a low portion of its rating to control large SPL.

5 Modelling

This chapter explored the simulation of active noise control (ANC) experiments. A sound transmission loss (STL) model was first developed and verified against published experimental data. ANC control sources were then included in the model. The anechoic room tests performed in chapter 4 were simulated and optimised, then compared to an optimised ideal ANC simulation. These simulations were performed for a 100Hz tone primary noise. The largest STL improvements theoretically possible are then presented, including their respective configurations. A summary of the model outlines the findings, limitations and any further development required.

5.1 Introduction

Computational modelling can be useful in the development of a ANC system. In this case the model is aimed at simulating the ANC tests that have been performed (see chapter 4). Once a model is verified it can significantly reduce the number of tests involved in the development of a new system.

The model implemented in this work was based on similar models described by Fuller et al. [64] and Howard [65]. Parts of each of these models were combined to create a model that would fit the experimental data. The verification of the model was performed using experimental data from other studies [16, 35].

Once the STL model was verified, it was used to find the ideal actuator locations within constraints as well as for the unconstrained case. This allowed the comparison of the theoretical maximum sound reduction due to ANC with that obtained from testing (see chapter 4). It is envisaged that this model would make a good tool for investigating actuator positions in future work.

5.2 Aims

The aim of this simulation work was to obtain a model that simulates ANC window testing results which were consistent with those observed in real tests (see chapter 4). This required a verified STL model and simulation of point control sources for the ANC part of the model.

Other benefits provided by this simulation work were:

- A more comprehensive understanding of STL in the low frequency range of 50Hz to 1000Hz where resonances dominate the STL curve.
- An indication of the most effective ANC control source locations.
- An understanding of panel vibration and how it is excited and the sound radiated.

5.3 Model Description

The MATLAB programming language was chosen for development of the model. The STL model was broken into three parts:

- A vibration model of the window (providing a modal analysis).
- A definition of the acoustic excitation of the window.
- And a definition of the acoustic radiation from the window.

The model was fundamentally based around a modal analysis model of the window. Once this was defined, the noise induced coupling to and from the model would enable calculation of the STL.

5.3.1 Modal panel vibration model

The modal analysis model of panel vibration formed the basis of the overall model upon which other components were added. Simply-supported boundary conditions were used for simplicity. However, in reality the boundary conditions of a window are likely to fall somewhere between clamped and simply-supported.

$$w(x,y,t) = \sum_{m=1}^{\infty}\sum_{n=1}^{\infty} W_{mn} sin(k_m x) sin(k_n y) e^{j\omega t} \qquad \text{Equation 5.1}$$

Where:

$$k_m = \frac{m\pi}{a}$$

$$k_n = \frac{n\pi}{b}$$

Fuller [64] defined his simply-supported model of a plate as in Equation 5.1. The model was to simulate a steady state response hence zero was substituted in for t in Equation 5.1, giving Equation 5.2.

$$w(x,y) = \sum_{m=1}^{\infty}\sum_{n=1}^{\infty} W_{mn} sin(k_m x) sin(k_n y) \qquad \text{Equation 5.2}$$

This model can be described as an infinite sum of plate mode shapes, each with a contribution factor that describes the influence of each mode on the overall plate response. These contribution factors were dependent on the manner of excitation, described in the next section.

This model is only concerned with frequencies up to 1000Hz therefore the number of modes will be limited to those relevant to this frequency range. The natural angular frequencies were calculated using Equation 5.3 [65]. Equation 5.4 shows the adjustment of natural frequency.

$$\omega_{mn} = \sqrt{\frac{D\pi^4}{\rho h}}\left(\left(\frac{m}{a}\right)^2 + \left(\frac{n}{b}\right)^2\right) \qquad \text{Equation 5.3}$$

$$f_{mn} = \frac{\omega_{mn}}{2\pi} \qquad \text{Equation 5.4}$$

Table 5.1 contains the properties of glass that were used in this model. These properties along with the glass window size were used to calculate the natural frequencies up to 1000Hz. The glass panel size was 1.13 x 0.735m. This corresponded to the window tested in the anechoic room tests (see chapter 4). The relevant natural frequencies are shown in Table 5.2. From these natural frequency calculations the maximum modal indices required are M = 7 and N = 11.

Property	Value Used
Young's Modulus	70e9 Pa
Poisson's ratio	0.23
Density	2500 kg/m^3
Thickness	4 mm (0.004 m)

Table 5.1 Table of glass properties used in this model.

		N modal index										
		1	2	3	4	5	6	7	8	9	10	11
M modal index	1	25.98	49.15	87.77	141.83	211.34	296.30	396.71	512.56	643.86	790.60	952.80
	2	80.75	103.92	142.53	196.60	266.11	351.07	451.47	567.33	698.62	845.37	0
	3	172.02	195.19	233.81	287.88	357.39	442.35	542.75	658.60	789.90	936.65	0
	4	299.81	322.98	361.60	415.67	485.18	570.13	670.54	786.39	917.69	0	0
	5	464.11	487.28	525.90	579.97	649.48	734.44	834.84	950.69	0	0	0
	6	664.92	688.09	726.71	780.78	850.29	935.25	0	0	0	0	0
	7	902.25	925.42	964.03	0	0	0	0	0	0	0	0

Table 5.2 Modal indices for natural frequencies below 1000Hz.

5.3.2 Excitation

The excitation of the vibration model (see section 5.3.1) simulates a tonal frequency airborne sound wave striking the window. This causes vibration in the window which was dependent on the frequency, pressure, and angle of incidence of the incident sound wave. Therefore, the excitation part of the model takes the frequency, pressure and angle of incidence of an incident sound wave and translates this into a set of modal contribution factors. These contribution factors essentially describe the vibration of the plate.

To calculate the modal contribution factors, the modal forces for each mode must be calculated first. Equation 5.5 shows this calculation for an obliquely incident plane wave impacting on the window. In this model P_i was derived from a 100dB sound pressure level (SPL) (P_i = 2Pa).

$$P_{mn}^{d} = 8P_i\bar{I}_m\bar{I}_n \qquad \text{Equation 5.5}$$

Where $\bar{I}_m$ and $\bar{I}_n$ are defined by:

$$\bar{I}_m = \begin{cases} \dfrac{-j}{2}sgn(\sin\theta\cos\varphi_i), & \text{when } (m\pi)^2 = [\sin\theta_i\cos\varphi_i]^2 \\ \dfrac{m\pi\{1-(-1)^m\exp[-j\sin\theta\cos\varphi_i\,(\omega a/c)]\}}{(m\pi)^2-[\sin\theta\cos\varphi_i\,(\omega a/c)]^2} & \text{when } (m\pi)^2 \neq [\sin\theta_i\cos\varphi_i]^2 \end{cases}$$

$$\bar{I}_n = \begin{cases} \dfrac{-j}{2}sgn(\sin\theta_i\cos\varphi_i), & \text{when } (n\pi)^2 = [\sin\theta_i\cos\varphi_i]^2 \\ \dfrac{n\pi\{1-(-1)^n\exp[-j\sin\theta_i\cos\varphi_i\,(\omega a/c)]\}}{(n\pi)^2-[\sin\theta_i\cos\varphi_i\,(\omega a/c)]^2} & \text{when } (n\pi)^2 \neq [\sin\theta_i\cos\varphi_i]^2 \end{cases}$$

Once the modal forces have been calculated, the modal contribution factors can be determined using Equation 5.6.

$$W_{mn} = \frac{P_{mn}^{d}}{\rho h(\omega_{mn}^2-\omega^2)} \qquad \text{Equation 5.6}$$

The modal contribution factors can then be used to fully describe the vibration of the glass window using Equation 5.2.

5.3.3 Radiation

The sound radiation component of the model was taken from Howard's work [65] where the equations are based on the Rayleigh integral. The Rayleigh integral calculates the radiated from the window sound power by summing all transmitted sound intensity components as per Equation 5.7. The sound intensity components were calculated using Equation 5.8. The sound intensity calculation required the sum of all pressure values due to each modal contribution factor, which is calculated in Equation 5.9. This was a computationally intensive calculation.

$$\prod_r = \int_{\varphi_t=0}^{2\pi} \int_{\theta_t=0}^{\pi/2} I^t r^2 \sin\theta_t d\theta d\varphi \qquad \text{Equation 5.7}$$

Where:

$$I^t = \left| \sum_m \sum_n p^t_{m,n} \right|^2 / 2\rho c \qquad \text{Equation 5.8}$$

Where:

$$p^t_{m,n} = \frac{W_{mn}\omega k \rho c}{2\pi} ab I_m I_n \qquad \text{Equation 5.9}$$

Where I_m and I_n are defined by:

$$\mathrm{I}_m = \begin{cases} \dfrac{-j}{2} sgn(\sin\theta\cos\varphi_i), & \text{when } (m\pi)^2 = [\sin\theta_i \cos\varphi_i]^2 \\ \dfrac{m\pi\{1-(-1)^m \exp[j\sin\theta\cos\varphi_i\,(\omega a/c)]\}}{(m\pi)^2 - [\sin\theta\cos\varphi_i\,(\omega a/c)]^2} & \text{when } (m\pi)^2 \neq [\sin\theta_i \cos\varphi_i]^2 \end{cases}$$

$$\mathrm{I}_n = \begin{cases} \dfrac{-j}{2} sgn(\sin\theta\cos\varphi_i), & \text{when } (n\pi)^2 = [\sin\theta_i \cos\varphi_i]^2 \\ \dfrac{n\pi\{1-(-1)^n \exp[j\sin\theta\cos\varphi_i\,(\omega a/c)]\}}{(n\pi)^2 - [\sin\theta\cos\varphi_i\,(\omega a/c)]^2} & \text{when } (n\pi)^2 \neq [\sin\theta_i \cos\varphi_i]^2 \end{cases}$$

5.3.4 Sound transmission loss calculation

Before the sound transmission loss could be determined, a value for the input sound power to the system must be calculated. The input sound power level was calculated using Equation 5.10, given an incident sound pressure P_i, as used in Equation 5.5.

$$\prod_i = \frac{|P_i|^2}{2\rho c} ab \cos\theta \qquad \text{Equation 5.10}$$

The STL can be calculated from the incident sound power and radiated sound power using Equation 5.11.

$$TL = 10 \log\left(\prod_i \Big/ \prod_r\right) \qquad \text{Equation 5.11}$$

The STL was calculated for 100 frequencies between 100Hz and 1000Hz. These frequencies were logarithmically spaced. The STL for each or these frequencies were then combined into third octave bands and averaged to give STL values for each third octave band. This allowed comparisons to be made with the experimental data easier.

5.4 Verification

To verify the model, STL data was sourced from Quirt [16] and a paper by Marsh [35] which contained data from Brandt, Wolley, and Saint-Roch. All of the STL data used in this verification were for 4mm single pane windows. The window sizes in each set of data vary but are all between $1m^3$ and $4m^3$ in area. Figure 5.1 shows all of the window STL data and the STL result calculated using the model developed in this chapter.

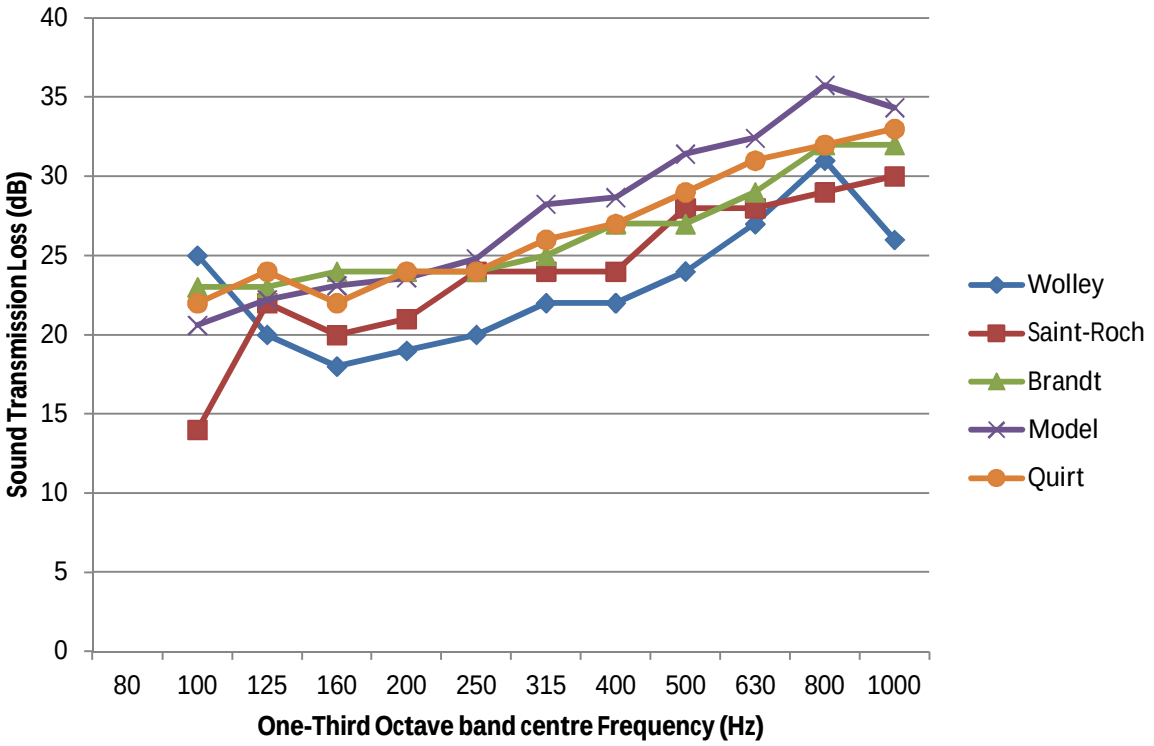

Figure 5.1 STL model compared to experimental STL data.

The model fits well with Quirt's and Brandt's experimental STL data, especially in the 100Hz to 250Hz third octave bands. Above 250Hz the model slightly overestimates the STL given by Quirt and Brandt. Overall the model fits the general trend of all measured data but most closely fits Quirt's data.

This fit of the model to experimental data allows the model to be used to investigate the effects of ANC point control sources on the window.

5.5 Active Noise Control Application

In order to investigate the effects of ANC the model was extended to include ANC point control source inputs. These sources were modelled as point sources which were to simulate the piezoelectric stack actuators used in testing (see chapter 4). These actuators can be modelled in a similar fashion to the acoustic excitation of the panel as in Fuller [64]. The modal forces can be calculated using Equation 5.12, which was then substituted into Equation 5.6 to determine the modal contribution factors.

$$P_{mn}^{c} = \frac{4F}{ab} \sin k_m x_f \cos k_n y_f \qquad \text{Equation 5.12}$$

A linear superposition of the control source and acoustic excitation modal contribution factors was performed to give the complete window vibration model. The model is then used to calculate the sound power radiated from the window and subsequently the STL. These calculations were required for each individual frequency.

ANC simulations with fixed actuator positions were performed using a brute force method of optimisation. Optimisation was performed by iterating through a range of different combinations of control force inputs (F) for each actuator. These combinations were initially very sparse but were progressively refined until an optimal gain was reached.

5.6 Active Noise Control Simulations

This section presents two sets of ANC simulations. The first is a simulation of the anechoic room tests performed in chapter 4 and the other is an ideal case of ANC without constraining the actuator placements.

5.6.1 ANC test simulations

ANC simulations were performed using the complete window vibration model to simulate the testing scenario in the anechoic room (see chapter 4). The actuator locations are indicated in Figure 5.2. All actuators are located 40mm in from the edge of the glass window. The exact locations of the actuators are stated in Table 5.3 where the bottom left corner was defined as the origin.

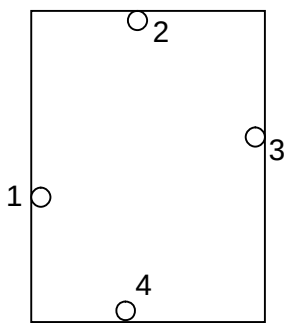

Figure 5.2 Actuator locations

Actuator	x	y
1	0.04m	0.45m
2	0.325m	1.09m
3	0.695m	0.63m
4	0.3m	0.04m

Table 5.3 Actuator locations

A single frequency of 100Hz was chosen for the simulation to reduce the calculation time. Before any ANC simulations were performed, a benchmark STL simulation was run for 100Hz. The STL result without ANC was 22.1dB. The plate vibration mode shape associated with 100Hz is shown in Figure 5.3(a). Figure 5.3(b) shows the nearest analytical mode shape which was the (1,3) mode, occurring at 88Hz.

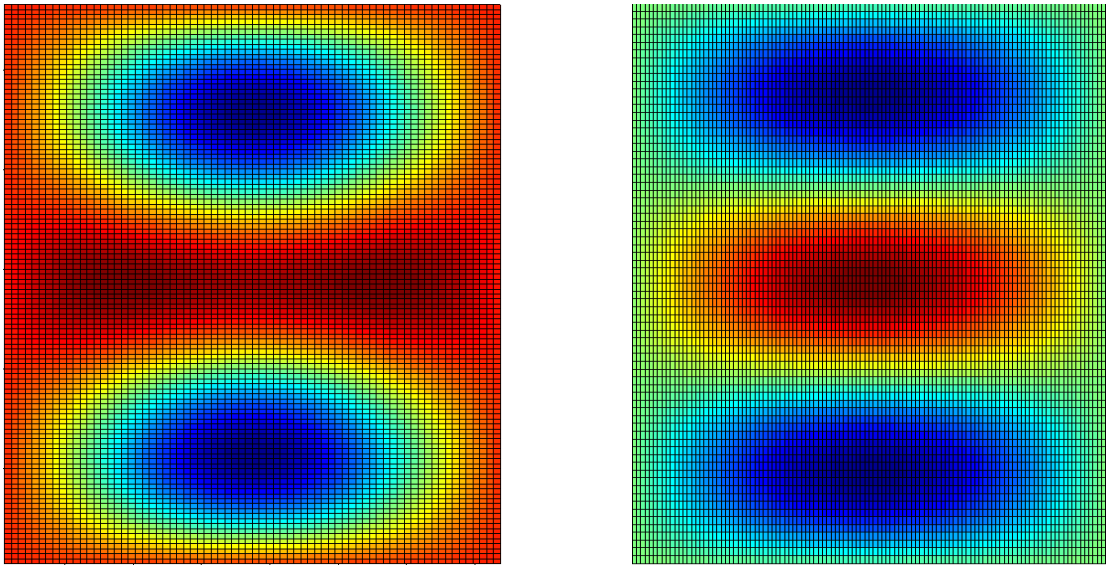

(a) (b)

Figure 5.3 Mode shapes of (a) the window at 100Hz and (b) the (1,3) mode which occurs fully at 88Hz.

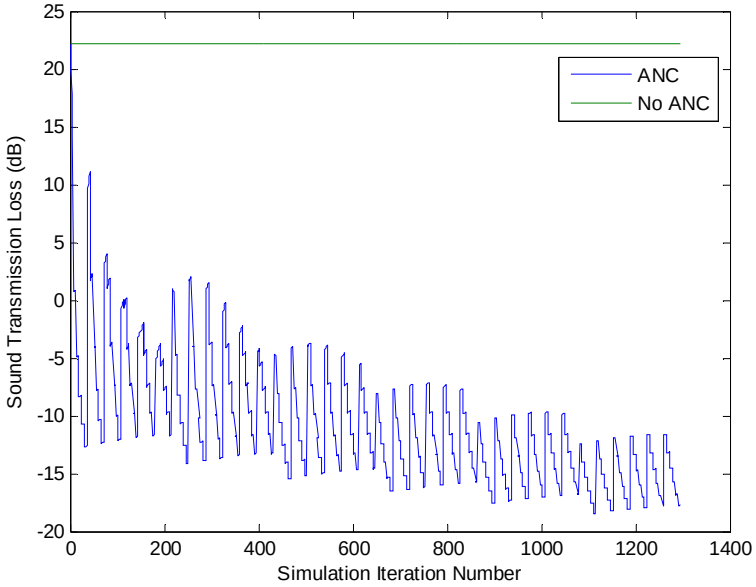

Figure 5.4 STL of first set of ANC control force combinations.

Figure 5.4 shows the first set of simulated ANC control force (F in Equation 5.12) combinations and their STL results. The horizontal axis in Figure 5.4 shows the simulation iteration number which corresponds to a particular combination of ANC control forces. The simulation presented in Figure 5.4 used control forces between 0N and 100N in increments of 20N. Since none of the results improved the STL of the 'No ANC' case, control source forces must be lower than 20N.

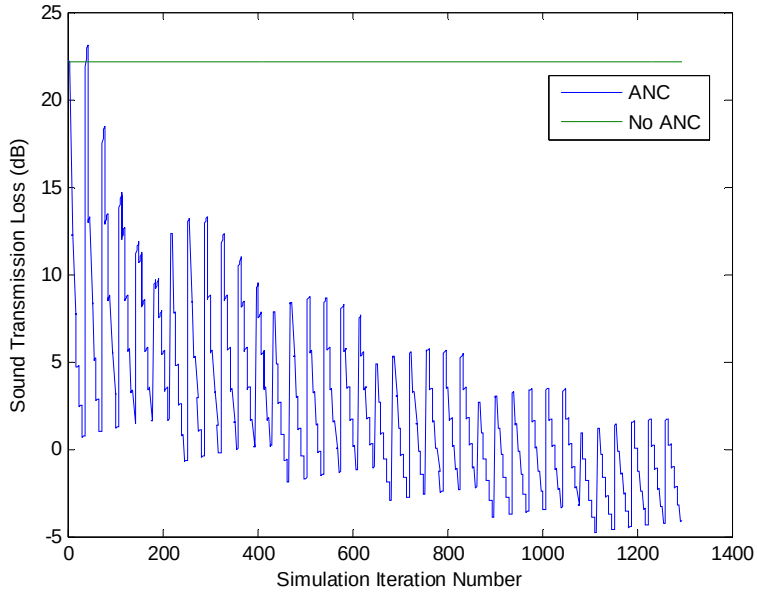

Figure 5.5 STL of second set of ANC control force combinations.

The next set of control force combinations used between 0N and 20N in increments of 4N for each control source. The results from this are shown in Figure 5.5. In these results there is a peak above the 'No ANC' line therefore there was an improvement using ANC. The control source combination that produced the maximum improvement was, source 1 = 20N, and source 3 = 4N. This was used to determine the next set of control forces to simulate. From here it was decided to drop control sources 2 and 4 and only consider sources 1 and 3 and use control forces:

- 12N to 20N in 0.5N increments for source 1.
- 0N to 8N in 0.5N increments for source 3.

Figure 5.6 shows the results from further optimisation. The overall maximum STL was 23.7dB and occurs when, the force used at control source 1 is 18N and the force used at control source 3 is 2.5N. This gives an overall theoretical improvement of 1.6dB due to ANC.

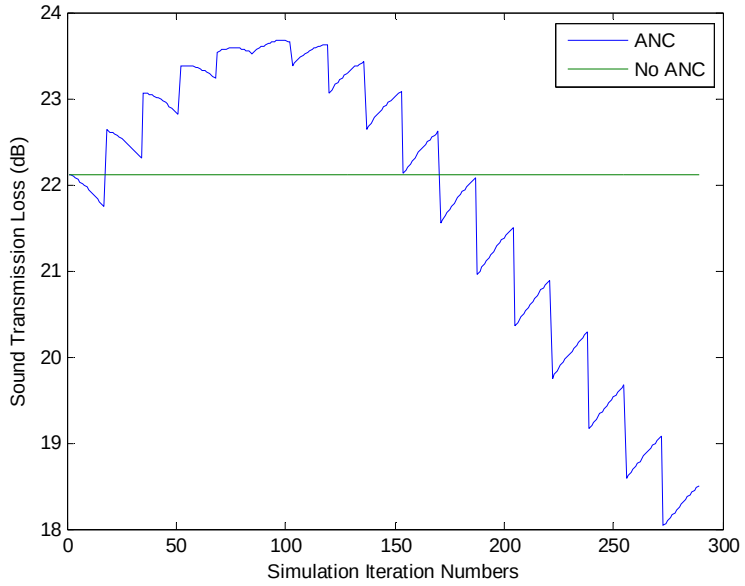

Figure 5.6 STL of third set of ANC control force combinations.

This 1.6dB reduction compares well with the anechoic room tests (see chapter 4). Since the model uses an input SPL of 100 dB it can adequately be compared to the higher power anechoic room tests. In these tests the 100Hz third octave band saw an improvement in STL of 0.8dB and 2dB for the broadband and third octave band tests respectively. This fits well with the model's prediction for the best case. Reductions of 10 dB were measured in the 100Hz octave band in the lower power anechoic room tests.

This could be explained by the measurement microphones not adequately capturing a representative sample of the radiated sound power.

5.6.2 ANC ideal simulations

The model was also used to simulate an ideal ANC situation without the constraints of placing the actuators close to the edge of the window. Again, this was carried out with a 100Hz disturbance. Figure 5.3 demonstrates that the 100Hz disturbance creates a vibration pattern very similar to that of the (1,3) mode shape. This helped determine ideal locations for the control sources.

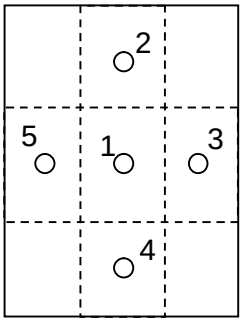

Figure 5.7 Actuator locations with the node lines of the (3,3) mode of vibration.

Figure 5.7 shows the control source locations chosen based on modes (1,1), (1,3), (3,1) and (3,3), which were the dominant modes of vibration around 100Hz. Table 5.4 shows the co-ordinates of each actuator position.

Actuator	x	y
1	0.3675m	0.565m
2	0.3675m	0.942m
3	0.6125m	0.565m
4	0.3675m	0.188m
5	0.1225m	0.565m

Table 5.4 Actuator coordinates

Optimisation of the ideal positions was conducted in a different manner than for the test case. First each ideal actuator position was simulated individually to determine whether it would improve the STL, considerably reducing the computational requirements of the

process. Figure 5.8 shows the simulation results for the individual actuator positions. Results for position 2 and position 3 are not visible as they exactly matched the results for positions 4 and 5 respectively, due to symmetry. No improvement in STL was seen due to positions 2 and 4. Therefore Positions 1, 3 and 5 were used in combination for the next optimisation iteration.

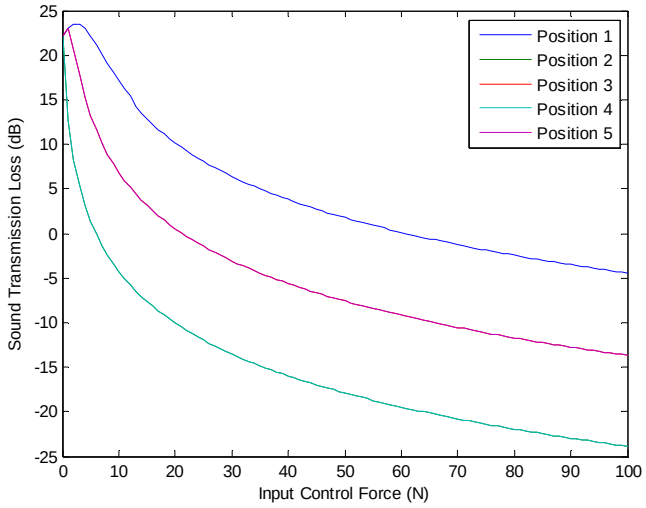

Figure 5.8 STL improvements achieved for different control inputs and actuator locations.

The next optimisation iteration used control inputs of 0N to 10N in increments of 1N and actuator positions 1, 3 and 5. The simulation results are shown in Figure 5.9. Significant improvements in STL were observed in these results. The highest STL was 32.2dB, which was a 10.1dB improvement due to ANC. This peak occurred at control force inputs of 0N, 2N and 2 N for actuators 1, 3 and 5 respectively.

Further optimisation of the control inputs are shown in Figure 5.10, which only used control positions 3 and 5 each with control inputs of 1N to 4N in 0.1N increments. This yielded a best performance of 34.1dB STL at control force inputs of 1.7N for both positions, corresponding to a STL improvement due to ANC of 12dB.

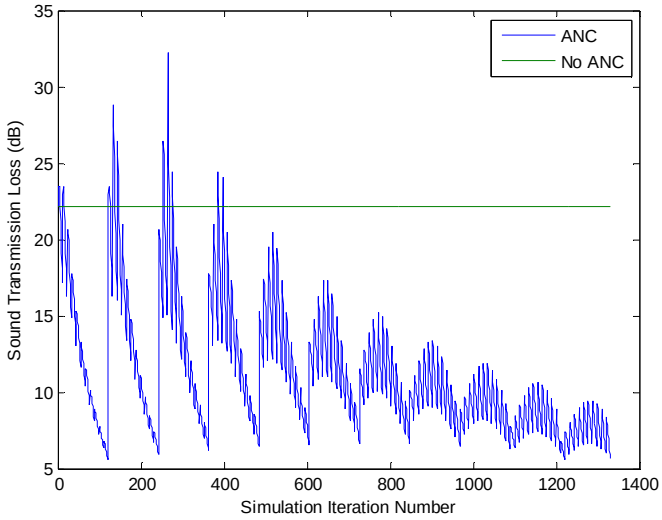

Figure 5.9 Optimisation of ANC system using control positions 1, 3, and 5 from Figure 5.8.

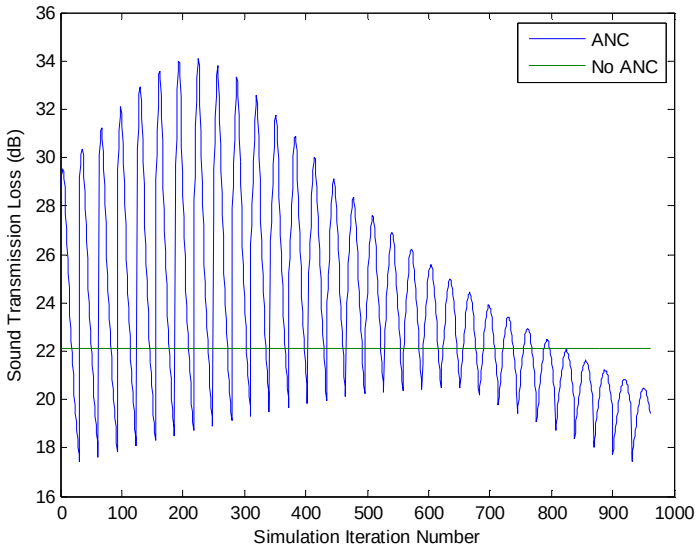

Figure 5.10 Third iteration of simulations for ideal ANC application.

From the optimised ANC simulations it can be concluded that the anechoic room tests achieve the best improvements in STL possible given the actuator locations. When compared with the ideal control source locations the test was achieving 13.3% (1.6dB) of the possible 12dB STL improvements due to ANC. This was based only on the 100Hz simulations performed.

If another frequency was chosen and simulated the mode of vibration would have been different. This is likely to change the optimal control locations and therefore more control sources would be needed for broader control. This adds to the expense and complexity of the problem. This is a major challenge for ANC windows if large frequency range coverage is desired. If a smaller band of frequencies were targeted the ANC performance would have more chance of obtaining optimal performance.

5.7 Summary

In this chapter a STL model was developed and verified. The model was extended to include control sources for ANC. Simulations were performed for a test case and an ideal case with an input frequency of 100Hz. The results from these were 1.6dB and 12dB additional STL, respectively.

The most effective ANC configurations both used 2 control sources. The test case used control sources 1 and 3 which are shown in Figure 5.2 and the ideal case used control sources 3 and 5 shown in Figure 5.7. It should be noted that control source 1 in the test case and control source 5 in the ideal case were in similar positions on the window as were control source 3 in both simulated cases. These positions were to the left and right of the true centre of the window. It would be interesting to investigate whether any improvement in STL is achieved as the control source locations of the test case converge on that of the ideal case.

The model was only able to consider a single frequency when optimising the ANC inputs. This limits the ability of the model to optimise the control source locations for bands of frequency. This model could be extended to consider a small selection of frequencies within a band of interest and optimise for this. Further development of this model would look at optimising the control source locations rather than just the control inputs on selected control source locations.

Overall this model could prove a useful tool in determining control source configurations for physical testing. This could reduce the number of future experiments to be carried out by only performing physical tests on configurations which have shown promise in the model first.

6 Project Findings

6.1 Introduction

This chapter is split into two sections; the first presents the findings as presented in each chapter while the second explores the potential avenues for future work.

6.2 Conclusions

Chapter two discovered that the 50Hz to 500Hz frequency range of interest dictated by resonance determined and mass determined sound transmission loss (STL). Review of previous active noise control (ANC) windows revealed panel control was light on previous work and did not suffer the thermal insulation issues that cavity control did. Therefore panel control was investigated in this work.

Chapter three found the PVDF film speaker, without window material, to be the best choice as a window speaker control source for ANC. The bowed film speakers outperformed the film speaker but were impractical for ANC use due to aesthetic reasons. All speakers tested in this work were short of the sound pressure level (SPL) response of 60dB to 80dB produced by Yu's window speaker [46].

The fourth chapter compared the tonal frequency ANC tests performed in both the ANC box and anechoic room. The anechoic room tonal results were more consistent then the ANC box tests with no substantial increases in sound energy seen below 500Hz. The ANC box tests found that using 8 corner located error microphones significantly outperforms a system using 4. The anechoic room band noise tests indicate that shorter band ranges were more likely to produce significant ANC reductions and ANC performs best at frequencies up to 200 Hz.

Chapter five investigated ANC window simulation and found some good agreement with the experimental results in chapter 4. The experimental case theoretically can only produce 13% of the ideal ANC reduction for a 100Hz tone due to the control source constraints of the experiment. The maximum sound energy reduction possible at 100Hz is 12dB.

6.3 Future Work

This project was mainly concerned with the implementation of an ANC window application. This section points out some potential areas where this work could be extended in future. The two main areas for future work are in modelling and experimental ANC window tests.

6.3.1 Modelling

The model developed in this work could be usefully developed so that theoretical control source number, locations and inputs are easily calculated. To do this the model would need to be adapted to optimise for multiple frequencies simultaneously, the control source inputs optimised given their locations, and then the control sources locations optimised. Development of a model this comprehensive would be an essential tool for the installation of ANC windows as windows are quite often custom sizes.

6.3.2 ANC window testing

Suggested future experimental work would investigate using the ANC control system in short frequencies bands (50Hz or less). Results from testing over the frequency range of interest in 50Hz bands (eg. .., 200-250Hz, 250-300Hz, ..) would provide a better indication of the highest controllable band of frequency. In any case future testing will need to focus on smaller frequency bands in order to be effective.

It is also suggested that larger piezoelectric stack actuators (PSAs) be used as this would ensure less distortion due to running the PSAs near their maximum rating.

References

[1] Zannin, P.H.T., Ferreira A. M. C., and Szeremetta B., Evaluation of Noise Pollution in Urban Parks, Environmental Monitering and Assesment, 2006, 118(1), 423-433.
[2] Broner, N., The Effects of Low Frequency Noise on People—A Review, Journal of Sound and Vibration, 1978, 58(4), 483-500.
[3] Kjellberg, A., et al., Fatigue Effects of Noise on Aeroplane Mechanics, Work & Stress, 1996, 10(1), 62-71.
[4] Passchier-Vermeer, W. and Passchier, W. F., Noise Exposure and Public Health, Environ Health Prospect, 2000, 108(1), 123-131.
[5] Leventhall, H., Low Frequency Noise and Annoyance, Noise and Health, 2004, 6(23), 2004.
[6] Hall, F., Papakyriakou, M., and Quirt, J., Comparison of Outdoor Microphone Locations for Measuring Sound Insulation of Building Facades, Journal of Sound and Vibration, 1984, 92(4), 559-567.
[7] Lercher, P., Environmental Noise and Health: An Integrated Research Perspective, Environment International, 1996, 22(1), 117-129.
[8] Rasmussen, B., Facade Sound Insulation Comfort Criteria in European Classification Schemes for Dwellings, Euronoise 2006, Tampere, 2006.
[9] Vermeir, G., Geentjens, G., and Bruyninckx, W., Measurement and Calculation Experiences on Façade Sound Insulation, Proceedings of Inter-Noise 2004, Prague, 2004, 115-122.
[10] Oldham, D. J., and Mohsen, E. A., The Acoustical Performance of Self-Protecting Buildings, Journal of Sound and Vibration, 1979, 65(4), 557-581.
[11] Shen, Y., and Oldham, D. J., Sound Radiation from Building Elements. Journal of Sound and Vibration, 1982, 84(1), 11-33.
[12] Yu, X., et al., Active Control of Sound Transmission through Windows with Carbon Nanotube-based Transparent Actuators, IEEE Transactions on Control Systems Technology, 2007, 15(4), 704-714.
[13] Beranek, L. L., Noise Reduction, McGraw-Hill: New York, 1960.
[14] Utley, W. A., Single Leaf Transmission Loss at Low Frequencies, Journal of Sound and Vibration, 1968, 8(2), 256-261.
[15] Jones, R. E., Intercomparisons of Laboratory Determinations of Airborne Sound Transmission Loss, The Journal of the Acoustical Society of America, 1979, 66(1), 148-164.
[16] Quirt, J. D., Sound Transmission through Windows. I. Single and Double Glazing, Journal of the Acoustical Society of America, 1982, 72(3), 834-844.
[17] Marsh, J. A., The Airborne Sound Insulation of Glass: Part 1, Applied Acoustics, 1971, 4(1), 55-70.
[18] Marsh, J.A., The Airborne Sound Insulation of Glass: Part 2, Applied Acoustics, 1971, 4(2), 131-154.
[19] Utley, W. A. and Fletcher, B. L., Influence of Edge Conditions on the Sound Insulation of Windows, Applied Acoustics, 1969, 2(2), 131-136.
[20] Oosting, W., "Investigation of the Sound Insulation of Flat Glass", Building Acoustics Technical Physical Service, TNO and TH, Delft, Report, 706(007), 1967.
[21] Michelsen, N., Effect of Size on Measurements of the Sound Reduction Index of a Window or a Pane, Applied Acoustics, 1983, 16(3), 215-234.
[22] *Mesures acoustique*. 1967, Office de Radiodiffusion-Television Franciase.
[23] Eisenberg, A., Die Schalldämmung von Gläsern und Verglasungen I - Fest eingebaute Einfachschreiben (The Sound Insulation of Glasses and Glazing - 1 - Firmly Fitted Single Panes), Glastechnische Berichte, 1958, 31, 297.

[24] Hood, M. J., The Transmission Loss and Vibration of Glass Panels in Non-Reverberative Conditions, Applied Acoustics, 1976, 9(4), 281-286.
[25] Utley, W. A. and Fletcher, B. L., The Effect of Edge Conditions on the Sound Insulation of Double Windows, Journal of Sound and Vibration, 1973, 26(1), 63-72.
[26] Lewis, P. T., Effect of Frame Construction on the Sound Insulation of Unsealed Windows, Applied Acoustics, 1979, 12(1), 15-24.
[27] "Sound Transmission through Glazing Materials", Libbey-Owens-Ford Glass Company, Manufacturer's data.
[28] London, A., Transmission of Reverberant Sound through Double Walls, The Journal of the Acoustical Society of America, 1950, 22(2), 270-279.
[29] Brüel, V., Sound Insulation and Room Acoustics, Chapman and Hall, 1951, Chapter 5.
[30] Bazley, E., "The Airborne Sound Insulation of Partitions", National Physical Laboratory, 1966.
[31] Woolley, R., "Sound Insulation of Windows", Building Research Station, 1967.
[32] Mackle, B. M., "Sound Transmission Loss of Non-Parallel Double Glazing", University of Canterbury, 1998.
[33] Tadeu, A. J. B. and Mateus D. M. R., Sound Transmission through Single, Double and Triple Glazing. Experimental Evaluation, Applied Acoustics, 2001, 62(3), 307-325.
[34] Quirt, J. D., Sound Transmission through Windows. II. Double and Triple Glazing, Journal of the Acoustical Society of America, 1983, 74(2), 534-542.
[35] Marsh, J. A., The Airborne Sound Insulation of Glass: part 3, Applied Acoustics, 1971, 4(3), 175-191.
[36] Quirt, J., "Measurements of Sound Transmission Loss", Division of Building, National Research Council of Canada, Ottawa, 1981.
[37] Kaiser, O. E., Pietrzko, S. J., and Morari, M., Feedback Control of Sound Transmission through a Double Glazed Window, Journal of Sound and Vibration, 2003, 263, 775-795.
[38] Jakob, A. and Moser, M., Active Control of Double-Glazed Windows. Part I. Feedforward Control, Applied Acoustics, 2003, 64, 163-82.
[39] De Man, P., Francois, A., and Preumont, A., Active Control of Noise Transmission through Double Wall Structures, An Overview of Possible Approaches, 6th National Congress on Theoretical and Applied Mechanics, Ghent, 2003.
[40] Jakob, A. and Moser, M., Active Control of the Cavity Sound Field of Double Panels with a Feedback Controller, *7th International Congress on Sound and Vibration*, Garmisch-Partenkirchen, Germany, 2000.
[41] Rubin, M. and C.M. Lampert, Transparent Silica Aerogels for Window Insulation, Solar Energy Materials, 1983, 7(4), 393-400.
[42] Jakob, A. and Moser, M., An Actively Controlled Double-Glazed Window with Small Pane Distance, Forum Acusticum, Sevilla, 2002.
[43] Fabio, S. and Fabrizio, V., Active Noise Control Applied to Buildings Components, Forum Acusticum, Sevilla, 2002.
[44] Jakob, A. and Moser, M., Active Control of Double-Glazed Windows. Part II. Feedback Control, Applied Acoustics, 2003, 64, 183-96.
[45] Jakob, A. and Moser, M., Active Control of Double-Glazing Windows: An Experimental Comparison between Feedback and Feedforward Controllers. Proceedings of 17th International Congress on Acoustics ICA, Rome, 2001.

[46] Yu, X., et al. Active Control of Sound Transmission through Windows with Carbon Nanotube based Transparent Actuators and Moving Noise Source Identification, *2006 American Control Conference,* Minneapolis, MN, 2006.
[47] Yu, X., et al., "Thin Film Transparent Acoustic Transducer", US Patent Office, United States, 2007.
[48] Zhu, H., et al., Active Control of Glass Panels for Reduction of Sound Transmission through Windows, Mechatronics, 2004, 14, 805-819.
[49] Sas, P., et al., Active Control of Sound Transmission through a Double Panel Partition, Journal of Sound and Vibration, 1995, 180(4), 609-625.
[50] Curie, J. and Curie, P., Développement, par pression, de l'électricité polaire dans les cristaux hémièdres à faces inclinées, Comptes rendus de l'Académie des Sciences, 1880, 91, 294-295.
[51] Curie, J. and P. Curie, Contractions et dilatations produites par des tensions électriques dans les cristaux hémièdres à faces inclinées, CR Acad. Sci, 1881, 93, 1137-1140.
[52] Gallego-Juarez, J. A., Piezoelectric Ceramics and Ultrasonic Transducers, Journal of Physics E, Science Instruments, 1989. 22(10), 804-816.
[53] Mason, W. P., Quartz Crystal Applications, Bell System Technical Journal, 1943, 22(2), 178-223.
[54] Kawai, H., The Piezoelectricity of Poly (vinylidene fluoride), Japanese Journal of Applied Physics, 1969, 8**,** 975-976.
[55] Gu, Y., et al., Experiments on Active Control of Plate Vibration Using Piezoelectric Actuators and Polyvinylidene Fluoride (PVDF) Modal Sensors, Journal of Vibration and Acoustics, 1994. 116(3), 303-308.
[56] Chandrashekhara, K. and Agarwal, A. N., Active Vibration Control of Laminated Composite Plates Using Piezoelectric Devices: A Finite Element Approach, Journal of Intelligent Material Systems and Structures, 1993. 4, 496-508.
[57] Gentry, C.A., Guigou, C., and Fuller, C.R., Smart Foam for Applications in Passive/Active Noise Radiation Control, Journal of the Acoustical Society of America, 1997, 101, 1771-1778.
[58] Tzou, H.S. and Gadre, M., Theoretical Analysis of a Multi-Layered Thin Shell Coupled with Piezoelectric Shell Actuators for Distributed Vibration Controls, Journal of Sound and Vibration, 1989, 132(3), 433-450.
[59] Davy, J., Challenges with the Active Sound Insulation of Windows, Acoustics 2001 Australian Acoustical Society Annual Conference Noise and Vibration Policy - The Way Forward?, Canberra, 2001.
[60] Trevathan, J., "Sound Transmission Through Walls: A Coupled BEM/FEM Approach", PhD Thesis, University of Canterbury, 2005.
[61] Monfared, V., Effect of Geometric Factor and Loading on Strength of Rectangular Plate Under Bending, Middle-East Journal of Scientific Research, 2012. 11(11), 1546-1549.
[62] Wilson, C. L. et al., Theoretical Active Control Analysis of Low Frequency Noise in a Mining Vehicle Cabin: Part 1, Inter-Noise and Noise-Con Congress and Conference Proceedings, Portland, 2011, 660-670.
[63] Hansen, C., Noise Control From Concept to Application, Taylor & Francis, 2005, 41.
[64] Fuller, C.C., S. Elliott, and P.A. Nelson, Active Control of Vibration, Academic Press, San Diego, 1996.
[65] Howard, C.Q., Transmission Loss of a Panel with an Array of Tuned Vibration Absorbers, Acoustics Australia, 2008. 36(3) 98-103.

Appendix A – Wooden Frame Drawings

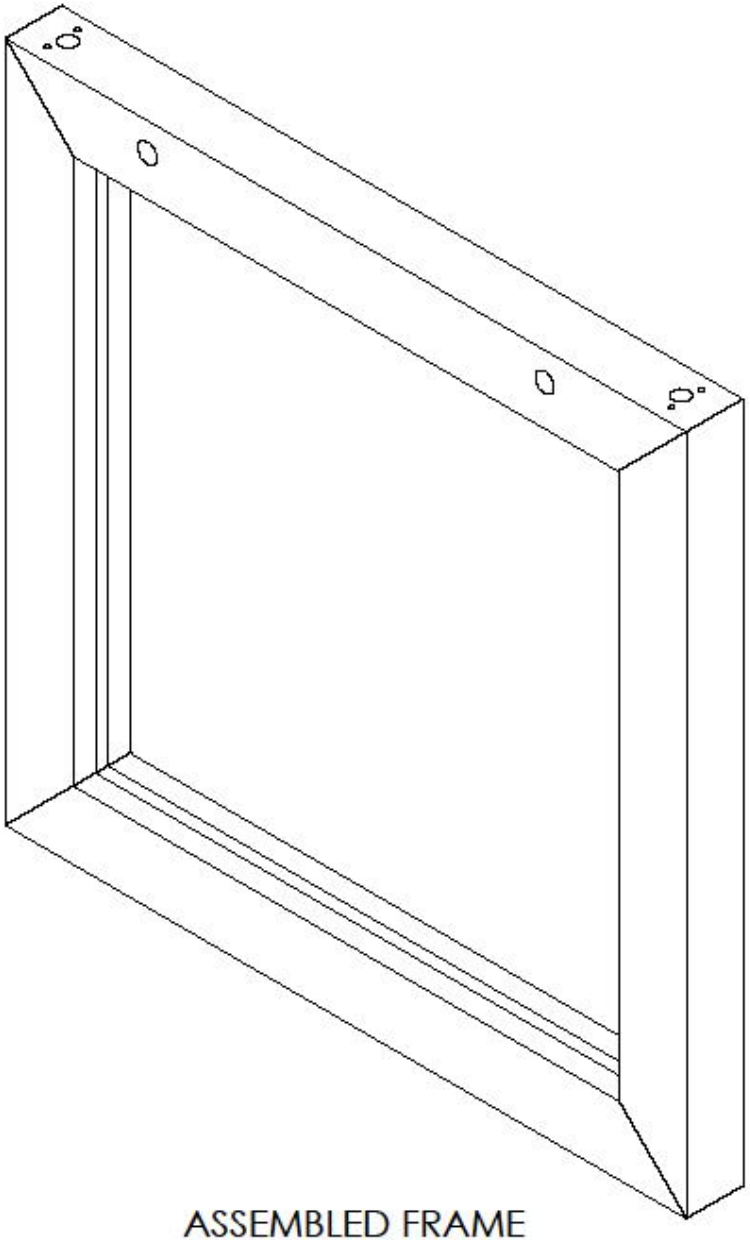

ASSEMBLED FRAME

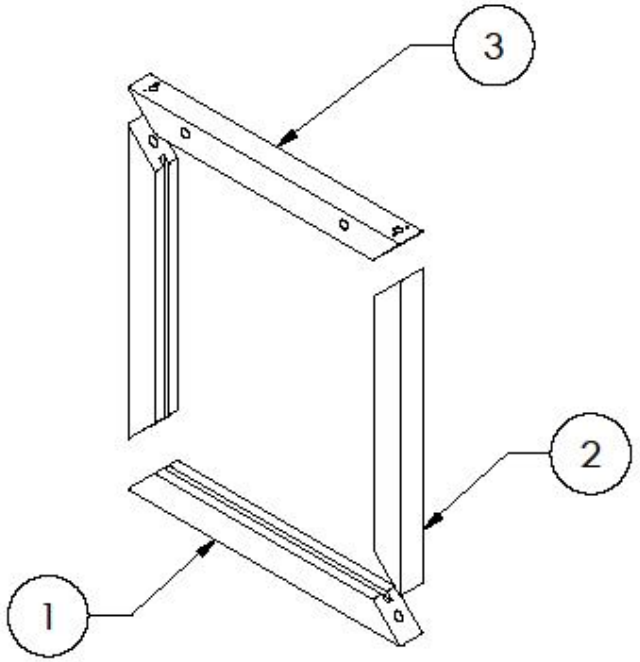

EXPLODED FRAME

ITEM NO.	DESCRIPTION	QTY.
1	Frame bottom	1
2	Frame side	2
3	Frame top	1

SHEET No. 1 of 1	UNIVERSITY of CANTERBURY MECHANICAL ENGINEERING DEPT. CH.CH. N.Z.	
Small Glass Frame	DRAWN :	DATE : 28/11/2011
Assembly	CHECKED :	DRG. No :
SCALE : 1:2 – (A3) ALL DIMENSIONS IN mm	APPROVED :	

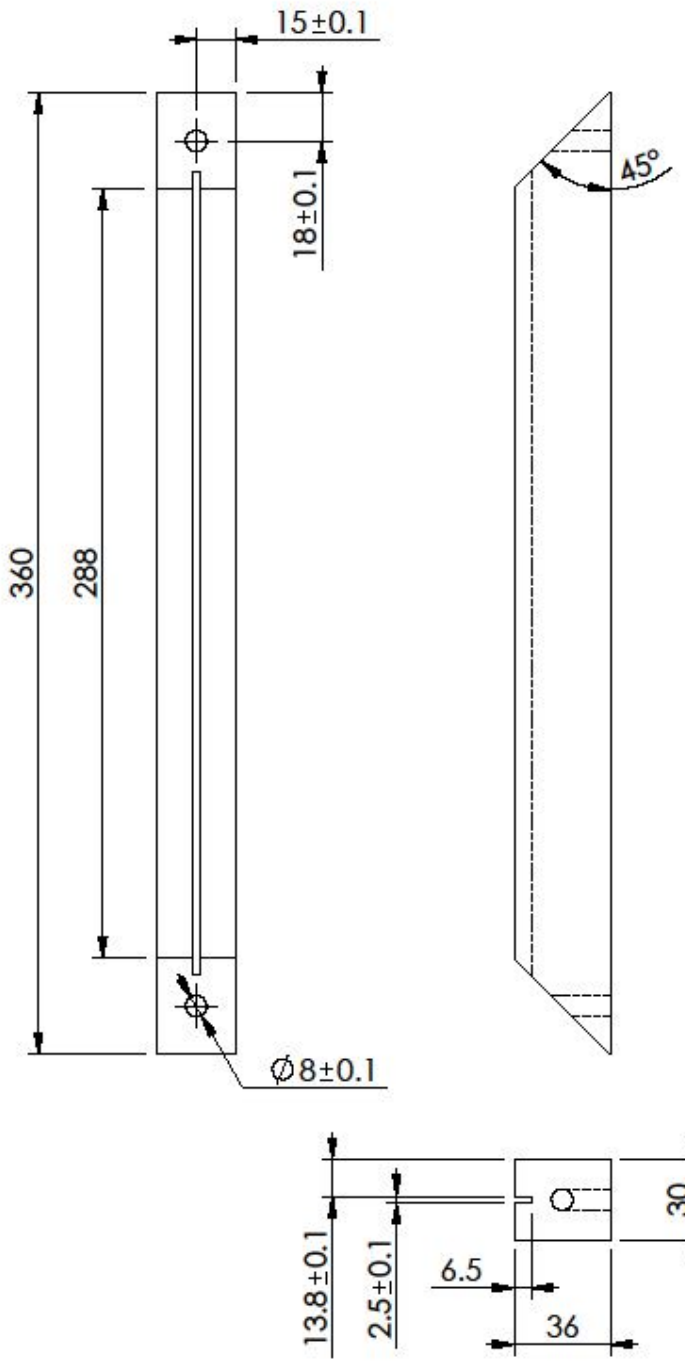

FRAME BOTTOM

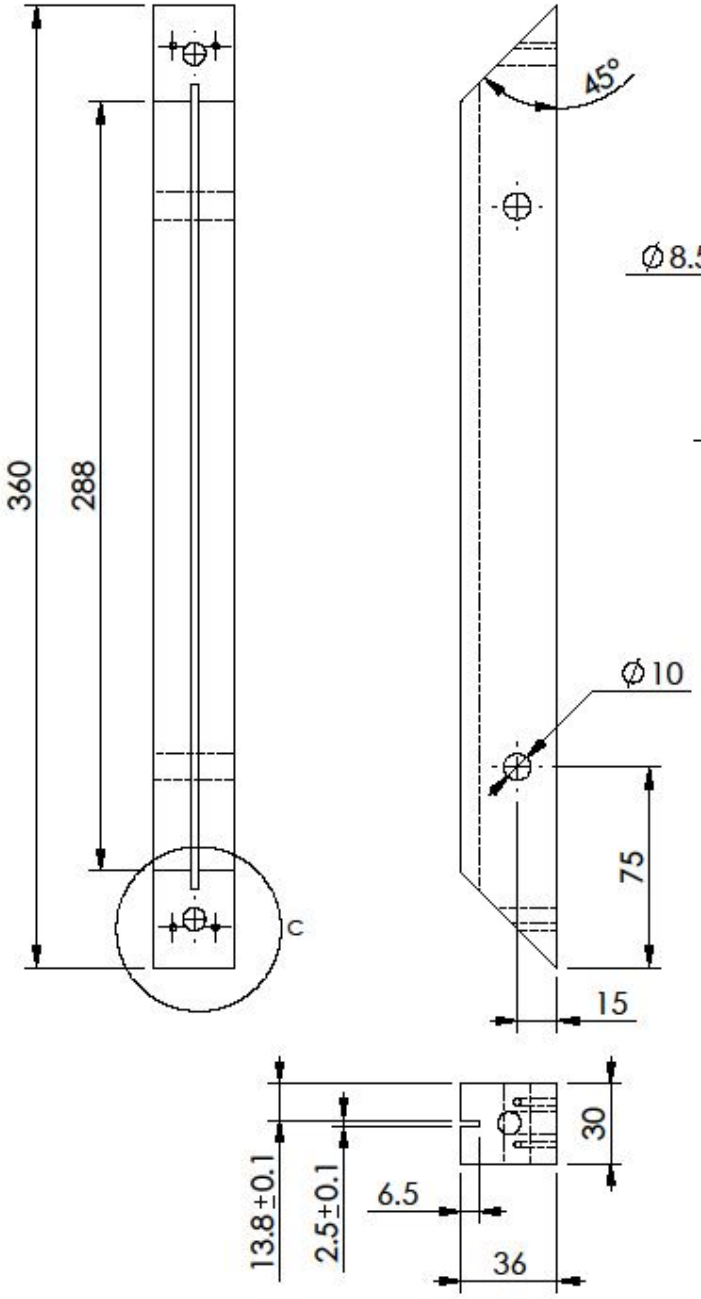

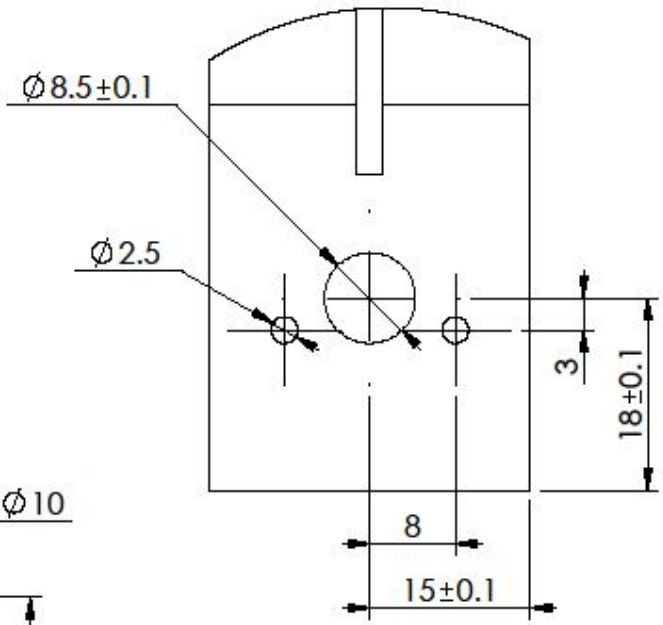

DETAIL C
SCALE 2 : 1

FRAME TOP

TOLERANCE: ± 0.2mm

SHEET No. 1 of 2	**UNIVERSITY of CANTERBURY** MECHANICAL ENGINEERING DEPT. CH.CH. N.Z.	
Frame - 2mm Glass	DRAWN :	DATE : 29/11/2011
Individual parts	CHECKED :	DRG. No :
SCALE : 1: 2 – (A3) ALL DIMENSIONS IN mm	APPROVED :	

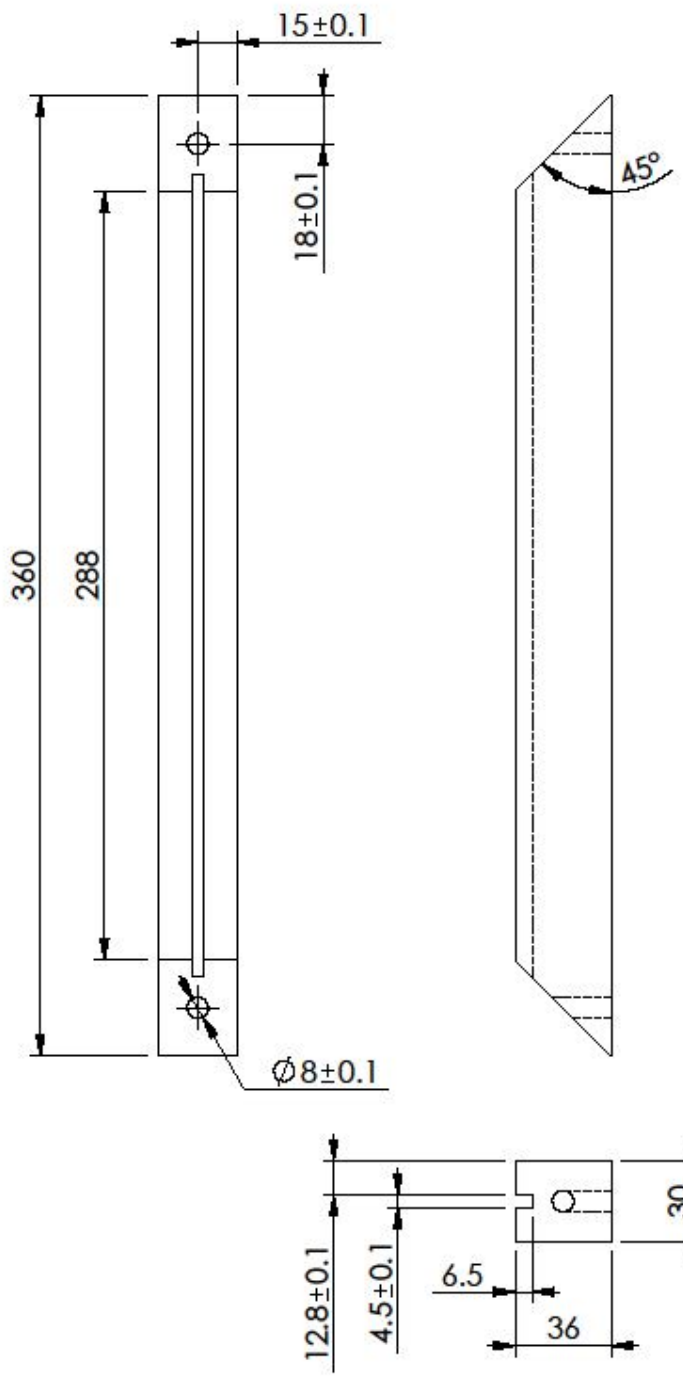

FRAME BOTTOM

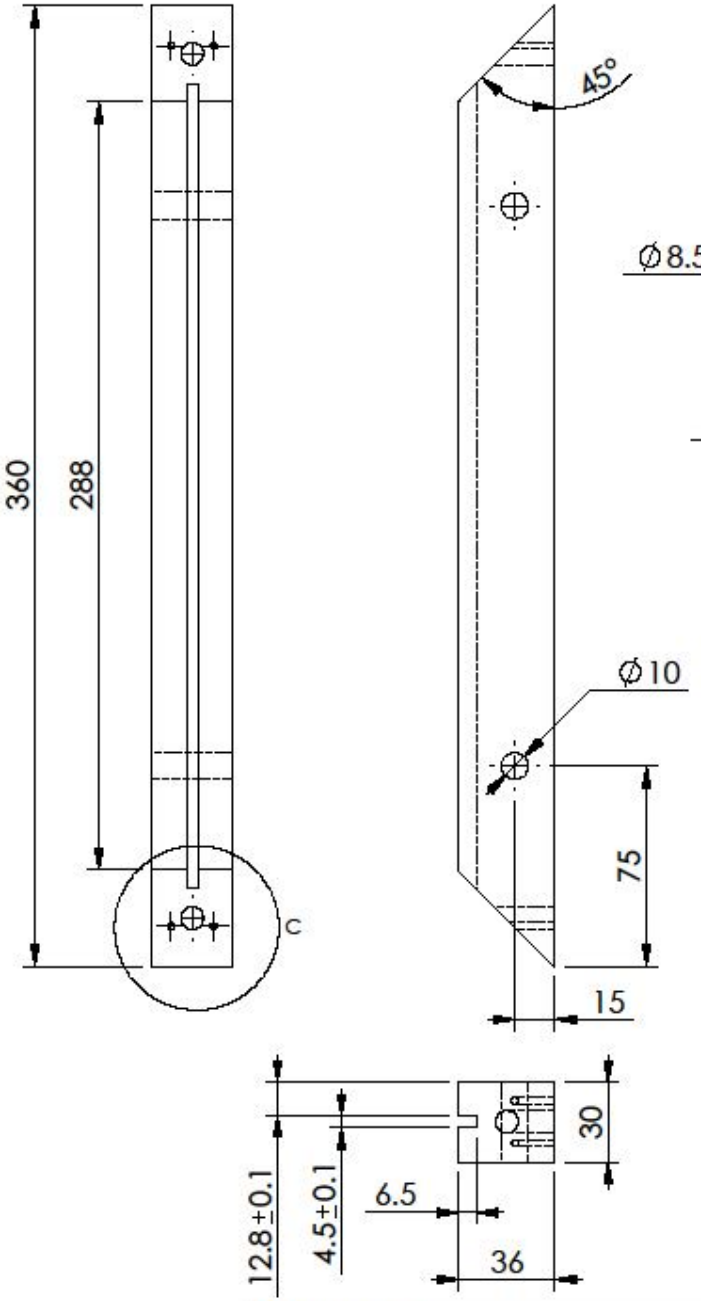

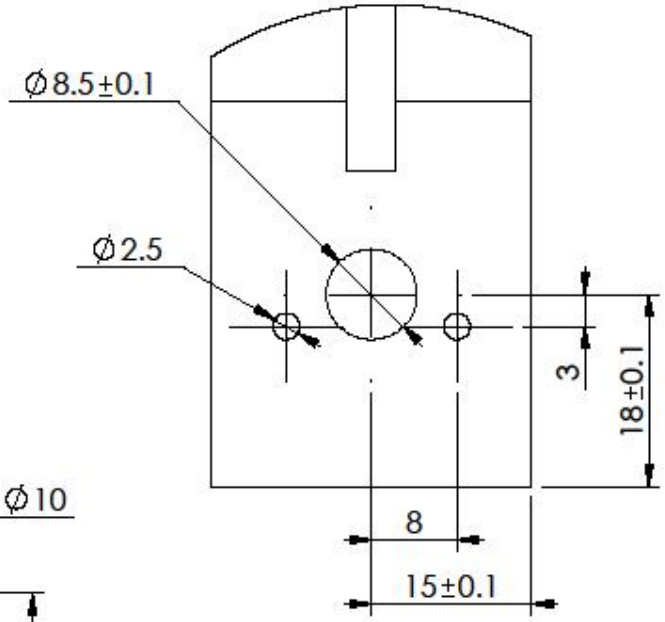

DETAIL C
SCALE 2 : 1

FRAME TOP

TOLERANCE: ± 0.2mm

SHEET No. 1 of 2	UNIVERSITY of CANTERBURY MECHANICAL ENGINEERING DEPT. CHCH N.Z.	
Frame - 4mm Glass	DRAWN :	DATE : 29/11/2011
Individual parts	CHECKED :	DRG. No :
SCALE : 1: 2 – (A3) ALL DIMENSIONS IN mm	APPROVED :	

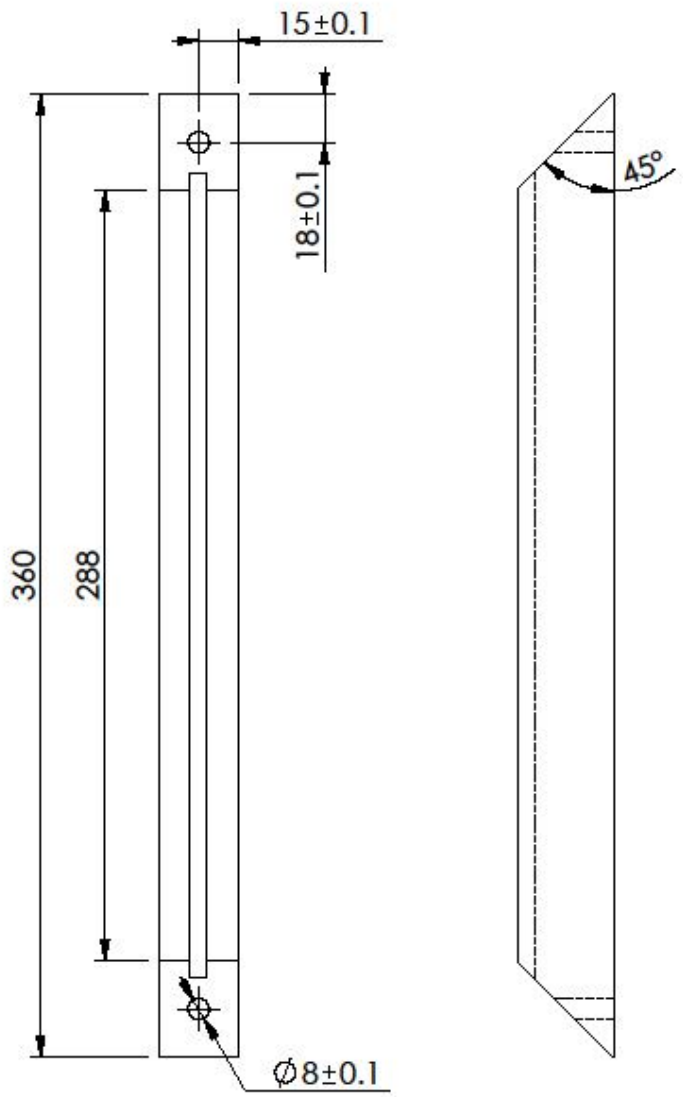

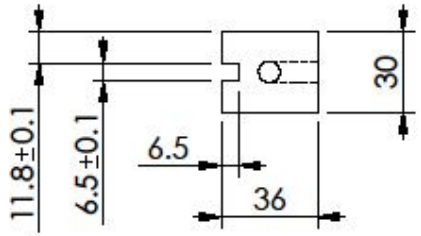

FRAME BOTTOM

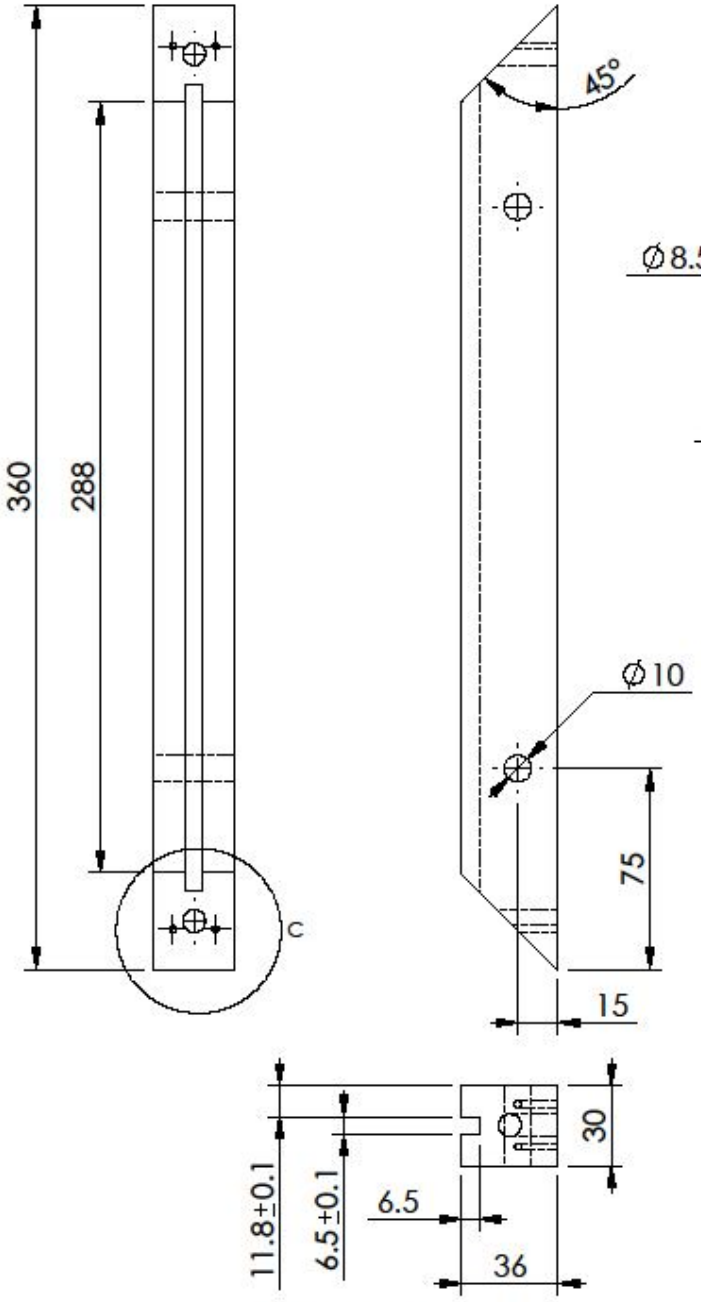

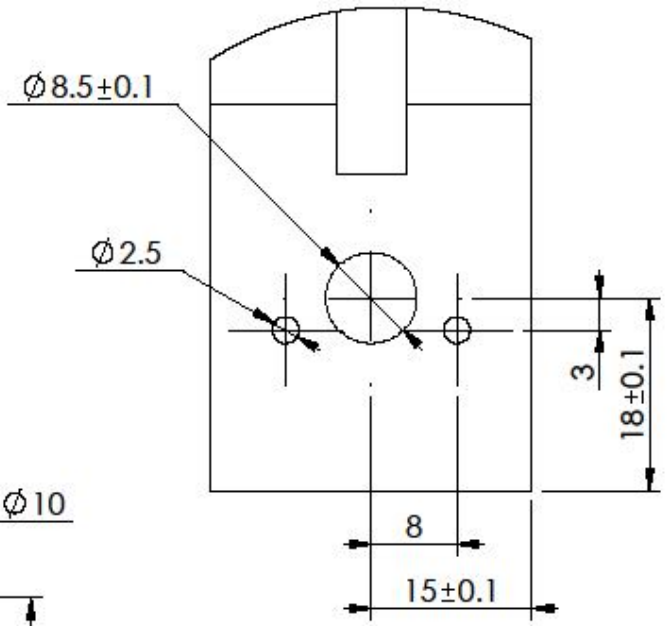

DETAIL C
SCALE 2 : 1

FRAME TOP

TOLERANCE: ± 0.2mm

SHEET No. 1 of 2		UNIVERSITY of CANTERBURY MECHANICAL ENGINEERING DEPT. CHCH N.Z.
Frame - 6mm Glass		DRAWN : DATE : 29/11/2011
Individual parts		CHECKED :
SCALE : 1: 2 – (A3)	ALL DIMENSIONS IN mm	APPROVED : DRG. No :

Appendix B – SPL Responses for PVDF Film Speakers

2mm responses:

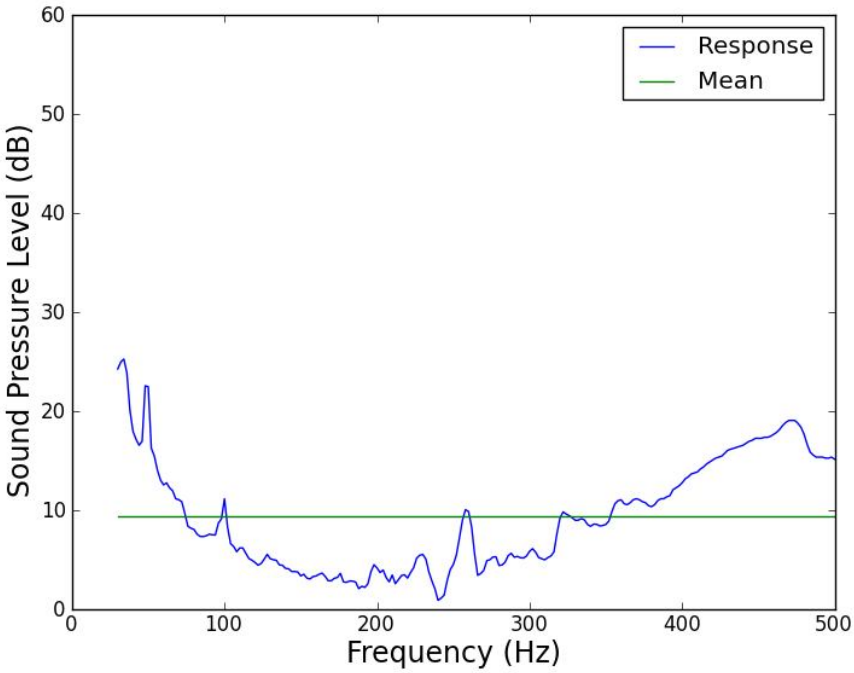

SPL frequency response for the tape attached PVDF film speaker on a 2mm glass sheet.

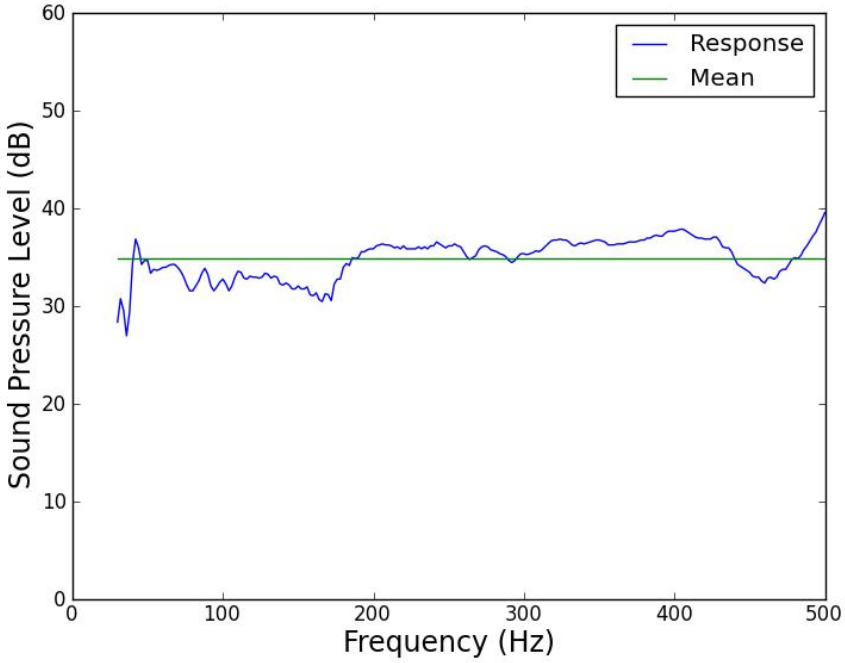

SPL frequency response for the tape attached PVDF film speaker on a 2mm acrylic sheet.

4mm responses:

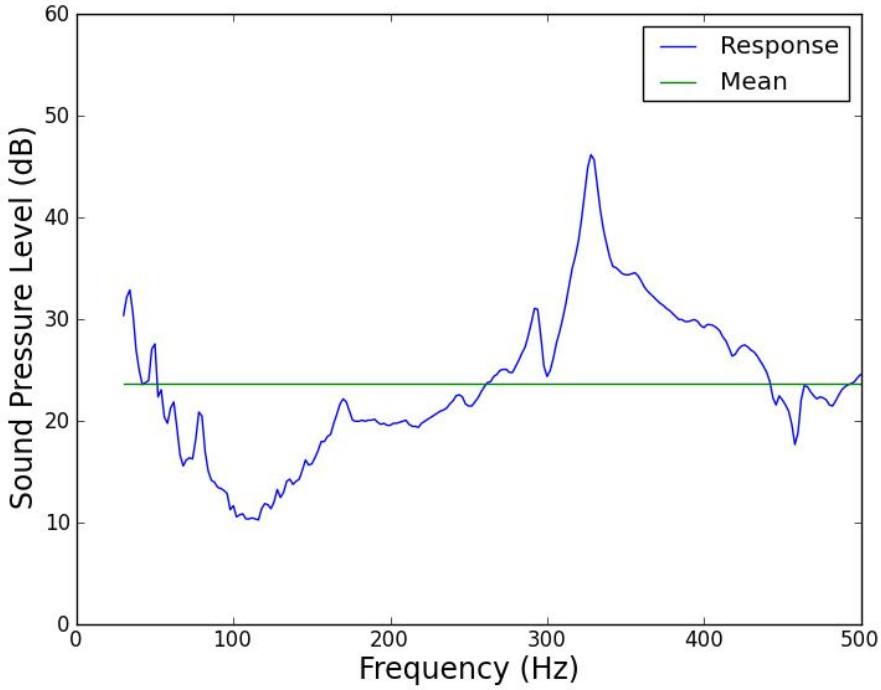

SPL frequency response for the tape attached PVDF film speaker on a 4mm glass sheet.

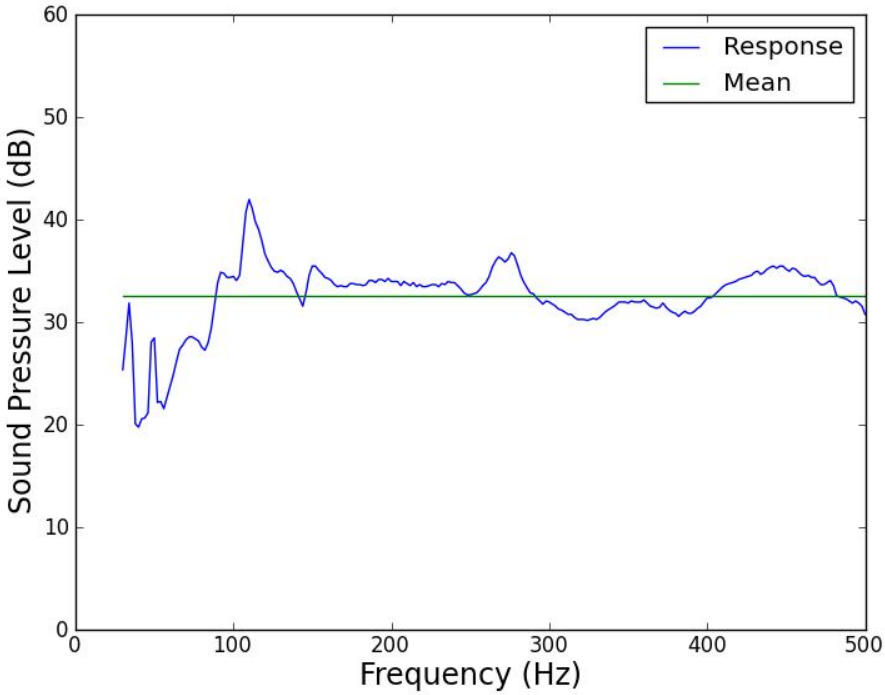

SPL frequency response for the tape attached PVDF film speaker on a 4mm acrylic sheet.

6mm Responses:

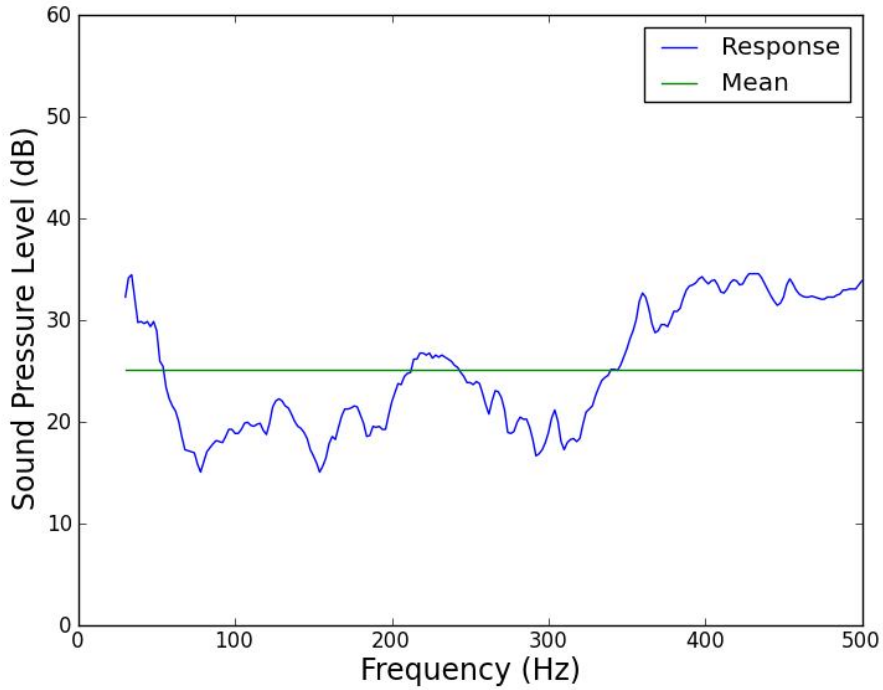

SPL frequency response for the tape attached PVDF film speaker on a 6mm glass sheet.

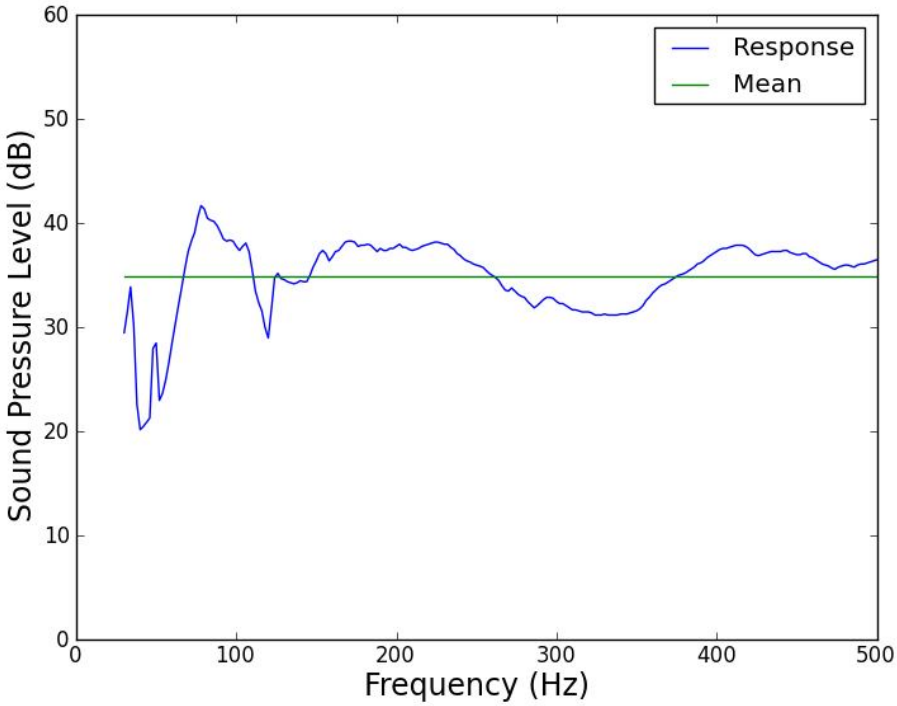

SPL frequency response for the tape attached PVDF film speaker on a 6mm acrylic sheet.

Appendix C – Energy Reductions for ANC Box Tests

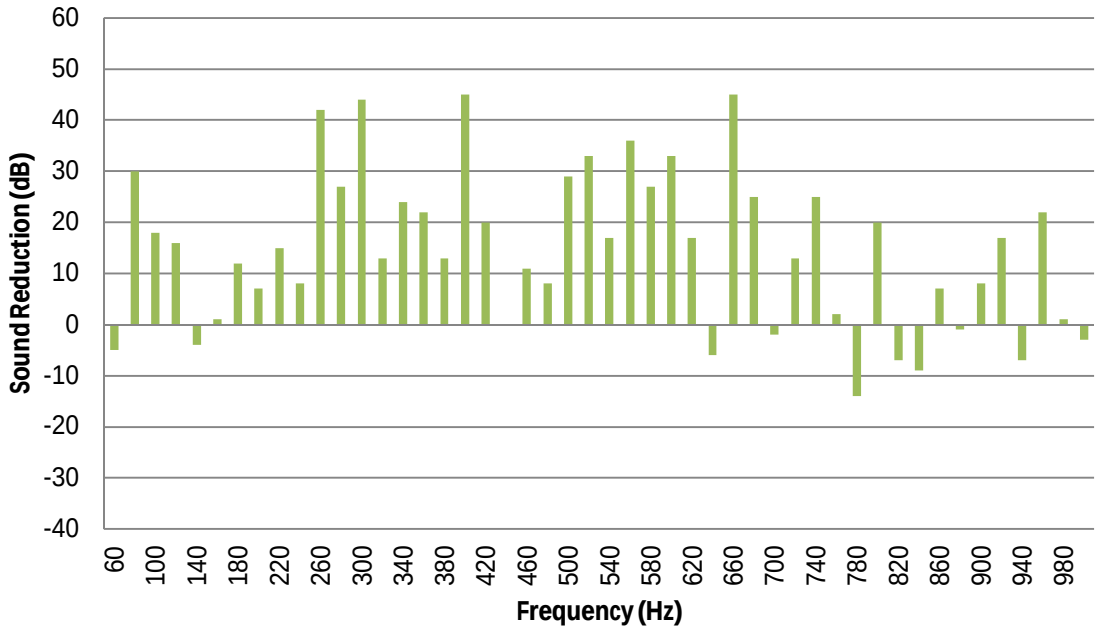

SPL reduction recorded at microphone 1 due to the 4x4 ANC control system tested in the ANC box

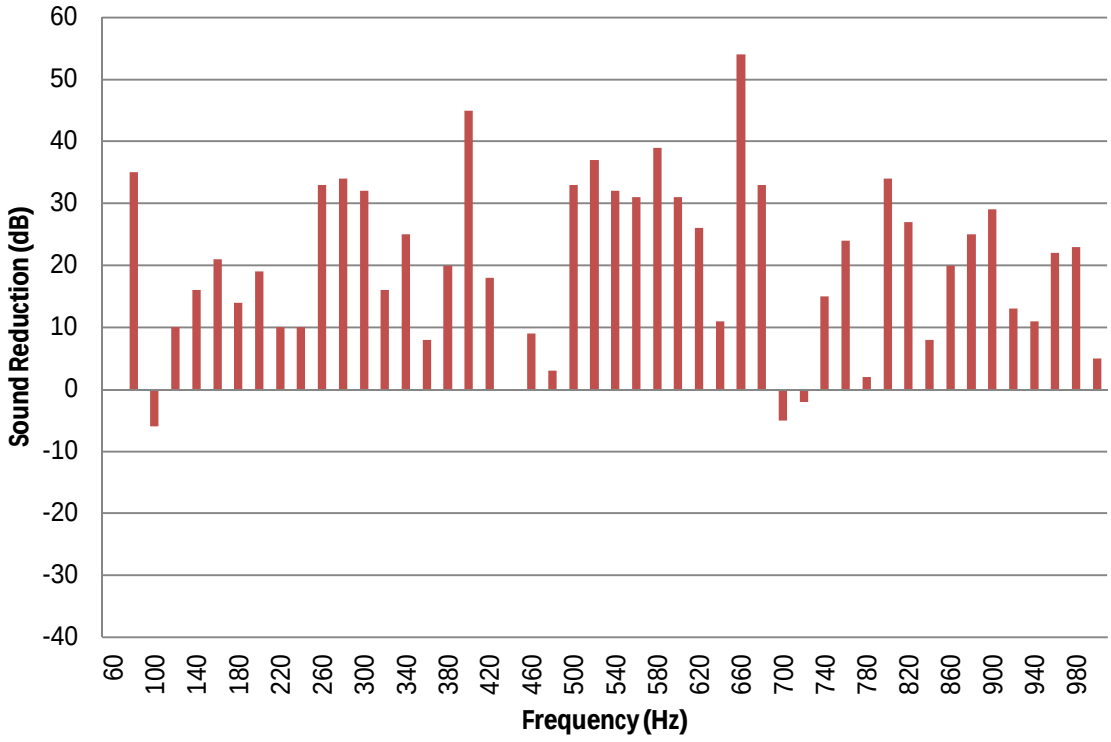

SPL reduction recorded at microphone 2 due to the 4x4 ANC control system tested in the ANC box

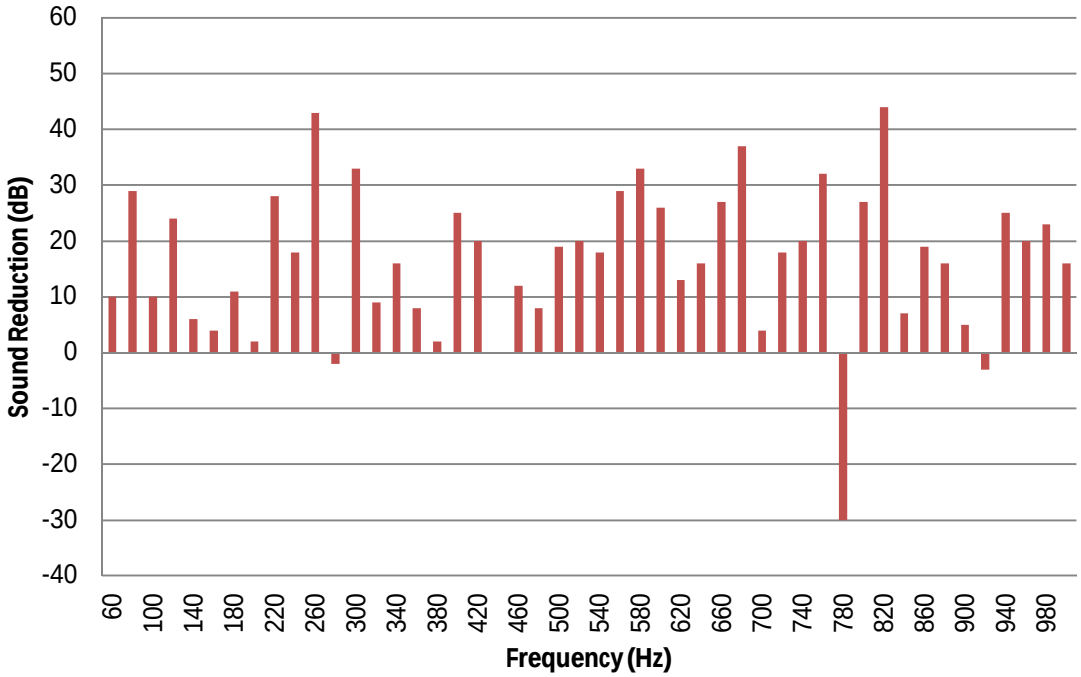

SPL reduction recorded at microphone 3 due to the 4x4 ANC control system tested in the ANC box

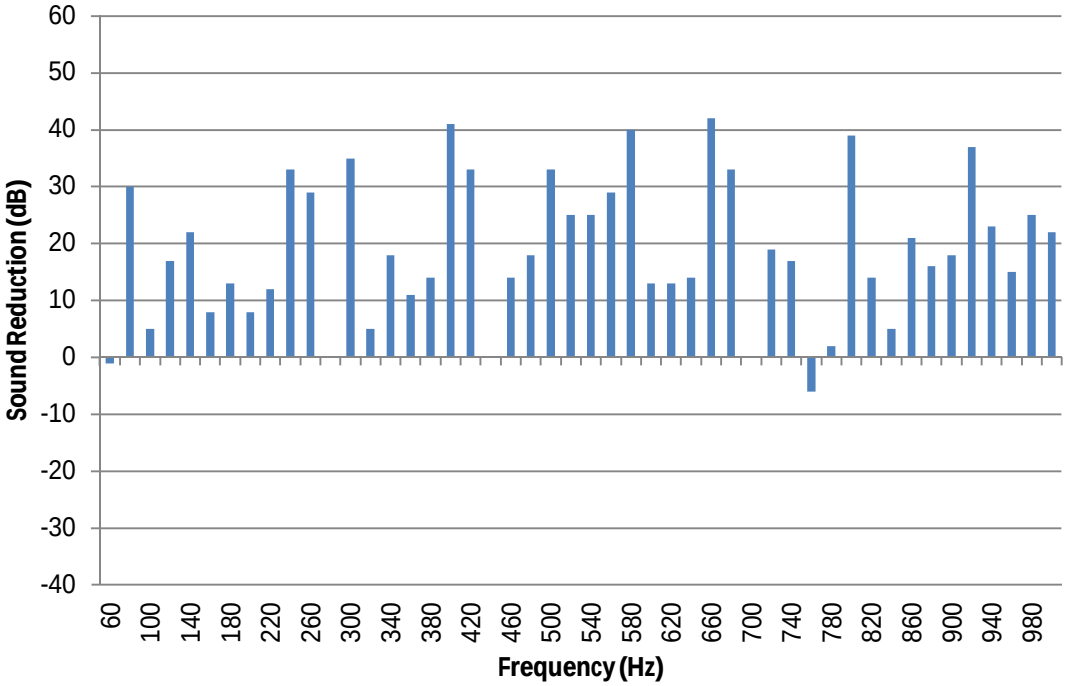

SPL reduction recorded at microphone 4 due to the 4x4 ANC control system tested in the ANC box